Investigation of novel dye anchoring and devices architecture for aiming at dye-sensitized solar cells with high efficiency

A thesis submitted in part of requirement to fulfill the degree

Doctoral Dissertation

Azwar Hayat / 12897014

Submitted to the Jury
Prof. Shuzi Hayase (Supervisor)
Prof. Tingli Ma
Prof. Wataru Takashima
Prof. Shyam S. Pandey
Prof. Hirokazu Yamane

Department of Biological Functions and Engineering
Graduate School of Life Science and System Engineering
Kyushu Institute of Technology
September 2015

Abstract

Current world population has reached 7.3 billion. With this huge population, demand of energy is rapidly increased. The standard of living is also growing, which increases demand of energy in near future. Fossil fuels are currently the main resource to provide energy which are not unlimited. Problems on fossil fuels energy are not only lack of resource but also creating the environmental problems. Oil based energy waste such as carbon monoxide (CO) and carbon dioxide (CO_2) block heat in atmosphere and accelerate earth surface temperature to trigger global warming. From this point of view, we need a suitable energy substitute as soon as possible.

Dye sensitized solar cell (DSSC) using the principle of natural photosynthesis are now currently at the verge of commercialization having similar photoconversion efficiency as compared to amorphous silicon solar cells. DSSCs or well known as Grätzel cells, consist of n-type semiconductor such as titanium dioxide (TiO_2), tungsten oxide (WO_3), zinc oxide (ZnO) or tin dioxide (SnO_2), with the light absorber. The structure is different from all solar cell mentioned above where light is being absorbed by the semiconductor materials itself. Relatively low cost and easy manufacturing process make DSSCs one of candidates for future solar energy resources. DSSCs reached up to 13% of efficiency in recent days. There are several barriers in DSSCs commercialization, for instance, utilization of only visible region of solar spectra, high cost of transparent conductive Oxide (TCO) glass, and so on. Our final goals are to extend the photo sensitivity of DSSCs to far-red and NIR area, to change the structure of DSSCs into back-contact DSSC in order to totally remove the TCO parts, and to fabricated cylindrical structure for harvesting more light in a day and decreasing wind resistance.

Chapter 1 deals with our research motivation, kinds of renewable energy, review about photovoltaics cell and propose of our present work. In chapter 2, the detail about the structure and working principle of DSSCs are discussed. The main components in DSSCs are explained in details and barriers of DSSCs commercialization also are discussed. In chapter 3, the DSSCs characteristics and cells performance calculation are deliberated. All experiments conducted in this thesis are described in this chapter.

Chapter 4 described the new dyes. Phosphorus-phthalocyanine dye was used to cover IR

region. Without conventional anchoring groups such as carboxylic acid (-COOH), phosporus-phthalocyanine dyes could be attached onto titania surface with P-O-Ti linkage. Furthermore, modification of the side chain at α-position of the sensitizer was done to optimize the HOMO-LUMO level.

In chapter 5, novel DSSC structure are discussed. Titanium sheet with micro holes (FTS-MH) was utilized as photo-anode and as counter electrode to completely eliminate TCO from DSSCs in flat as well as in cylinder structure. In flat back-contact DSSC, hydrogen peroxide treatment was used to modifu the titanium surface to make TiO_2 nanosheets, which leads to enhancement of short circuit current and open circuit voltage. Reduction of electrolytic gap was carried out to optimize IPCE in 300-400 nm wavelength region. In cylindrical structure, TCO-less cylinder DSSCs ware fabricated by folding the FTS-MH sheet and Ti-based counter electrode and inserted into heat shrinkable tubes. It was proved that the process enhanced the photovoltaic performance to the cylinder DSSC.

In last chapter we discuss about results and further optimizations prospect from current works and hopefully help researcher and industry to accelerate commercialization of DSSCs in near future.

Azwar Hayat

Contents

5. TCO free Dye sensitized solar cell using flat Titanium sheet

6. Conclusions and future prospects

1 Introduction

1.1 Global Energy Consumption

The governments in many countries have realized the energy problems to be faced if they did not manage and reserve their energy resources wisely. Energy regulations related to energy consumption and energy management have been more and more strictly applied to ensure energy availability[1]. Rising of global population and increasing of standard of living makes energy demand doubled within 40 years[2]. Figure 1.1 shows world energy supply in 2012. Almost half of our global consumptions still relay on oil and within 40 years the utilizations of other types of fuels also increase to support high energy demand.

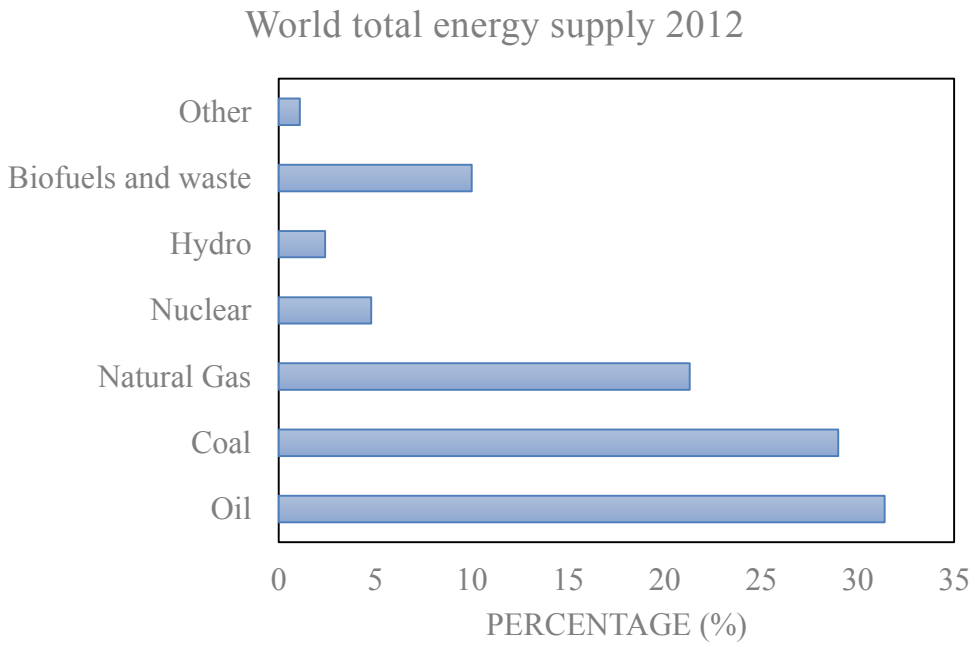

Figure 1.1 *World total energy supply in 2012.*

According to US Informational Administration, world annual energy demand has exceed 524 quadrillion Btu (1 Btu: 1055.05 joules) in 2012[3]. In another report in international energy outlook in 2014, global energy consumption is predicted to increase 56% from 520 quadrillion in 2010 step up to 820 quadrillion Btu in 2014[4]. The strong

demand comes from non-OECD (non-Organization for Economic Cooperation and Development) countries including China, India and Brazil. Emerging economics of China and India will stimulate oil demand in next 30 years while other countries incorporated in OECD will well-established since the oil markets seems have peaked.

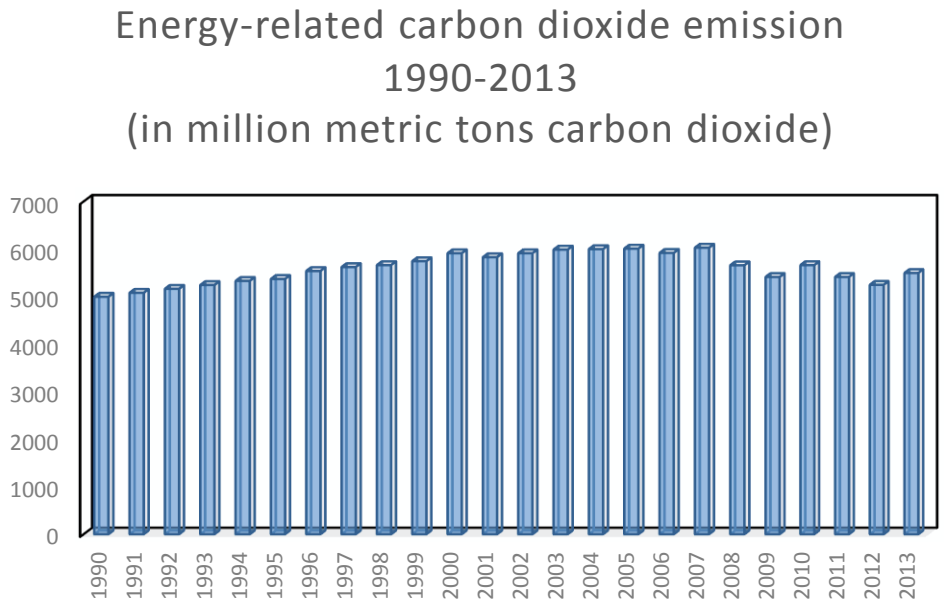

Figure 1.2 *Energy-related carbon dioxide emissions, 1990-2013.*

Among fossil fuels, the main global consumption still relay on Oil. Oil is the main players to provide energy which are limited in supply showing a declining trend against the current global demand. Oil not only lack of resource but also one of the trigger for generating the environmental problems, which needs an appropriate substitute as soon as possible. Burning Oil to create energy will produce waste product such as carbon monoxide (CO) and carbon dioxide (CO_2). These gases will trap the heat on earth and consequently will rise earth surface temperature to trigger greenhouse effect or global warming. Figure 1.2 shows number of carbon dioxide from 1990 ton 2013[5]. CO_2 emission increased 2.5% from 5.267 million metric tons (MMmt) in 2012 to 5.396 MMmt in 2013. It was found that earth temperature heated up 18.5% in 2013 versus 2012. Regardless of the rise in 2012, emissions in 2013 were still 10% lower than CO_2

emissions level in 2005. With the growth of global energy demand and human population in recent year, CO_2 concentration level will continuously increase[6].

1.2 Renewable energy sources

Fossil fuels based energy is still main resource for our energy demand. Therefore, the effect triggered by this choice will lead us to environmental damage for us now and for our future generations. In 1997, The Tokyo Protocol had been signed (and extended with Doha Amendment) as an effort to reduce the greenhouse. The next step is to reduce dependence at fossil based fuel, particularly oil, and escalation of renewable energy form usage. The sources of energy such as wind, biomass and bioenergy, hydropower, nuclear and sun are some of our alternative choices. The wind based energy potential power is vast which is 20 times of human population needs. The wind turbines could extract kinetic energy at a rate of at least 400 TW, whereas high-altitude places wind power could create more than 1,800 TW[7]. Therefore, the wind power`s cost-effectiveness is still a matter of argument and the other problems for example is noise problem and unpredictable availability makes wind power still hardly apply in wide scale. Biomass and bioenergy are self-renewing energy that can be understood as regenerative organic material. Biomass is recycling energy stored in organic matter such as wood products, corps, manure, dried vegetation and aquatic plants. Using biomass as energy sources can reduce greenhouse gas emissions. Burning biomass and fossil fuel will release the same amount of carbon dioxide. Therefore, burning fossil fuel will release "new" greenhouse gas. Biomass fuels like methanol from corn grain[8] and biodiesel from soybeans[9] can be used to substitute current vehicle fuels. However, biomass is still expensive and inefficient as compared with fossil fuels. It also consumes more fuel in the process to convert the organic matter into the energy form.

Hydropower uses water to generate electricity. Water cycle is endless processes from evaporating from lakes and oceans, creating clouds, falling down as rain or snow, flowing back to the ocean. This makes hydropower consider as renewable energy. Large hydropower has capacity more than 30 megawatts[10]. Small hydropower produces 100

kilowatts to 30 megawatts[11] and micro hydropower has capability up to 100 kilowatts for home or farm[12]. On the other hand, limitation of use and expensive installation and maintenance cost makes hydropower still rarely use as main energy sources for now.

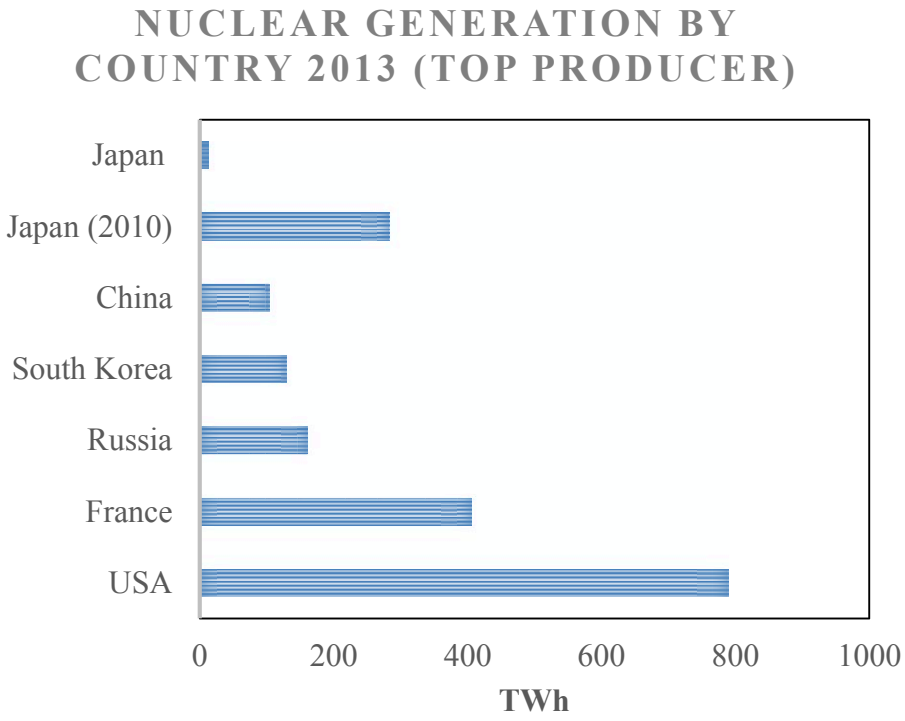

Figure 1.3 *Top nuclear power producer in 2013.*

Nuclear power is the primary choice to generate massive energy. It is forms by splitting atoms of certain elements. In 1940s, nuclear power initially were developed as weapons in World War II by splitting certain isotopes of either plutonium or uranium. The first commercial nuclear power station in the world was operated in 1950s. Today, 31 countries operate more than 430 commercials nuclear reactors including USA, Russia, China and Japan[13]. USA, France and Japan (in 2010 before tsunami disaster) are the top nuclear power producer in the world. In Japan, first commercial nuclear power was operated in mid-1966 and now more than 50 reactors support 30 % of country`s electricity needs. It is predicted to increase at least 40% by 2017[14]. Large power-generating capacity and low carbon dioxide make it a prominent alternative to fossil based fuel, however, safety concern such as controlling the radiation and maintaining radioactive waste still make this kind of energy form get resistant from society. Tsunami

struck in Japan in 2011 made one of its nuclear power plants in Fukushima broke down. Learning from this disaster event, we need safer energy form to fulfill our needs.

1.3 Photovoltaic

Sun is the main energy source for all the living being on this planet Earth. It contains massive amount of energy and transports through hundreds of kilometers to earth. Energy from sunlight is utilized by plant for photosynthesis process. Except the nuclear power, all the different forms of energy such as coal, oil, natural gas, biomass, hydropower and wind eventually originate from the sun. Learning from nature about application of sunlight to harvest energy in plants via the photosynthesis process, solar cells realize direct conversion of solar energy into usable electric power. Beyond that benefit, solar cells work without creating additional greenhouse gas emission. There are various different types of solar cells available at this time, such as mono-crystalline, polycrystalline, thin film, dye sensitized solar cell, organic photovoltaic (OPV), and perovskite solar cells are among the most popular.

Mono-Crystalline Silicon cells are produced by growing high purity of single crystal Si rods. To make a single crystal wafer cells is not cheap and it require high energetic resource for purification. They are cut from cylindrical ingots and the wafers do not completely cover a square solar cells module. The efficiency of mono-crystalline silicon cells remains around 22-25% depend on the purity level[15]. Poly-crystalline silicon cells are made from sawing a cast block of silicon into bars and then into thin wafers. This technology is also known as Multi crystalline technology[16]. Poly-Si cells are less expensive than single crystal silicon cells. Poly-Si solar cells are manufactured with efficiency more than 18 %[17]. Cadmium telluride (CdTe) solar cell is an efficient light-absorbing material for thin-film cells. The layer can be very thin in micrometer order. CdTe is easier to deposit and more suitable for large-scale production compared with other thin-film materials. It requires less resource to produce and manufacture technology significantly refined over the past few years[18]. On the downside, Cadmium

is a toxic heavy metal which make some environmental groups concern about it safety for long term usage.

Heterojuction solar cells are uniquely capable of producing low-cost modules, high-volume and affordable solar electricity. III-V heterojunctions are appropriate for fabrication of single junction solar cells, Aluminum-Gallium-Arsenide/Gallium-Arsenide (AlGaAs/GaAs) heterostructures have been found for solar cells application due to the well-matched lattice parameters of Gallium-Arsenide (GaAs) and Aluminum-Arsenide (AlAs), and on the other hand, GaAs has an optimal band gap for effective sunlight conversion. In AlGaAs/GaAs heterojunctions, the basic narrow band gap material was GaAs. A wide band gap window was made of AlGaAs close in the composition to AlAs, which is almost completely transparent to sunlight, making solar cells very sensitive in the short wavelength range of the sun spectrum[19]. Another type of solar cells is Copper Indium Gallium Selenide (CIGS). CIGS technology has achieved efficiency levels of 20% in the laboratory[20].

Learning from photosynthesis process, Dye sensitized solar cell (DSSC) is one of promising low cost solar cells. DSSCs research came in light when M. Grätzel and O`Regan reported a record photo-conversion efficiency of 7.1% using 10 μm thick nanoporous titanium dioxide (TiO_2) electrode in 1991[21] and currently DSSCs are also being popularly known as Grätzel Cell. Later invention of N3, N719 and Black dye sensitizer pushed the external power conversion efficiency well over 10%[22,23]. Using Ruthenium based novel sensitizers and cobalt electrolyte, 13 % of efficiency had been achieved[24]. The detail about DSSCs will be present in next chapter. The new golden boy in photovoltaic is Perovskite solar cell. Perovskite solar cells originally from DSSCs field when Prof. Miyasaka from Japan proposed it with liquid redox couple iodine as electrolyte in 2009[25]. Perovskite got its momentum when liquid electrolyte was replaced with solid state holes transport materials (Spiro-OMeTAD) that boost the efficiency[26]. Prof. Shuzi Hayase *et al* also succeed to extend perovskite solar cell coverage up to 1000nm[27]. Perovskite now reached 20% of efficiency[28] and this result reached within short time makes the golden boy one of the best candidate for future low cost solar cell. However, Perovskite is still prone to be damaged by moisture (water) and efficiency

depend on how we measured the cells (the hysteresis)[29]. This make it still long way to mass production.

1.4 Outline of the thesis

In chapter 2, the detail about structure and working principle of DSSCs are discussed. The main components in DSSCs are explained in details and barriers of DSSCs commercialization are also discussed.

In chapter 3, the DSSCs characteristics and cells performance calculation is deliberated. All experiment conducted in this thesis are presented in this chapter. Chapter 2 and 3 are based on knowledge from literature and recent publications. My research is presented in following chapters.

Axial ligation of phosphorous-phtalocyanine dyes as far red sensitizer for DSSCs application is studied in chapter 4. Without conventional anchoring groups such as carboxylic acid (-COOH), phosporus-phthalocyanine dyes could be attached onto titania surface with P-O-Ti linkage. Furthermore, modification of side chain at α-position of sensitizer moves the HOMO-LUMO level of dye to optimize electron injection and dye regeneration.

Device architecture modifications into transparent conductive-less (TCO-less) is discussed in chapter 5. TCO-less DSSCs using flat titanium sheet with micro holes (FTS-MH) employed as base for photo-anode is studied. In flat back-contact DSSC, flat titanium sheet sputtered with platinum (Pt) as counter electrode is compared with standard fluorine doped tin oxide (FTO) sputtered Pt. Hydrogen peroxide treatment also used to modified titanium surface from TiOx into TiO_2 nanosheets. Reduction of electrolytic gap also carried out to optimize IPCE in 300-400 nm wavelength region. In cylindrical structure, TCO-less DSSCs was carried out by folding the FTS-MH and Ti-based counter electrode to 360 degree and inserted into heat shrinkable tube led to high efficiency cylindrical TCO-less DSSCs.

Chapter 6 gives brief summary of the thesis and future optimization possibilities in this field.

1.5 References to chapter 1

1) Worldwide trends in energy use and efficiency, International Energy Agency, (2008).

2) Key world energy statistics, International Energy Agency, (2014)

3) "International Energy Statistics". Energy Information Administration. Website: http://www.eia.gov/consumption/ Retrieved 31 March 2015.

4) International Energy Outlook, U.S. Energy Information Administration, (2014).

5) U.S. Energy-Related Carbon Dioxide Emission, U.S. Energy Information Administration, (2013).

6) Intergovernmental Panel on Climate Change (IPCC) "Second Assessment Report - Climate Change 1995", (1995) Web site: www.meto.gov.uk.

7) K. Marvel, B. Kravitz and K. Caldeira, *Nature Climate Change*, **3**, 118-121, (2013).

8) H.L. Chum and R.P. Overend, *Fuel Processing Technology,* **71,** 1-3, 187-195, (2001).

9) H. Noureddini, X. Gao and R.S. Philkana, *Bioresource Technology*, **96**, 7, 769-777, (2005).

10) M. Barros, F. Tsai, S. Yang, J. Lopes, and W. Yeh, *J. Water resources Planning and Management*, **129**, 3, 178-188, (2003).

11) F. Onen and M. Eminoglu, *European Scientific Journal,* **SE 3**, (2013).

12) Y.R. Pasalli and A.B. Rehiara, *Procedia Environmental Sciences,* **20**, 55-63, (2013).

13) IAEA, *Nuclear Engineering International*, June 2014.

14) The 4th Strategic Energy Plan of Japan, (2014).

15) M.A. Green, K. Emery, Y. Hishikawa, W. Warta and E.D. Dunlop, *Progress in Photovoltaics,* **23**, 1, 1-9, (2015).

16) D. Macdonald, A. Cuevas, A. Kinomura, Y. Nakano, and L.J. Geerligs, *Journal of Applied Physics*, **97***,* 3, 033523, (2005).

17) P. Engelhart, J. Wendt, A. Schulze, C. Klenke, A. Mohr, K. Petter and P. Wawer, *Energy Procedia*, **8**, 313-317, (2011).

18) M. Woodhouse, A. Goodrich, R. Margolis, T. James, R. Dhere, T. Gessert and D. Albin, *Solar Energy Materials and Solar Cells*, **115**, 199-212, (2013).

19) Y. Özen, N. Akın, B. Kınacı and S. Özçelik, *Solar Energy Materials and Solar Cells*, **137**, 1-5, (2015).

20) P. Jackson, D. Hariskos, E. Lotter, S. Paetel, R. Wuerz, R. Menner and M. Powalla, *Progress in Photovoltaics: Research and Applications*, **19***,* 7, 894-897, (2011).

21) B. O'Regan and M. Grätzel, *Nature*, **353**, 737–740, (1991).

22) M.K. Nazeeruddin, A. Kay, I. Rodicio, R. Humphry-Baker, E. Muller, P. Liska, N. Vlachopoulos, M. Grätzel, *J. Am. Chem. Soc.,* **115**, 6382, (1993).

23) M.K Nazeeruddin, P. Pechy and M. Grätzel, *Chemical Communications*, **18**, 1705-1706, (1997).

24) S. Mathew, A. Yella, P. Gao, R. Humphry-Baker, B.F. Curchod, N. Ashari-Astani and M. Grätzel, *Nature chemistry*, **6***,* 3, 242-247, (2014).

25) A. Kojima, K. Teshima, Y. Shirai and T. Miyasaka, *Journal of the American Chemical Society*, **131***,* 17, 6050-6051, (2009).

26) H.J. Snaith, *The Journal of Physical Chemistry Letters*, **4**, 21, 3623-3630, (2013).

27) Y. Ogomi, A. Morita, S. Tsukamoto, T. Saitho, N. Fujikawa, Q. Shen, T. Toyoda, K. Yoshino, S.S Pandey, T. Ma and S. Hayase, *The Journal of Physical Chemistry Letters*, *5*(6), 1004-1011, (2014).

28) N.G Park, *The Journal of Physical Chemistry Letters*, **4**, 15, 2423-2429, (2013).

29) H.J. Snaith, A. Abate, J.M. Ball, G.E. Eperon, T. Leijtens, N.K. Noel and W. Zhang, *The Journal of Physical Chemistry Letters*, **5***,* 9, 1511-1515, (2014).

Chapter 2 Dye sensitized solar cells

2.1 A brief history of DSSCs

In 1839, Becquerel laid the foundation of the application of photochemistry when he observed the first photovoltaic effect. He found that current passing between two platinum electrodes when they immersed in electrolyte contain metal halide in the present of sunlight[1)]. Almost at the same time Louis Daguerre, a French artist and photographer, with mirror-polished of silver halide particles he made first photographic image. Silver halide based photography is the major application of photosensitization effect in industry until digital photography appears. Silver halide particles are not photoactive for wavelength longer than 460 nm since it band gap ranging from 2.7 to 3.3 eV. A substantial development happened when Hermann Wilhelm Vogel, a German photo-chemist, in 1873 discovered dye sensitized silver halide emulsions for rendering first black and white photographic films[2,3)].

In 1972, Honda and Fujishima reported water splitting by illumination of TiO_2. This opened explanation about electron injection from photo-exited state into conduction band of TiO_2[4)]. However, efficiency obtained was low due to narrow absorption range of TiO_2 which was limited to ultraviolet region only. With the purpose to enhance the photon harvesting, Tsubomura reported a structure of a working dye-sensitized solar cell with porous zinc oxide (ZnO) photocell along with a platinum counter electrode and an iodide/tri-iodide redox couple with ruthenium dye as sensitizer[5)]. Dye sensitized solar cells (DSSCs), are utilizing *n*-type semiconductor for instance tin dioxide (SnO_2), titanium dioxide (TiO_2), tungsten oxide (WO_3) and zinc oxide (ZnO) as photo anodes, with the light absorber attached onto it which is different with all solar cell mentioned before, where light was being absorbed by the semiconductor materials itself. Desilvestro (1985) proposed the ruthenium complex sensitizer with rough TiO_2 electrode to enhance photovoltaic performance[6)]. DSSCs research gain its momentum when M. Grätzel and O`Regan reported a breakthrough with photo-conversion efficiency of 7.1% through 10 μm thick nanoporous TiO_2 photo anode and DSSCs are also being popularly known as Grätzel Cell[7)]. This field started to gain more interaction

from researches. Invention of ruthenium dye family of sensitizer such as N3, N719 and Black dye bumped the external power conversion efficiency (PCE) up to 10%[8-11]. DSSCs with TiO_2 photo anodes with ruthenium based novel sensitizers have reached PCE between 10-13 %[12-15].

All researchers in the world are working on not only to enhance the efficiency but the recent trends of DSSCs now are heading in the direction of the development of new flexible and light weight structure[16-18], cylindrical structure for optimum light harvesting[19,20] and type of hybrid or multi junction cells (tandem)[21-23]. There are some limitations of ruthenium for example, its absorption limited to visible rang and the dyes high production cost. Researchers seek for alternative sensitizer with metal free organic sensitizers which are cheaper and easy to synthesize[24-26]. Some research groups proposed dyes with absorption beyond visible range to far red and near infrared dyes[27-30]. TCO-less DSSCs for lower production cost applications[31-35] and flexible indoor applications[36-38] are also currently being actively tracked. Furthermore, solidification of DSSCs with hole transport material (HTM) to address leaking problems of liquid electrolyte and extend the DSSCs life time endurance[39-41].

Dye sensitized solar cells had currently initiated in mass commercialization stage. For example, G24i has stated the commercial production of solar back packs and iPad case based on DSSCs[42,43].

2.2 Structure of Dye sensitized Solar Cell.

A DSSC is fundamentally a thin-layer solar cell formed with sandwich structure of working electrode (photo anode) and counter electrode, with redox couple mediator containing electrolytes to fill the gap between these two electrodes. Figure 2.1 shows the detailed structure of DSSCs. First part is working electrode made of 10-15 micrometer thick *n*-type semiconductor such as TiO_2, SnO_2, ZnO *etc.*, coated on the top of TCO glass like Fluorine-doped tin oxide (FTO) or Indium-doped tin oxide (ITO). Light absorbing materials (sensitizing dyes) which are coated on nanoporous TiO_2 to construct

the photo anode. Mostly common dyes utilized till date for high efficiency are the ruthenium based dye sensitizer.

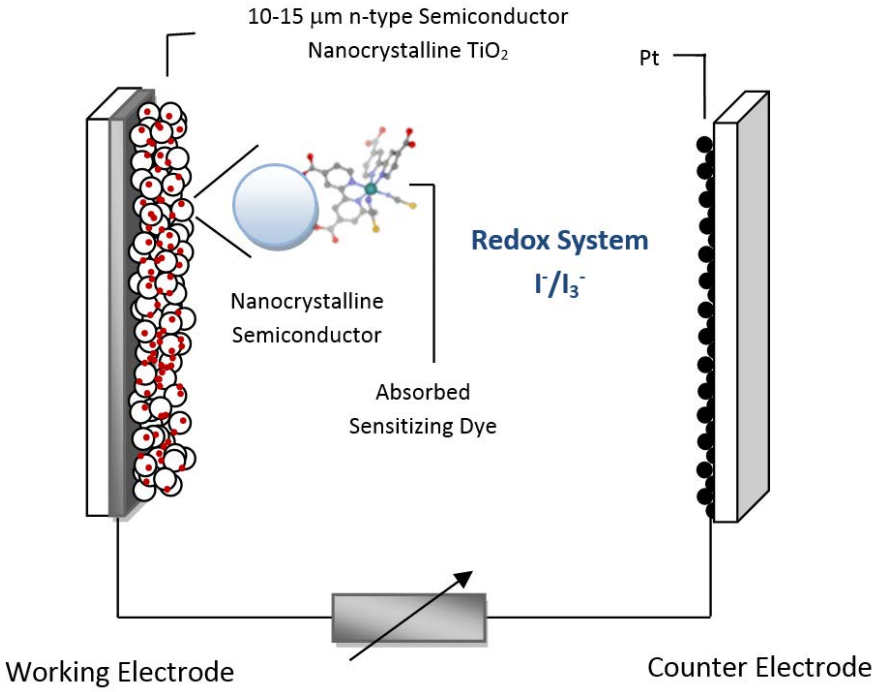

Figure 2.1 *Dye sensitized solar cells schematic illustrations.*

To sustain power regeneration on DSSCs systems, redox couple (iodide/tri-iodide) electrolyte in organic solvent is needed. Electron regeneration takes place from counter electrode back to the oxidized dye (hole) created after the photo excitation of the dye. The counter electrode is typically made by FTO sputtered with platinum or thin layer of carbon for low cost cells. To control gap between working and counter electrodes a spacer is placed. It also functions to determine volume of the electrolyte. Without spacer, direct contact between working electrode and counter electrode will lead to short-circuit or failure of the system.

2.3 Working principle of DSSCs

DSSCs like others type of solar cells is functioning to directly convert photon into electricity. The main process of DSSCs can be divided into three basic steps which

are light absorption, charge separations and charge collections. For more clear view about these three processes see Figure 2.2. First process is light absorption, i.e. dye molecules are photoexcited to form Dye* (Eq. 2.1).

$$Dye + hv \rightarrow Dye^{*} \text{ (Photoexcitation)} \quad (2.1)$$

The photo-excited dye molecules can decay back to the ground state (Eq. 2.2) or inject the electron into TiO_2 conduction band creating the oxidized dye molecules (dye cation or hole) (Eq. 2.3).

$$Dye^{*} \rightarrow \text{Dye} + hv' \ (emission) \quad (2.2)$$

$$Dye^{*} + \text{TiO}_2 \rightarrow Dye^{*} + \ \text{TiO}_2(e^{-})(TiO_2 \ charge \ injection) \quad (2.3)$$

Charge separation takes place at the semiconductor/dye/electrolyte interface when electron is located in TiO_2 conduction band and hole is located on the oxidized dye molecules. The injected electrons percolate through porous nanocrystalline TiO_2 to the conductive glass where charge collection occurs. Injected electron travels through TiO_2 interface flow to external circuit and collected at the counter electrode. At counter electrode, electrons are rapidly transferred to triiodide ion in electrolyte changing I_3^- into iodide (Eq. 2.4). The sequence gets finally closed by reduction of the oxidized dye to the ground state using iodide ion (Eq. 2.5).

$$I_3^- + 2e^- \rightarrow 3I^- \ (regeneration \ of \ I^-) \quad (2.4)$$

$$2Dye^{*} + 3I^- \rightarrow 2\text{Dye} + I_3^- \ (regeneration \ of \ Dye) \quad (2.5)$$

Redox reaction in equation 2.4 and 2.5 has to be unmistakably understood. Triiodide ions diffuse to counter electrode to receive electron and are converted into iodide ion. Iodide ion then returns back to filling the hole of oxidized dyes. Charge recombination takes place between electrons in TiO_2 oxidized dye leading to any photocurrent (Eq. 2.6).

$$Dye^{*} + \ e^{-}(\text{TiO}_2) \rightarrow Dye \ (recombination) \quad (2.6)$$

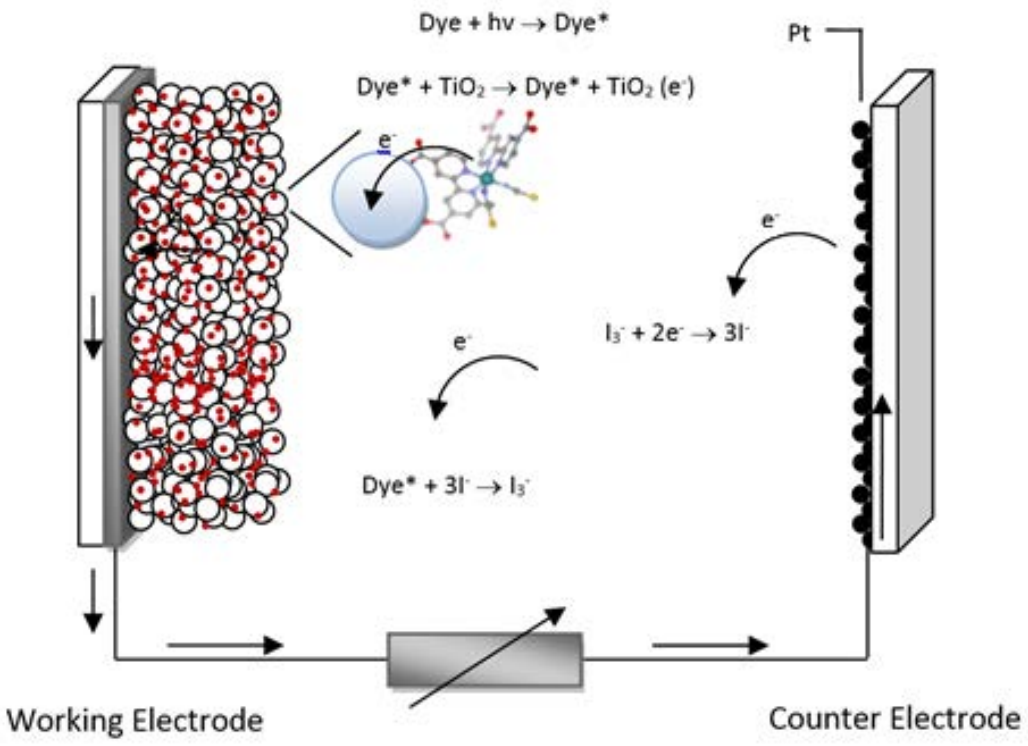

Figure 2.2 *Electron transport process in DSSCs.*

2.4 Component of DSSCs

2.4.1 Working Electrode

A. Substrates for DSSCs

DSSCs consist of two TCO substrates. TCO should be highly transparent in the visible region and maintain low sheet resistance after 450-500 ^{O}C for TiO_2 calcination. The sheet resistance commonly used as TCO is 5-15 Ω/square. The cost of TCO is nearly a quarter of total cost of the solar cell. Conductive oxide layer can be deposited in various types of substrates like plastic coated with conductive layer, and this makes make DSSCs lightweight and flexible. However, Plastics substrates are limited to low temperature process and its sheet resistance is relatively high (60 Ω/square for ITO-PET). Another

alternative is thin metal sheet or foils such as titanium or stainless steel. These metal substrates have higher temperature tolerance.

B. Semiconductors for photo-electrode

Working electrode also known as photo anode of the DSSCs consists of *n*-type semiconductor material. Due to the variety in band gap of the semiconductors, care must be taken for the thoughtful combination of semiconductor band gap and light absorption edge. Band gap energy, Eg, and threshold wavelength, λg, relationship between bandgap energy (Eg) and threshold wavelength is given by equation 2.7.

$$\lambda g = 1240/Eg \text{ (eV)} \qquad (2.7)$$

Wide band gap semiconductor with Eg > 3 are highly desired to make the stable and efficient DSSCs. The most widely used semiconductor material in the DSSCs research community is anatase form of titanium dioxide (TiO_2). It is abundantly available material, non-toxic and widely used in paint, sunscreens and food with the band gap and an absorption edge (~390 nm) make the TiO_2 the most useful *n*-type material. Apart from the TiO_2, other *n*-type wide gap semiconducting materials such as zinc oxide (ZnO)[44,45], tin dioxide (SnO_2)[46,47], and tungsten oxide (WO_3)[48,49] have also been used for the preparation of DSSCs.

Doctor-blade, screen printing and spray methods are most widely used techniques for coating TCO glass with nanoparticle based mesoporous TiO_2. Metal masks are used as a pattern on the top of transparent conductive glass. Suitable thickness of the nanoporous TiO_2 layer depends on the nature of the paste, its particle size and viscosity. Most suitable thickness of nanoporous TiO_2 layer for DSSCs has been found to be less than 15 μm. In order to make inter-particle connectivity or necking of TiO_2 layer, its calcination at high temperatures about 450-500ºC is required. Highly porous TiO_2 sizes are about 20-30 nm in diameters for light absorber, 200-400 nm for scattering

layers and 10-18 nm for transparent applications. In 10 μm thickness of TiO_2, 50-70 % porosity is appropriate for high efficiency DSSCs.

2.4.2 Sensitizing Dye

Dye plays a very important role in DSSCs. It makes DSSCs essentially different from most of the solar cells. In the conservative solar cell, light absorber is the semiconducting material itself while in DSSCs light absorption is achieved by additional dye molecules anchored on the semiconducting surface. This process is analogous with the phenomenon of natural photosynthesis. Research on sensitizing dyes is the one of main concerns in this field. Thousands of dyes have been intensively studied as prospective candidates to boost efficiency. Designing a dye requires several criteria. Highest occupied molecular orbital (HOMO) and Lowest unoccupied molecular orbitals (LUMO) of dye should match with the energy level of photo anode semiconductor and redox couple used to ensure optimum electron injection and dye regeneration. It also should have good chemical and thermal stability, good solubility in organic solvent and appropriate anchoring ligand.

The role of the dye in DSSC is a molecular electron pump. It absorbs light and pushes an electron into the semiconductor, and then, accepts an electron from the redox couple in the electrolyte. Ruthenium (Ru) based dyes attached on TiO_2 are still the preferred choice for achieving the best performance till date. In 1993, Nazeeruddin and co-worker are the pioneer in Ru-type dyes. They introduced the N3 dye or usually called "red" dye, at that time and could reach 10% of efficiency. Later N719[41] and 749 "black" dye from the same group was introduced with efficiency above 10%. Now, these three dyes become benchmark for developing others dyes or components in DSSCs. Ru dye with longer alkyl chain coded Z-907 was also proposed to counter instability problem due to water content on oxide layers[50].

Another important factor in designing a dye is anchoring groups. Ru-based dyes (N3, N719 and Black dye) showing high performance use carboxylic group (-COOH) to

attach on TiO_2 surface. Anchoring method without inserting carboxylic group is also intensively studied since inserting COOH ring is not easy. In chapter 4, attaching dye without conventional anchoring groups is discussed.

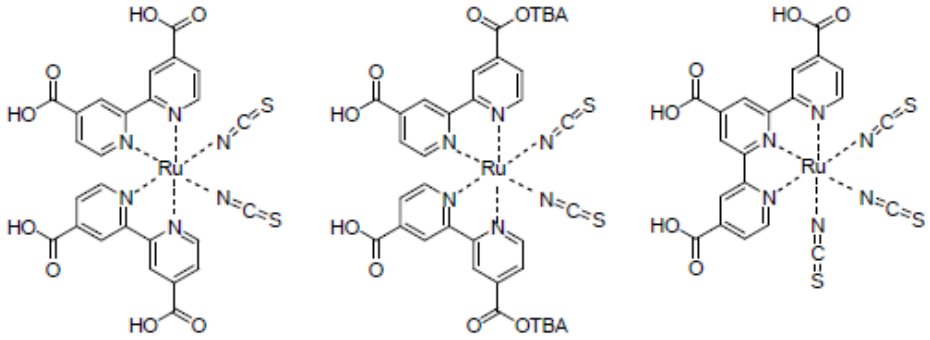

Figure 2.3 *Structure of sensitizing dye N3 (left), N719 (middle) and Black dye (right).*

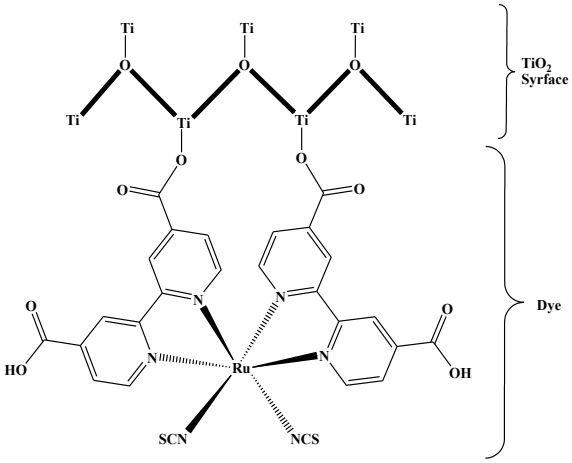

Figure 2.4 *Anchoring of dye on TiO_2 nanoparticle through ester linkage.*

As mentioned before, Ruthenium based sensitizer is expensive and difficult to synthesize. Organic dye is one of alternatives to Ru based dyes. Remarkable photovoltaic performance with 8-10% efficiency has been reported[51-53]. The concern for the metal free organic dyes lies in the fact that they do not use rare metals and that their light absorption property can be synthetically tailored. Organic dyes usually have higher

extinction coefficient, resulting into narrow absorption bands as compared to metal based dyes. High extinction coefficients of organic dyes allowing us to fabricate DSSCs with thinner photo anode while the light harvesting.

In order to enhance DSSCs efficiency, panchromatic photon harvesting from visible to near infra-red (NIR) region is highly required for enhancing the PCE. Phthalocyanines have intense light absorption and high thermal stability. This makes them one of the potential candidates amongst the NIR sensitizers[54-57]. Details about phthalocyanine dyes will be deliberated in Chapter 4.

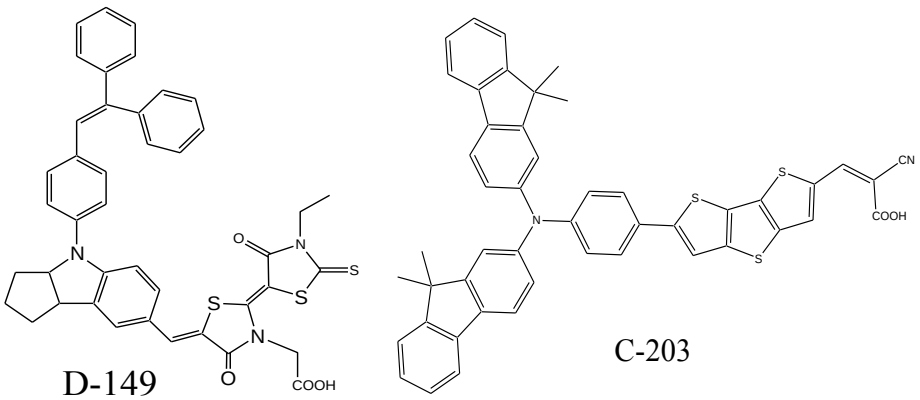

Figure 2.5 *Structure of the some efficient organic dye*

2. 4. 3 Redox Mediators

Redox mediators enable the charge transport between working electrode and counter electrode. Electrons are collected at counter electrode and distribute them to hole on oxidized dye. Redox mediators for liquid DSSCs also known as electrolyte consist of redox couple iodide (I^-) and triiodide (I_3^-) in solvent such as acetonitrile. I^- concentration is usually a few millimolar and that of I_3^- is ten times higher. Since I^-/I_3^- absorb visible light (in 360 nm wavelength), they are better combine with low-viscosity solvent such

as acetonitrile in order to keep their concentrations low. Although I^-/I_3^- electrolyte with acetonitrile already gives high efficiency, but there are some demerit such as corrosiveness, leakages, and low boiling point. New type redox mediators are needed to fulfill the requirement of industrial standard for future mass production.

Another liquid type electrolyte that gain more attentions is Cobalt complex (Co(II)/Co(III)) having deeper HOMO energy level than I^-/I_3^- redox couple. This allows to get higher open circuit voltage (Voc)[58,59]. Cobalt electrolyte combine with porphyrin dye has realizes DSSC`s highest efficiency of 13% with more than 0.9 V of Voc. Ionic liquid (IL) also has been proposed by some researchers including our group[60-62] which have many advantages over liquid electrolyte, for instance, chemical stability and high thermal stability. However, IL still need more improvement on issues such as high viscosity, mass transport limitation etc.

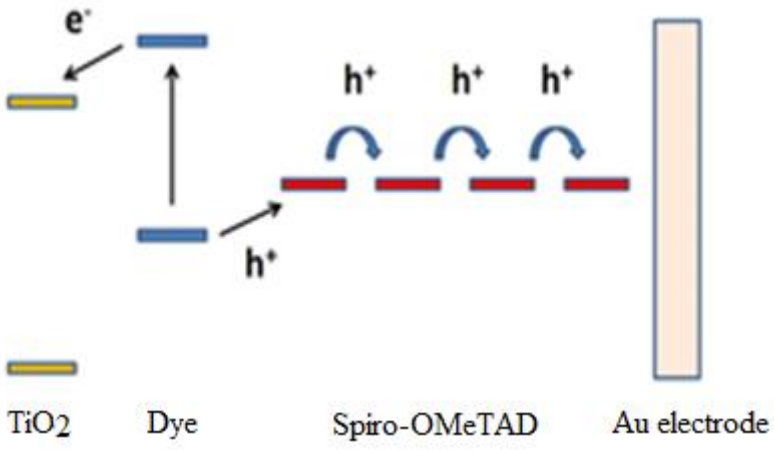

Figure 2.6 *Charge balancing in Solid State DSSCs*

For solid state DSSCs, redox mediator are not employed. Instead of this, Hole transport material (HTM). HTMs are contacted on porous TiO_2/dye layer. Electron transport in solid state is directly from dye to the hole transporter. This electrons diffuse by hopping in the HTM layer from counter electrode back to oxidized dye (see Figure 2.6). The most well-known HTM is spiro-OMeTAD molecule (2,2',7,7'-tetrakis(N,N-di-p-methaoxypheny-amine)-9,9'-spirobi-fluorene) proposed by M.Grätzel[63] in 2005.

The advantages using Spiro-OMeTAD as redox mediator are higher open circuit voltage (due to deeper HOMO). However, Spiro-OMeTAD also have limitation on charge carrier mobility, higher price and poor pore filling. The future challenge is to find best redox mediator to increase stability and enhance DSSCs performance.

2. 4. 4 Counter Electrode

Widely used material for counter electrode in DSSCs is Platinum (Pt). In earlier publication, Pt counter electrode was prepared using thermal deposition of H_2PtCl_6[55]. In recent years, Pt can be prepared using Paste. Solaronix made Pt-catalyst T/SP, a transparent and activated Pt, prepared with screen printing method. At present, a layer of platinum coated on TCO substrate is commonly used as counter electrode in DSSCs. CE is usually made by coating a few $\mu g/cm^2$ of Platinum (Pt) on FTO glass. Pt layer preparation is done by sputtering process.

The other alternative materials as counter electrode are carbon black[64,65], carbon nanotubes[66,67] and conductive polymer PEDOT-PSS[68,69]. Graphene is another candidate for the counter electrode.

2.5 Main problems for decrease in the DSSCs efficiency

Electron transport of DSSCs systems is schematically illustrated in Figure 2.7. Among them, charge recombination process should be suppressed. After electrons are injected from dyes to TiO_2 conduction band, electron will diffuse in TiO_2 layer to conductive glass. Sometime electrons get trapped or recombine with hole on sensitizing dye. Charge recombination between electrons in TiO2 and oxidized sensitizer, and that between electrons in TiO_2 and I_3^- have to be suppressed. In order to do that, fabrication of trap free material and interface is needed.

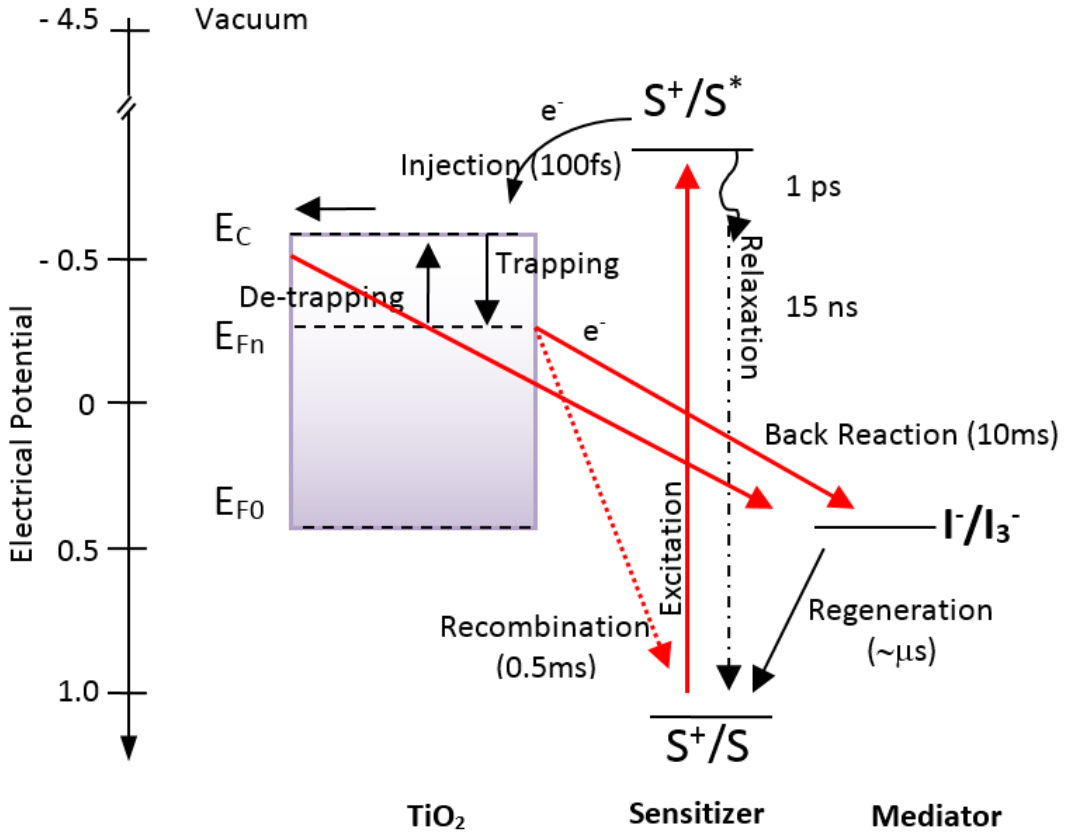

Figure 2.7 Illustration of DSSCs electron transport process

2.6 References to chapter 2

1) A.E Becquerel, *Comptes Rendues Acad. Sci.,* **9**, 145, (1839).

2) W. West, *Photogr. Sci. Eng.*, **18**, 35, (1974).

3) J. Moser, *Monatsch. Chem.*, **8**, 373, (1887).

4) A. Fujishima, T. Watanabe, O. Tatsuoki, K. Honda, *Chem. Lett.*, **4**, 13, (1975).

5) H. Tsubomura, M. Matsumura, Y. Noyamaura, T. Amamyiya, *Nature*, **261**, 402, (1976).

6) J. DeSilvestro, M. Grätzel, L. Kavan, J. Moser, J. Augustynski, *J. Am. Chem. Soc.*, **107**, 2988, (1985).

7) B. O'Regan and M. Grätzel, *Nature*, **353**, 737–740, (1991).

8) C.J. Barb, F. Arendse, P. Comte, M. Jirousek, F. Lenzmann, V. Shklover and M. Graetzel, *J. Am. Cer. Soc.*, **80**, 12, 3157-3171, (1997).

9) Md. K. Nazeeruddin, R. H.-Baker, P. Liska and M. Grätzel, *J. Phys. Chem. B*., **107**, 34, 8981-8987, (2003).

10) M.K. Nazeeruddin, F.D. Angelis, S. Fantacci, A. Selloni, G. Viscardi, P. Liska, S. Ito, B. Takeru and M. Grätzel, *J. Am. Chem. Soc*., **127**, 48, 16835-16847, (2005).

11) M.K. Nazeeruddin, P. Pechy, T. Renouard, S. M. Zakeeruddin, R. H.-Baker, P. Comte, P. Liska, L. Cevey, E. Costa, V. Shklover, L. Spiccia, G. B. Deacon, C.A. Bignozzi and M. Grätzel, *J. Am. Chem. Soc*., **123**, 8, 1613-1624, (2001).

12) F. Gao, Y. Wang, D. Shi, J. Zhang, M. Wang, X. Jing, R. Humphry-Backer, P. Wang, S.M. Zakeeruddin and M. Grätzel, *J. Am. Chem. Soc.*, **130**, 10720-10728, (2008).

13) F. Gao, Y. Wang, J. Zhang, D. Shi, M. Wang, R. Humphry-Backer, P. Wang, S.M. Zakeeruddin and M. Grätzel, *Chem. Commun*., 2635-2637, (2008).

14) M. Grätzel, "The Advent of Mesoscopic Solar Cells", International Symposium on Innovative Solar Cells 2009, Tokyo, Japan, (2009).

15) S. Mathew, A. Yella, P. Gao, R. Humphry-Baker, B.F. Curchod, N. Ashari-Astani and M. Grätzel, *Nature chemistry*, **6***,* 3, 242-247, (2014).

16) F. Huang, D. Chen, Q. Li, R.A. Caruso and Y.B. Cheng, *Applied Physics Letters*, **100***,* 12, 123102, (2012).

17) V.D. Dao, C.Q. Tran, S.H. Ko and H.S. Choi, *Journal of Materials Chemistry A*, **1***,* 14, 4436-4443, (2013).

18) Y. Peng, J. Zhong, K. Wang, B. Xue and Y.B. Cheng, *Nano Energy*, **2***,* 2, 235-240, (2013).

19) J. Usagawa, T. Kogo, K. Sadamasu, S.S. Pandey, Y. Ogomi and S. Hayase, *Journal of Photonics for Energy*, **2***,* 1, 021011-1, (2012).

20) J. Usagawa, B.W. Park, Y. Ogomi, S.S. Pandey and S. Hayase, *MRS Proceedings,* **1435**, pp. mrss12-1435, (2013).

21) K. Uzaki, S. S. Pandey and S. Hayase, *J. Photochem. Photobiol. A.*, **216**, 104, (2010).

22) K. Uzaki, S. S. Pandey, Y. Ogomi and S. Hayase, *Jap. J. Appl. Phys.*, **49**, 082301, (2010).

23) A.K. Baranwal, T. Shiki, Y. Ogomi, S.S. Pandey, T. Ma and S. Hayase, *RSC Advances*, **4***,* 88, 47735-47742, (2014).

24) P. Qin, H, Zhu, T. Edvinsson, G.Boschloo, A. Hagfeldt and L. Sun, *J.Am.Chem.Soc.*, **130**, 8570-8571, (2008).

25) H. Choi, C. Baik, S.O. Kang, J. Ko, M.-S. Kang, Md.K. Nazeeruddin and M. Grätzel, *Angew. Chem.*, 333-336, (2008).

26) D. Kuang, S. Uchida, R. Humphry-Backer, S.M. Zakeerudding and M. Grätzel, *Angew.Chem.Int.Ed.*, **47**, 1923-1927, (2008).

27) B. Lim, G.Y. Margulis, J.H. Yum, E.L. Unger, B.E. Hardin, M. Grätzel and A. Sellinger, *Organic letters*, **15***,* 4, 784-787, (2013).

28) J. Park, G. Viscardi, C. Barolo and N. Barbero, *CHIMIA International Journal for Chemistry*, **67**, 3, 129-135, (2013).

29) J.H. Yum, E. Baranoff, S. Wenger, M.K. Nazeeruddin and M. Grätzel, *Energy & Environmental Science*, **4***,* 3, 842-857, (2011).

30) C. Magistris, S. Martiniani, N. Barbero, J. Park, C. Benzi, A. Anderson and B. O'Regan, *Renewable Energy*, **60**, 672-678, (2013).

31) H.C. Ki, H.Y. Jung, S.H. Kim, D.G. Kim, T.U. Kim and H.J. Kim, *SPIE Advanced Lithography,* 90521S-90521S, (2014)

32) N. Vyas, D.A. Wragg, C. Charbonneau, M. Carnie and T.M. Watson, *ECS Transactions*, **53**, 24, 39-46, (2013).

33) M.G. Choi and Y.M. Sung, *Optical Materials*, **36**, 8, 1430-1435, (2014).

34) M. Yanagida, Y. Numata, K. Yoshimatsu, M. Ochiai, H. Naito and L. Han, *Electrochimica Acta*, **87**, 309-316, (2013).

35) M. Molla, N. Mizukoshi, H. Furukawa, Y. Ogomi, S.S. Pandey, T. Ma and S. Hayase, *Progress in Photovoltaics: Research and Applications* (2014).

36) W.H. Howie, F. Claeyssens, H. Miura and L.M Peter, *J.Am.Chem.Soc.*, **130**, 1367-1375, (2008).

37) L. Schmidt-Mende and M. Grätzel, *Thin Solid Film,* **500**, 296-301, (2006).

38) P. Wang, S.M. Zakeeruddin, J.E. Moser, M.K. Nazeeruddin, T. Sekiguchi and M. Grätzel, *Nature*, **2**, 402-407, (2003).

39) E. Diau, *227th ECS Meeting,* (2015).

40) C.T. Weisspfennig, D.J. Hollman, C. Menelaou, S.D. Stranks, H.J. Joyce, M.B. Johnston and L.M. Herz, *Advanced Functional Materials*, **24**, 5, 668-677, (2014).

41) J.K Koh, J. Kim, B. Kim, J.H. Kim and E. Kim, *Advanced Materials*, ***23***, 14, 1641-1646, (2011).

42) GCell by G24 Power for DSSCs application, http://gcell.com/product/graetzel-solar-backpack, Retrieved 30 April 2015.

43) GCell by G24 Power for DSSCs application, http://gcell.com/product/solar-powered-keyboard-folio-for-ipad-air-2, Retrieved 30 April 2015.

44) K. Keis, E. Magnusson, H. Lindstrom, S. E. Lindquist, A. Hagfeldt, *Sol. Energy Mater. Sol. Cells, **73***, 51, (2002).

45) G. Chen, K. Zheng, X. Mo, D. Sun, Q. Meng and G. Chen, *Materials Letters*, **64**, 1336-1339, (2010).

46) A. N. M. Green, E. Palomares, S. A. Haque, J. M. Kroon, J. R. Durrant, *J. Phys. Chem. B, **109***, 12525, (2005).

47) H.-M. Kwon, D.-W. Han, D.-J. Kwak and Y.-M. Sung, *Current Applied Physics*, **10**, S172-S175, (2010).

48) P. Qin, H. J. Zhu, T. Edvinsson, G. Boschloo, A. Hagfeldt, L. C. Sun, *J. Am. Chem. Soc.,* **130**, 8570, (2008).

49) Y. Saito, S. Uchida, T. Kubo and H. Segawa, *Thin Solid Films*, **518**, 3033-3036, (2010)

50) P. Wang, S.M. Zakeeruddin, I. Exnar and M. Grätzel, *Chemical Communications*, **24**, 2972-2973, (2002).

51) S. Hwang, J.H. Lee, C. Park, H. Lee, C. Kim, C. Park, M.-H. Lee, W. Lee, J. Park, K. Kim, N.-G. Park and C. Kim, *Chem. Commun.,* 4887-4889, (2007).

52) K. Pei, Y. Wu, W. Wu, Q. Zhang, B. Chen, H. Tian and W. Zhu, *Chemistry-A European Journal*, **18**, 26, 8190-8200, (2012).

53) Y. Wu, M. Marszalek, S.M. Zakeeruddin, Q. Zhang, H. Tian and M. Grätzel, *Energy & Environmental Science*, **5***,* 8, 8261-8272, (2012).

54) S. Mori, M. Nagata, Y. Nakahata, K. Yasuta, R. Goto, M. Kimura and M. Taya, *Journal of the American Chemical Society*, **132**, 12, 4054-4055, (2010).

55) S. Eu, T. Katoh, T. Umeyama, Y. Matano and H. Imahori, *Dalton Transactions*, **40**, 5476-5483, (2008).

56) T. Komori and Y. Amao, *Journal of Porphyrins and Phthalocyanines*, *7*, 02, 131-136, (2003).

57) T. Ikeuchi, H. Nomoto, N. Masaki, M.J. Griffith, S. Mori and M. Kimura, *Chemical Communications*, **50***,* 16, 1941-1943, (2014).

58) M.K. Kashif, J.C. Axelson, N.W. Duffy, C.M. Forsyth, C.J. Chang, J.R. Long and U. Bach, *Journal of the American Chemical Society*, **134**, 40, 16646-16653, (2012).

59) E. Mosconi, J.H. Yum, F. Kessler, C.J.G. García, C. Zuccaccia, A. Cinti and F. De Angelis, *Journal of the American Chemical Society*, **134**, 47, 19438-19453, (2012).

60) Y. Shibata, T. Kato, T. Kado, R. Shiratuchi, W. Takashima, K. Kaneto and S. Hayase, *Chem.Communication.*, **21**, 2730-2731, (2003).

61) M. Gorlov and L. Kloo, *Dalton Transactions*, **20**, 2655-2666, (2008).

62) S. Sakaguchi, H. Ueki, T. Kato, T. Kado, R. Shiratuchi, W. Takashima, K. Kaneto and S. Hayase, *Journal of Photochemistry and Photobiology A: Chemistry*, **164**, 1, 117-122, (2004).

63) M. Grätzel, *MRS bulletin*, *30*, 01, 23-27, (2005).

64) P. Li, J. Wu, J. Lin, M. Huang, Y. Huang and Q. Li, *Solar Energy*, **83***,* 6, 845-849, (2009).

65) M. Chen, L.L. Shao, X. Qian, L. Liu, T.Z. Ren and Z.Y. Yuan, *Chemical Engineering Journal*, **256**, 23-31, (2014).

66) D. Sebastián, V. Baglio, M. Girolamo, R. Moliner, M.J. Lazaro and A.S. Arico, *Journal of Power Sources*, **250**, 242-249, (2014).

67) B. He, Q. Tang, J. Luo, Q. Li, X. Chen and H. Cai, *Journal of Power Sources*, **256**, 170-177, (2014).

68) G. Yue, X. Ma, Q. Jiang, F. Tan, J. Wu, C. Chen, F. Li and Q. Li, *Electrochimica Acta*, **142**, 68-75, (2014).

69) B.W. Park, M. Pazoki, K. Aitola, S. Jeong, E.M. Johansson, A. Hagfeldt and G. Boschloo, *ACS applied materials & interfaces*, **6**, 3, 2074-2079, (2014).

Chapter 3 Experiment and Measurements

3.1 Device Characterizations

3.1.1 I-V characteristics

As mentioned in the introduction, DSSCs and all other kinds of solar cells convert solar irradiance directly into electricity. The characteristics of a typical current-voltage (I-V) curve at certain temperature and illumination have been shown in Figure 3.1.

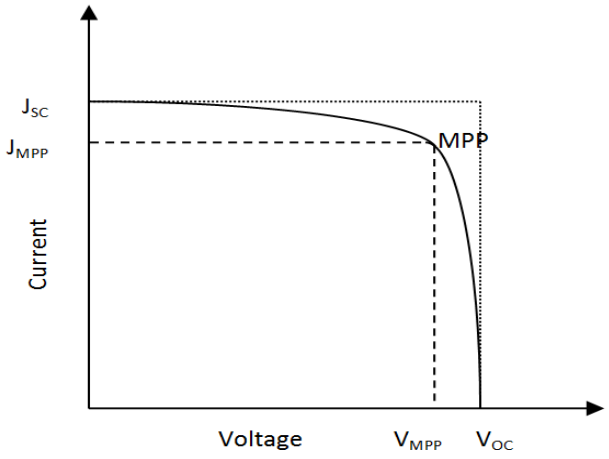

Figure 3.1 *A typical I-V Curve for a solar cell*

Short circuit current density (Jsc) is the maximum current under illumination, while at the open circuit voltage (Voc) there is no flow of the current. Point where maximum power obtained is known as the maximum power point (MPP). Another important parameter for DSSCs is fill factor (FF) and can be written as equation below.

$$FF = \frac{V_{MPP} \cdot J_{MPP}}{V_{OC} \cdot J_{SC}} \qquad (3.1)$$

Using fill factor, the maximum power can be written as,

$$P_{MAX} = V_{OC} \cdot J_{SC} \cdot FF \qquad (3.2)$$

With I-V characteristic curve, DSSCs can be compared with each other based on open circuit voltage, short circuit current density and fill factors. The efficiency of solar cells depends on temperature and illumination. Therefore it is needed to make standards for measurement condition. Efficiency is given by equation 3.3.

$$\eta = \frac{P_{MAX}}{P_{light}} \quad (3.3)$$

P_{MAX}: maximum power, P_{light}: power of incident light.

A. Short Circuit current density (Jsc)

Jsc is expressed by Eq. 3.4,

$$J_{sc} = \frac{hc}{q} \int \frac{Psun(\lambda) \cdot EQE(\lambda)}{\lambda} d\lambda \quad (3.4)$$

where, *h* is the Planck's constant, *c* the speed of light, *q* the elementary charge, and P_{sun} the solar irradiance.

B. Open circuit voltage (Voc)

As explained before, Voc is one of the main factors to control the photovoltaic efficiency of dye sensitized solar cells. There are a number of sensitizing dyes exhibiting very high Jsc but the overall power conversion efficiency is low which could be attributed to its low Voc. Theoretically, Voc is determined by the energy gap between *n*-type semiconductor conduction band and redox potential of the redox couple under investigation. Since in this thesis TiO_2 is employed as *n*-type semiconductor having conduction band edge at -4.0 eV and using iodide/triiodide (-4.9 eV) as the redox mediator, the maximum theoretical open circuit voltage should be 0.9 V as shown in the Figure 3.2.

The actual Voc in DSSCs is generally lower than 0.9V due to the recombination losses occurring in the system.

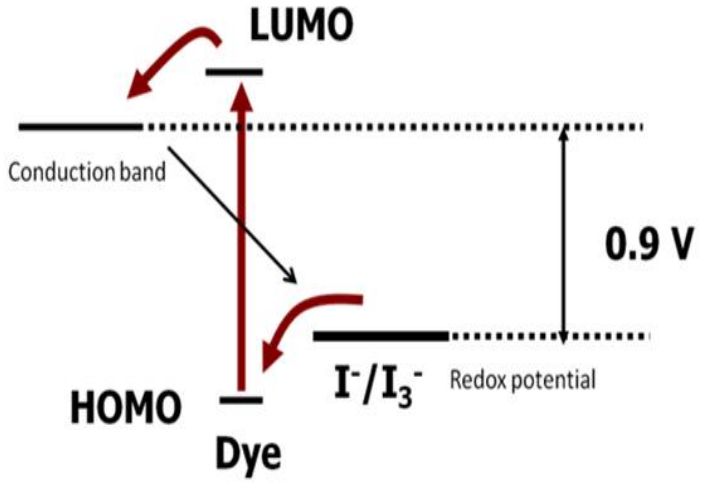

Figure 3.2 Energy band diagram for DSSC to define the Voc

C. Fill Factor (FF)

Fill factor means the squareness of the I-V curve. FF is directly affected by carrier mobility, balanced charge transport and planar polymer structure for molecular packing in the organic photovoltaic devices. In addition, the active layer/cathode interface can play a major role in determining fill factor.

The shape of FF is also important. It is dependent on series and shunt resistances. The influence of increasing series resistance, Rs, and decreasing shunt resistance, Rsh on the current-voltage characteristic will affect the FF. To gain high fill factors, Rs has to be as small as possible while Rsh needs to be as high as possible.

3.1.2 Incident Photon-to-current efficiency

Incident photon-to-current efficiency (IPCE) or Quantum efficiency (QE) show the effectiveness of device converting the incident light or photon into electrical energy at certain wavelength. There are two types of QE; Internal Quantum Efficiency (IQE) and External Quantum Efficiency (EQE). IQE is the ratio of the number of collected carriers devided by the number of all absorbed

photon. EQE is the ratio of the number of collected carrier devided by the number of incident photon. IQE is always higher than EQE. In order to measure IQE, one first gets EQE value and then measures its transmission and reflectance and then finally combines them to get the IQE. Fig. 3.3 show the IPCE curves for DSSC.

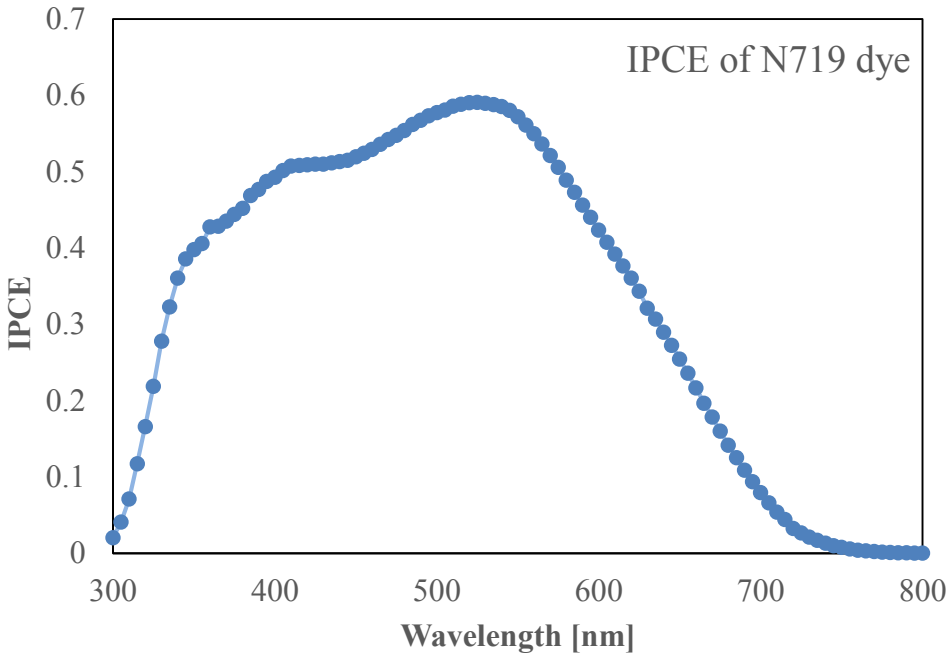

Figure 3.3 *Example of IPCE spectrum of N719 dye.*

IPCE measurement is also beneficial for studying degradation properties of devices. The change of the IPCE curve may indicate degradation of specific layers.

3.2 Solar simulator and spectro-radiometer

The spectrum at the Earth's surface horizontal with sun zenit is called AM1 (Air Mass 1) as shown in Fig. 3.4. AM 1.5 spectrum (1kW/m^2) is used for the standard light for measuring PV performance. The AM1.5 is defined as shown in Fig. 3.4. In order to simulate AM1.5 solar spectrum, the solar simulator is calibrated with LS-100 spectro-radiometer. The intensity of the lamp and the mounting position of the cell are set by

matching these two graphs. This calibration is very important factor to eliminate over estimation and miscalculation of devices photovoltaic performance.

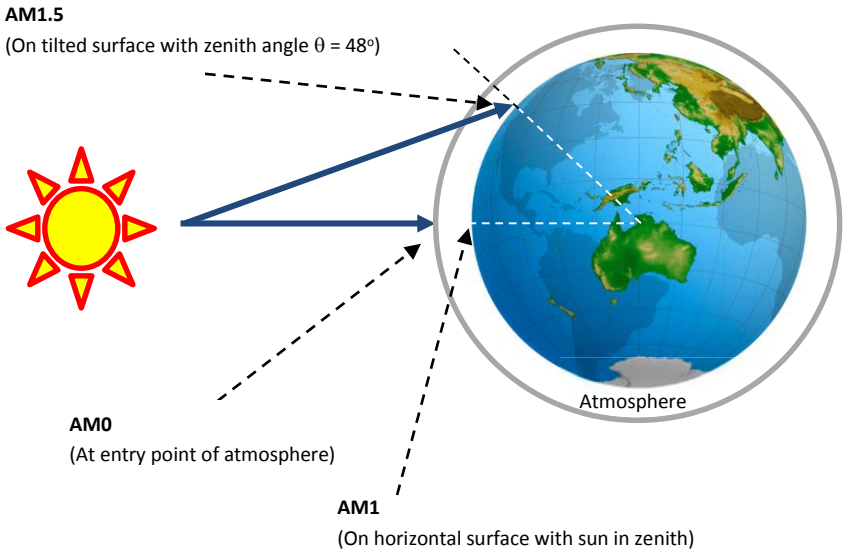

Figure 3.4 *Air Mass represents on earth.*

3.3 Thickness Measurement

Dektak 6M Stylus profiler from Veeco was used to measure thickness profile. The thickness was measured by moving the sample under a diamond-tipped stylus. The length, speed and stylus force pressure are adjustable via user-programed. The stylus is mechanically coupled to the core of an LVDT (Linear Variable Differential Transformer). As the stage moves the sample, the stylus runs over the sample surface. Surface variations cause the stylus to move vertically. Electrical signals corresponding to stylus movement are produced as the core position of the LVDT changes. The LVDT scales an AC reference signal relative to the position change, which in turn is conditioned and transformed to a digital format through a high precision, integrating, analog-to-digital converter. The digitized signals from printing

a single scan are stored in computer memory for display, manipulation, measurement, and printing.

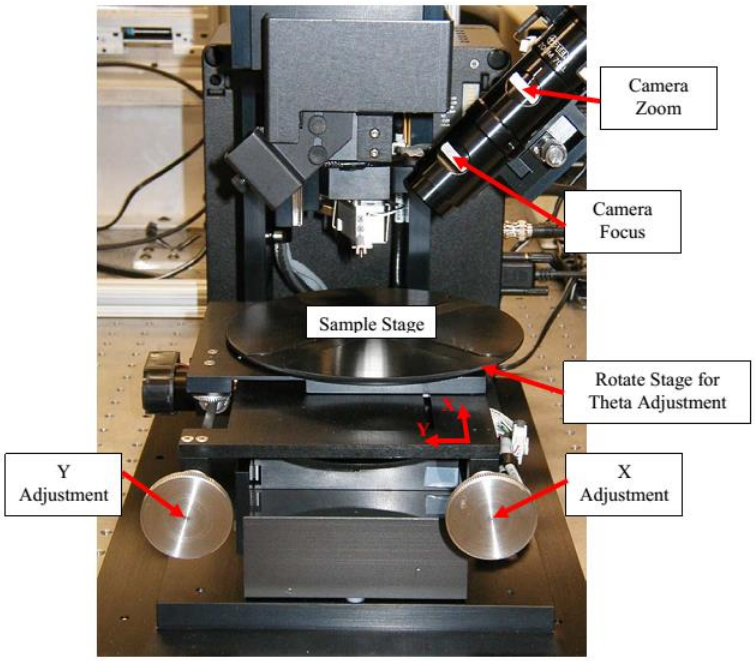

Figure 3.5 *Dektak 6M Stylus Profiler*

3.4 UV-Visible spectroscopy

UV-Visible Spectrophotometer is an instrument used to measure absorbance in ultraviolet light (200-400nm) and visible light (400-750nm) wavelength regions. Light sources in UV-Vis spectrometers are deuterium lamp for UV region and tungsten lamp for visible light wavelengths. In UV region, absorbance is measured from transitions of electrons from ground state to excited state when molecule absorbs light energy. Absorbance in visible region is measured directly from electromagnetic spectrum absorptions. The molecule will only absorb a photon which carries sufficient energy which is greater than the band gap of the molecule under investigation.

Using the UV-visible spectrophotometry, it is possible to determine the concentration of desired molecule using well known Beer-Lambert law as shown in Fig. 3.6. This law relates the absorption of light to the properties of the material through which the light is traveling. The Beer-Lambert law determines the absorbance of a solution directly and is proportional to the concentration of absorbing species and the path length. Mathematically it can represented as

$$A = -\log\left(\frac{I_o}{I}\right) = - \varepsilon cL \qquad (3.5)$$

where A is absorbance, I_o is intensity of incident light before entering, I is transmitted intensity after absorption, c is concentration, L is path length through the sample and ε is constant for molar absorptivity. Negative (-) sign in the equation because of decrease in intensity of the light so the value in always positive.

UV-Vis spectrophotometers can be used to determine the concentration of absorber in solution.

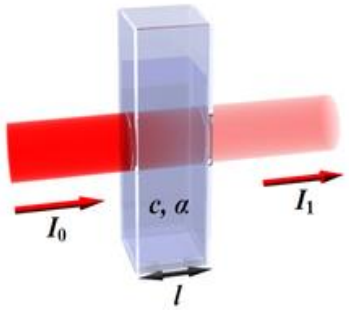

Figure 3.6 *Illustration of light absorption/transmission in UV-Vis spectrophotometer*

3.5 Fluorescence lifetime

As shown in Figure 3.7, the fluorescence lifetime, t, is the time at which the intensity has decayed to 1/e of the original value. The decay of the intensity as a function of time is given by equation below.

$$I_t = \alpha\, e^{-t/\tau} \qquad (3.6)$$

where, I_t is the intensity at time t, α is a normalization term (the pre-exponential factor) and τ is the lifetime. Information of the excited state lifetime of a fluorophore is important for quantitative understandings of numerous fluorescence measurements such as quenching, polarization and fluorescence resonance energy transfer (FRET).

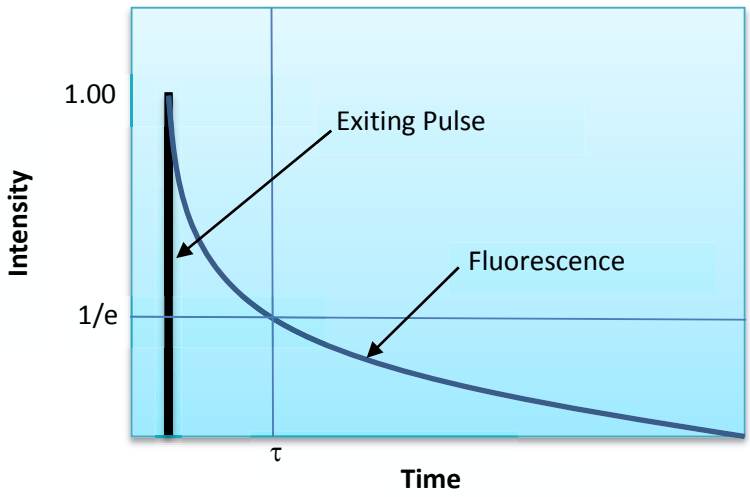

Figure 3.7 *Intensity decay for Fluorescence lifetime*

3.6 Electrochemical impedance spectroscopy

Electrochemical Impedance Spectroscopy (EIS) is a very useful diagnostic tool that can be used to characterize and improve the performance of solar cells. There are three fundamental sources of voltage loss in solar cells: kinetic losses, ohmic losses, and mass transfer losses.

Among other factors, EIS is an experimental technique that can be used to separate and quantify these sources of polarization. The equivalent circuit models a network of resistors, capacitors and inductors. This can extract qualitative and quantitative information regarding the sources of impedance within the cell. EIS is useful for research and development of new materials and electrode structures, as well as for product verification and quality assurance in manufacturing operations. EIS data for electrochemical cells such as solar cells are most often characterized in Nyquist (cole-cole) plot and Bode plots as shown in Figure 3.8. Bode plots refer to

illustration of the impedance magnitude in this case for the real or imaginary components of the impedance and phase angle as a function of frequency.

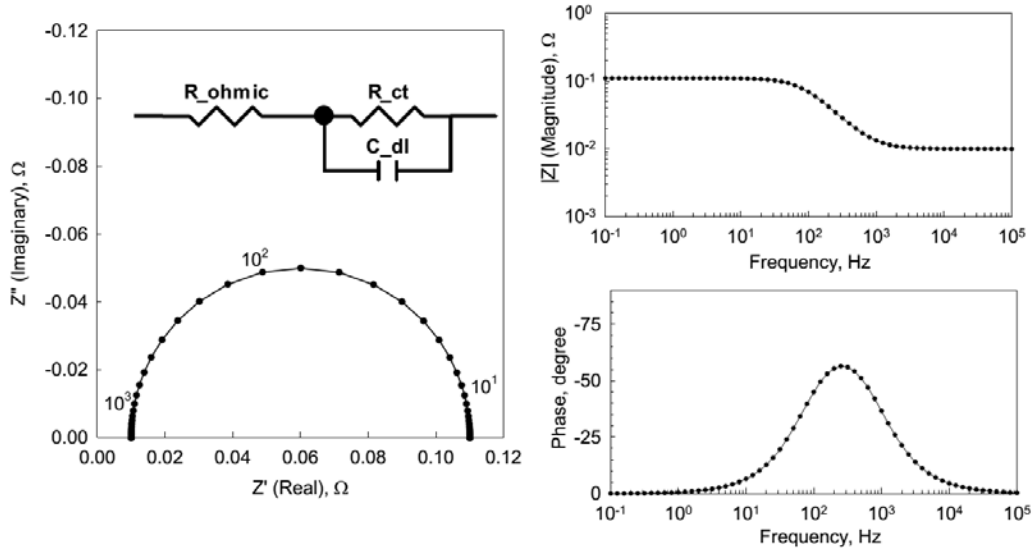

Figure 3.8 *Nyquist plot (left) and Bode plots (right)*

3.7 X-ray Photoelectron Spectroscopy

X-ray photoelectron spectroscopy (XPS) is a surface investigation technique, which is based upon the photoelectric effect. Photoelectric effect concept was proposed by Einstein and received Nobel Prize for this works in 1921. This concept was developed by Kai Seigbahn into useful measurement method, namely for Photoemission as an analytical tool.

Every single atom in the surface has core electron with the representative to binding energy that is theoretically equal to the ionization energy of electron. In order to measure the binding energy, an X-ray beam point towards to the sample. The energy of the X-ray photon is adsorbed completely by the core electron of an atom. However, if the photon energy, h, is high enough, the core electron will then escape from the atom and emit out of the surface. The emitted electron with the kinetic energy of E_k from this process is referred to as the photoelectron. The binding energy (E_b) of the core electron is given by the Einstein relationship:

$$E_b = hv - E_k - \Phi \quad (3.7)$$

where, h is the X-ray photon energy; E_k is the kinetic energy of photoelectron, which can be measured by the energy analyzer; and Φ is the work function induced by the analyzer.

Chapter 4 DSSCs based on axially ligated phosphorus-phthalocyanine dyes

Dye-sensitized solar cells with axially anchored phosphorous-phthalocyanine dyes were fabricated for the first time. Although the phosphorus-phthalocyanine dyes do not have a conventional anchoring group (–COOH), these dyes could be absorbed on a TiO_2 semiconductor surface. After the optimization of energy levels, a 24% incident photon-to-current efficiency (IPCE) was observed at 710 nm with an IPCE curve edge of 800 nm. The efficiency was 2.67%, which was higher than those of previously reported dye-sensitized solar cells with axially anchored phthalocyanine dyes (less than 1%).

4.1 Introduction

Dye-sensitized solar cells (DSSCs) are attracting attention owing to their high efficiency and low cost of production[1)]. The most widely employed dyes in DSSCs are ruthenium (Ru) dyes[2)]. Previous Ru dyes cover only the area of the visible region up to 800 nm. Recently, Segawa and colleagues have reported Ru dyes covering a wide range of wavelengths from 400 to 1000 nm[3)]. Panchromatic photon harvesting from visible-to-near-infrared (NIR) region is ideal; however, dyes with both high incident photon-to-current efficiency (IPCE) in the IR region and high open circuit voltage (Voc) have not yet been realized. Recently, metal-free dyes having nearly quantitative photon harvesting in the visible light region have been reported[4)]. However, NIR dyes with high photoconversion quantum efficiency have not been reported so far. Macrocyclic dyes such as phthalocyanines having intense light absorption are one of the candidates for NIR dyes[5–7)]. Some phthalocyanine derivatives have absorption in IR regions[8)]. In the course of study, we accidentally found that phthalocyanine dyes without conventional anchoring groups such as carboxylic acid are adsorbed on porous titania layers and show photovoltaic properties. Macor et al. have already reported on the carboxylic moiety-free silicon naphthalocyanine NIR dye adsorbed on a nanoporous titania layer, where the dye was linked with the titania surface by Ti–O–Si lingkage, which is substituted at the axial position of the naphthalocyanine ring. The efficiency was about 0.1%[9)].

Recently, we have reported that axially anchored Sn naphthalocyanine was adsorbed on porous tin oxide layers by a Sn–O–Sn bond and showed photovoltaic performance, where electrons are injected from the naphthalocyanine ring to tin oxide through the narrow space between them[10]. The advantage of the axially anchored phthalocyanine on TiO_2 is that symmetrical phthalocyanine derivatives can be used. They can be prepared much more easily than unsymmetrical phthalocyanine derivatives, and a variety of symmetrical cyclic structures can be applied to DSSCs. In this report, the photovoltaic performance of DSSCs with axially anchored phosphorous(III)phthalocyanine (PPc) adsorbed on porous titania layers is described.

4.2 Experimental detail

4.2.1 Materials

A working electrode was fabricated by coating paste containing titania nanoparticles (Solaronix D paste) on a fluorine-doped tin oxide layered glass (FTO glass, Asahi Glass). The sample was baked at 450°C for 30 min to obtain a 12-μm-thick porous titania layer, and was immersed in a 40 mM $TiCl_4$ solution in distilled water for 30 min at 80°C, followed by heating this at 500°C for 30 min. The sample was immersed in a 0.2 mM solution of PPc in ethanol at 60°C to enhance the adsorption of the dye on the porous titania layer.

A Pt-sputtered FTO layered glass working as a counter electrode was coupled with the working electrode using a spacer (Solaronix Meltonix 1170-25F, thickness: 25 μm). Three dyes (PPc-1, PPc-2, and Ref-Pc-1) with a symmetrical ring structure shown in Fig. 4.1 were synthesized by the method described in our earlier publication.[11,12] Electrolyte (E1) was injected into the gap between the two electrodes consisting of 500 mM lithium iodide (LiI), 50 mM iodine (I_2), 600 mM ethylmethylimidazolium dicyanoimide (MeEtIm-DCA), and 580 mM 4-*tert*-butylpyridine (TBP) in acetonitrile.

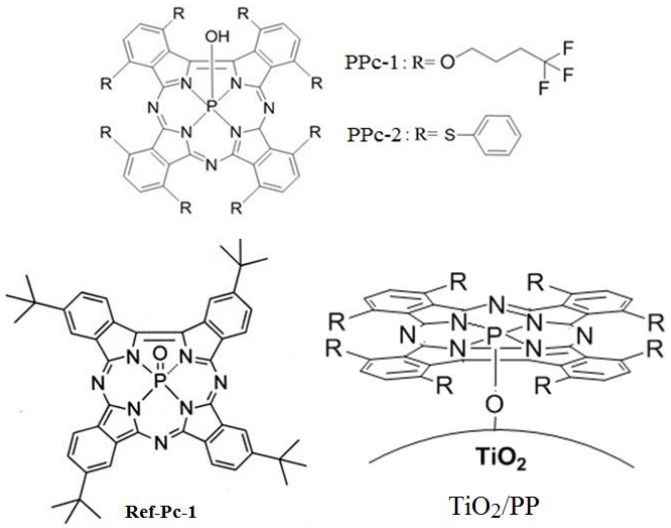

Figure 4.1 *Chemical structures of phosphorous-phthalocyanine dyes and its attachment on nanoporus TiO_2 layer.*

4.2.2 Cell Fabrication and Measurement

A. Working electrode

Figure 4.2 shows photo-electrodes prepared for conventional type DSSCs. FTO glass (Asahi Glass), used as working electrodes, cut with diamond cutter into desired size. FTO glass was cleaned with ultrasonic cleaner in distilled water, isopropanol and acetone for 15 minutes in each process. After drying with blower, FTO glass was cleaned again with UV-Ozone cleaner for 20 minutes. TiO_2 paste (Solaronix D paste) was screen printed into FTO glass using metal mask (thickness: 30µm) and dried in open air for 10 minutes. After drying, FTO coated with TiO_2 was baked at 450^oC for 30 minutes. After cooling down into room temperature, TiO_2 paste was coated and baked again until desired thickness was achieved. In this work, the optimum thickness was 12µm which was measured with Dektak 6M Stylus Profiler.

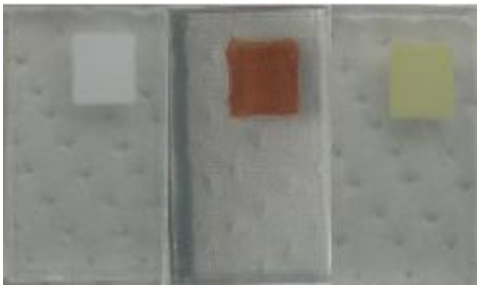

Figure 4.2 *Bare TiO_2 (left), TiO_2 coated PPc-1 (middle) and TiO_2 coated PPc-2 (right).*

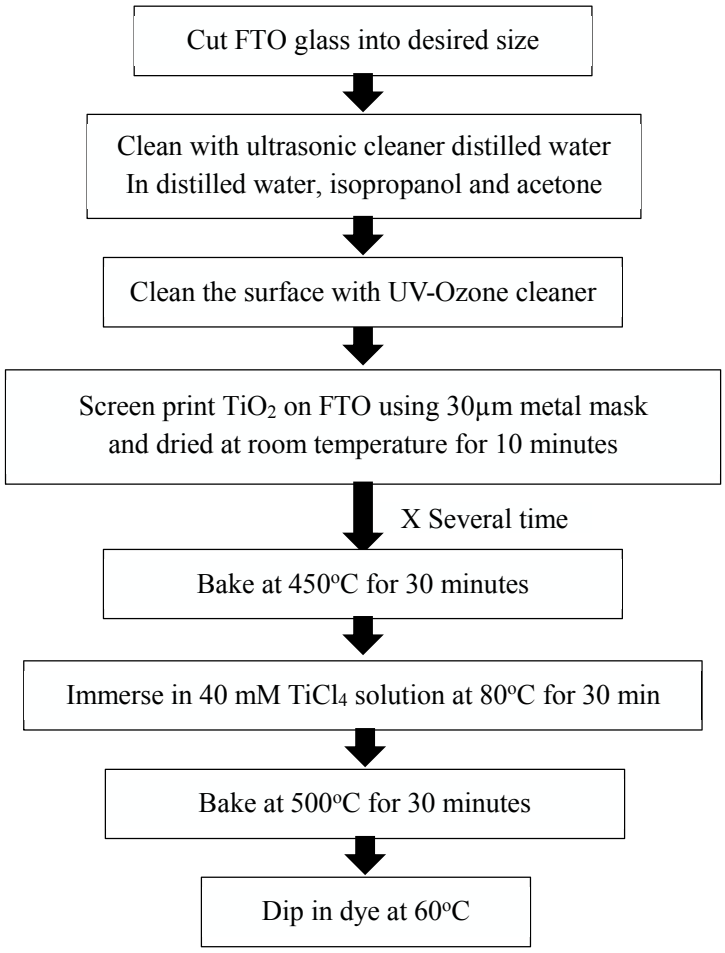

Figure 4.3 *Flowchart for fabrication of TiO_2 electrodes of DSSCs*

Sintered TiO_2 was dipped in 40 mM $TiCl_4$ solution at 80ºC for 30 minutes, rinsed with distilled water and ethanol and dried again at 500ºC for 30 minutes. After temperature was down to 80ºC, $TiCl_4$ treated TiO_2 was immersed in 0.2 mM PPc-1 and PPc-2 (in ethanol solution) while maintaining the dye solution temperature at 60ºC with coil heater. This was then dipped for 24 hours for attaching the dyes on TiO_2 surface. Dipped photo anode was finally rinsed with ethanol to remove excess dyes. Flowchart for fabrication of photo anode is shown in Figure 4.3.

B. Counter electrode

Counter electrode prepared by cutting and cleaning FTO glass in distilled water, isopropanol and acetone with ultrasonic cleaner for 15 minutes. FTO glass was cleaned again with UV-Ozone cleaner. Platinum target used for sputtering Pt on top of cleaned FTO glass by radio frequency magnetron sputtering machine (Shibaura, I-Miller, CFS-4EF-LL). The optimized conditions are in argon atmosphere (99.99%) with a base of plasma chamber of $4x10^{-4}$ Pa and working pressure of $2x10^{-1}$ Pa.

C. Dye Absorption on Titania film

Dye absorption measurement on Titania film was done by following steps. Slide glass was cut and cleaned with ultrasonic cleaner in distilled water, isopropanol and acetone for 15 minutes, respectively. After drying, glass surface was cleaned again with UV-Ozone cleaner for 20 minutes. Cleaned glass coated with transparent TiO_2 paste (Solaronix HT/SP) using 50µm thick metal mask and dried at 450ºC for 30 minutes. One layer of TiO_2 was 5µm which is enough for absorption measurement. Glass coated TiO_2 was dipped in dye solution for 24 hours at 60ºC. Figure 4.4 shows the adsorption of PPc-1 and PPc-1 on HT/SP. Finally, absorption spectrum was measured with UV-VIS spectrophotometers using Jusco V-670. LUMO level of dyes was also determined by its absorption edge which was obtained from this graph.

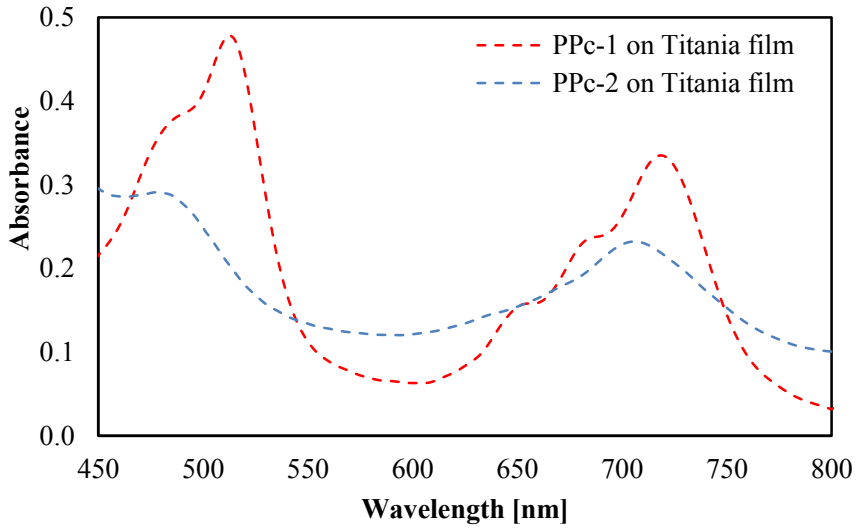

Figure 4.4 *PPc-1 and PPc-2 absorption on Titania film.*

D. DSSCs assembling

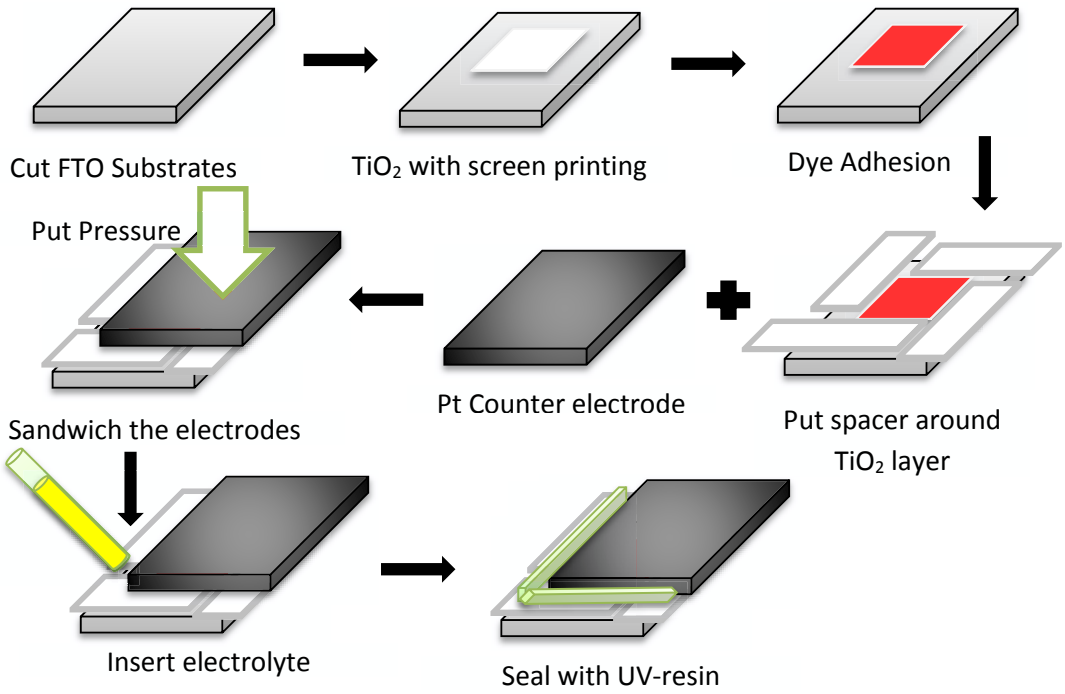

Figure 4.5 *DSSCs assembly*

Working electrode and counter electrode ware assembled into sandwich structure with 25µm thick spacer as a gap. To stick these both electrodes, hotplate at 120ºC was used to melt the spacer while applying a pressure on the sandwich structure. Electrolyte (E1) inserted into the gap between spacer. Finally, four sides of device is sealed with UV resin and solidified with UV-light. In order to have a good electrical contact, silver paste was applied on both poles. Preparation and assembly process can be seen on Figure 4.5.

E. HOMO-LUMO

The lowest unoccupied molecular orbital (LUMO) level was estimated by adding the energy gap calculated from the absorption spectrum edge to the HOMO energy level. Figure 4.6 shows HOMO level measured from dye powder of PPc-1 and PPc-2 with Photo-Electron Spectroscopy in Air (PESA) AC-3 Riken. HOMO level of PPc-1 and PPc-2 are 5.28eV and 4.95eV, respectively. The absorption edge values acquire from UV-Vis spectrophotometer measurement mentioned above.

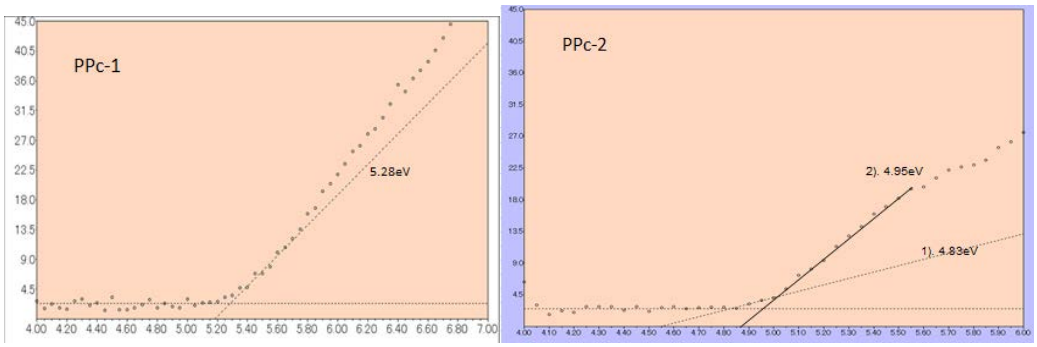

Figure 4.6 *HOMO level for PPc-1 and PPc-2*

F. Emission lifetime

Emission lifetime was measured using the fluorescence lifetime spectrometer Quantaurus-Tau C11367 and was analyzed with the fluorescence lifetime measurement software Hamamatsu Photonics U11487. Emission lifetime of phtalocyanine dyes ware measured in ethanol solution, on titania film and on zirconia film.

G. Impedance spectra

Impedance spectra were measured by Z-View Software (Solarton Analytical) with a frequency response analyzer (Solarton Analytical 1255B) connected to a potentiostat (Solarton Analytical 1287) under illumination (Yamashita Denso YSS-50A) at 1mA constant current.

H. Dye loading

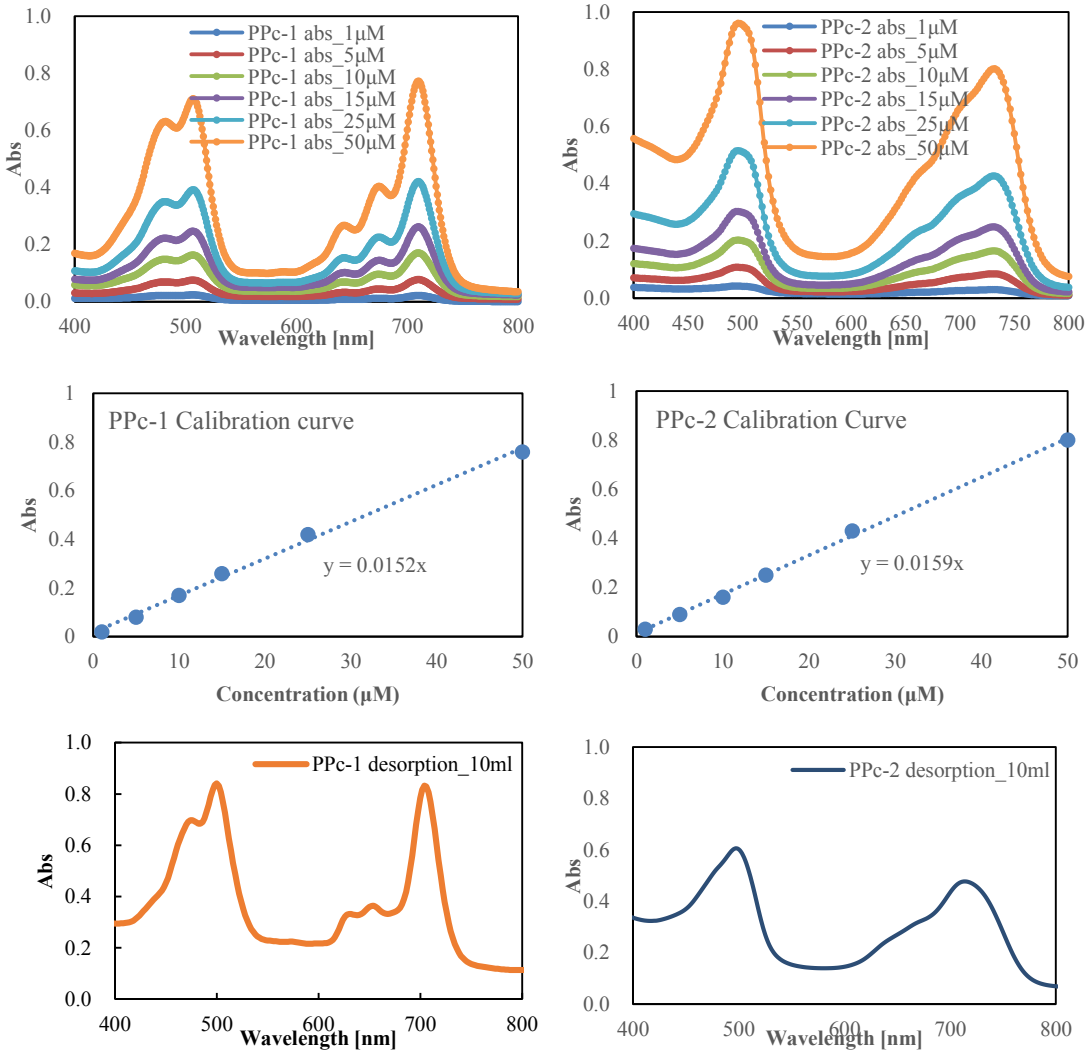

Figure 4.7 Calibration curves and desorbed dye absorptions for PPc-1 and PPc-2.

Dye loading of dye measured and calculated by comparing the desorption of dyes with calibration curve from known concentration of dye and divided by the total area of titania layer. Dye solutions with certain concentration was measured with UV-vis spectroscopy and plotted to determine the equation for calibration curve. The mixture of NaOH (0.1mM), ethanol, t-butyl alcohol and acetonitrile (vol 1:1:1:1) was used to desorbed the dyes from titania surface. Desorption dye solution is taken and calculated with calibration curve of knowing concentration. At last, the concentration of desorbed dyes divided by the active area. For example, PPc-1 has absorption peak for desorbed dye of 0.83, which corresponds to concentration of 53.48 μM. Since the concentration was 10 ml, the concentration of dye desorbed was 534.8 nmole. The active area of titania is 4 cm^2, gave final dye loading for PPc-1 was 133.7 nmole/cm^2. Same method was done for PPc-2. PPc-2 has absorption peak for desorbed dye of 0.48, which corresponds to concentration of 29.40 μM. Since the concentration was 10 ml, the concentration of dye desorbed was 294 nmole. The active area of titania was 4 cm^2, gave final dye loading for PPc-2 was 73.5 nmole/cm^2.

4.3 Result and discussion

It has been reported that the absorption spectrum edge shifts to the longer wavelength region (900 nm) by substituting the α-position of the phthalocyanine rings with ether or thioether groups[13]. Kobayashi et al. have reported on phosphorus-phthalocyanine covering up to 1000nm[14]. However, the LUMO was −5.8 eV, which was deeper than that of the TiO_2 conduction band (-4.0 eV). Since electron injection does not occur from the dye to titania, we were not able to expect photovoltaic performance. The reason for the low LUMO level is associated with the phosphorous (V) cation located at the center of the phthalocyanine ring. Therefore, we focused on PPc. It is known that the absorption spectrum peak of Ref-Pc-1 is 680nm (Q-band) with the 700nm absorption edge. The coverage of the spectrum area by Ref-Pc-1 is not sufficiently wide. In addition, the HOMO of Ref-Pc-1 was -4.80 eV, which was shallower than that of I^-/I_3^- (−4.9 eV). Therefore, the oxided Ref-Pc-1 is not reduced by I^-. In order to cover the wide range of wavelengths, an ether or thioether group was introduced into the α-position of the phthalocyanine ring, as shown in Figure 4.1.

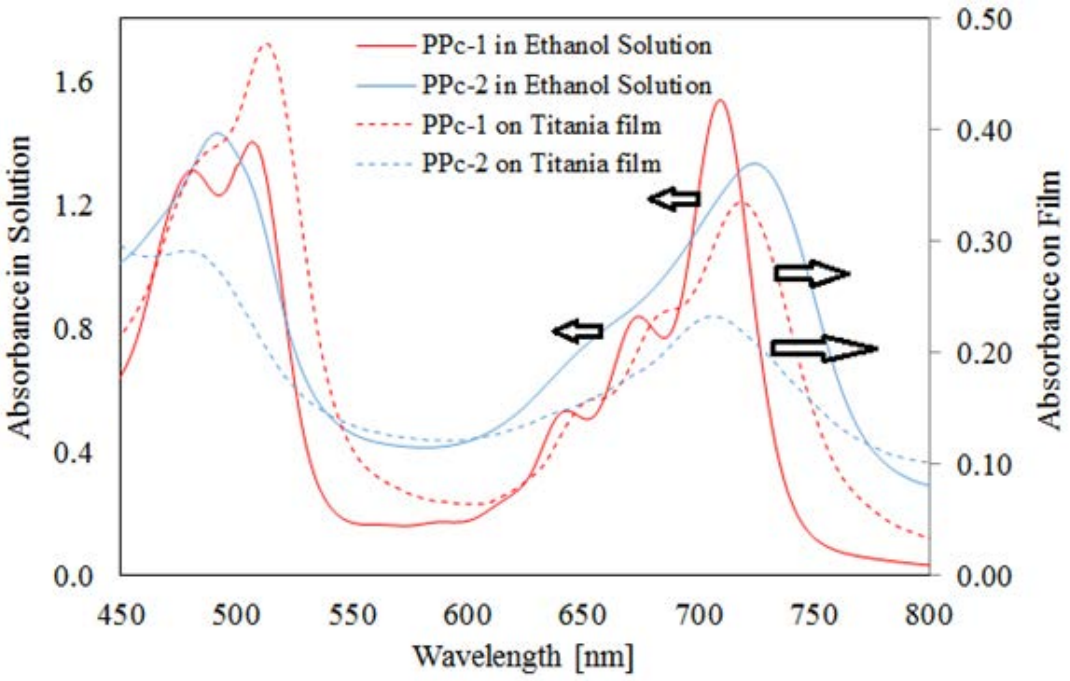

Figure 4.8 *Electronic absorption spectra of phosphorus-phthalocyanine dyes in solution and in solid state (TiO_2 surface)*

The electronic absorption spectra of these dyes in solution and on a porous titania layer are shown in Fig. 4.7 PPc-1 has absorption peaks at 710 and 507 nm (in solution), assigned to the Q and Soret bands, respectively. The Q band of Ref-Pc-1 in solution shifted from 680 to 710 nm with the introduction of $–O–CH_2–CH_2–CH_2–CF_3$(TFB) at the α-position of phthalocyanine rings. When the substituent (TFB) was replaced with –S-Ph (SPh), the absorption peak in solution was shifted to a longer wavelength (724 nm), suggesting that the electronic properties of the phthalocyanine ring are affected by the substituents. The full widths at half maximum (FWHMs) in solution were 39 nm for PPc-1 and 119 nm for PPc-2. The larger FWHM for PPc-2 is probably due to some aggregations in the solvent[15]. It has been reported that dye aggregation makes the dye excited state lifetime shorter and degrades the solar cell performance[16]. From the viewpoint of dye aggregation, PPc-1 may have some advantages over PPc-2. After a glass substrate with a porous titania layer was dipped in the dye solution, the substrate became coloured even without COOH anchoring groups.

In Figure 4.7 also shows the spectra of dyes that are adsorbed on the porous titania layer. The absorption peak of PPc-1 shifted from 710 nm in solution to 719 nm on titania. On the other hand, that of PPc-2 shifted from 725 nm in solution to 706 nm in titania. The shift of PPc-1 after adsorption was opposite to that of PPc-2. The FWHMs of PPc-1 and PPc-2 became larger from 39 nm (solution) to 82 nm (on TiO_2) and from 119 nm (solution) to 175 nm (on TiO_2), respectively, after these dyes were adsorbed on the porous titania layer, suggesting that these dyes were bonded to the surface of titania and the motions on the porous titania layer were restricted more than those in the solutions. PPc-1 and PPc-2 do not have a conventional anchoring group such as carboxylic moieties; however, adsorption actually occurred. The adsorption by the P–OH group probably occurs at the center of the phthalocyanine ring to make the P–O–Ti (porous titania) linkage (TiO_2/PP in Fig. 4.1).

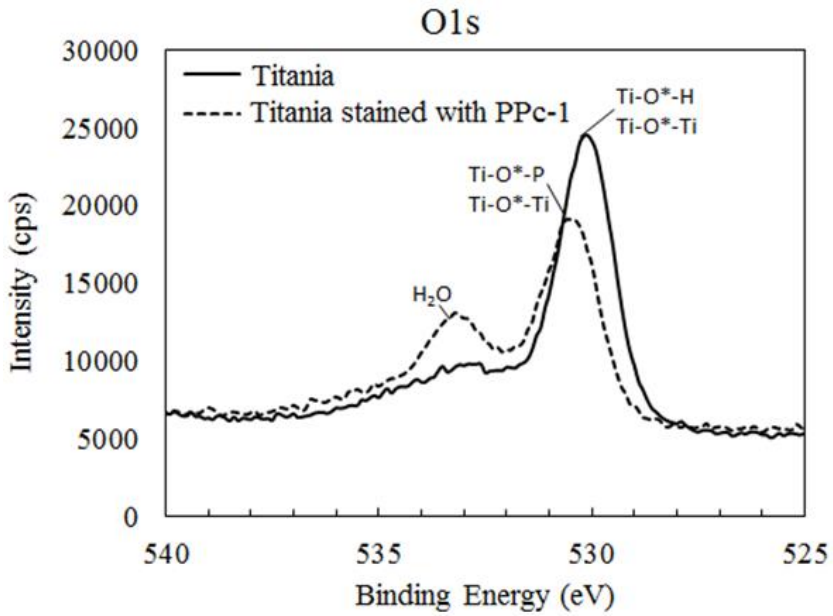

Figure 4.9 *Shift of binding energy on TiO_2 as reference and after stained with PPc-1 dye.*

The binding energy of O 1s of the porous TiO_2 film was shifted from 530.1 to 530.5 eV, after the porous TiO_2 layer was stained by PPc-1, as shown in Figure 4.8. Unfortunately, P was not detected probably because of the low P density of the titania surface. It has

been reported that the binding energies of O 1s for Ti–OH and Ti–O–P are 529.3 and 529.7 eV, respectively[17]. After P was introduced, the binding energy of O 1s increased by 0.4 eV. The trend of the shift was the same as that in this experiment. The results strongly support the presence of the Ti–O–P linkage.

Table 4.1 shows the emission lifetimes of PPc-1 and PPc-2 in ethanol solution on the ZrO_2 and TiO_2 substrates (details are shown in Figure 4.9 and 4.10, respectively). ZrO_2 was employed for measuring the emission of the adsorbed dye. Since ZrO_2 has a shallow conduction band energy level, emission from adsorbed dyes is observed without being affected by electron injection. When the dye is adsorbed on porous TiO_2, emission competes with electron injection and the emission lifetime is not compared with those in ethanol solution. The emission lifetime of PPc-1 in solution is 1.93 ns, which is longer than that of PPc-2 (1.57 ns) in solution. PPc-1 on ZrO_2 has a longer emission lifetime (1.02 ns) than PPc-2 (0.42 ns).

Table 4.1 *Excitation life time*

	PPc-1 (Ethanol)	PPc-2 (Ethanol)	PPc-1 (Zirconia)	PPc-2 (Zirconia)	PPc-1 (Titania)	PPc-2 (Titania)
Excitation life time	1.93 nsec	1.57 nsec	1.02 nsec	0.42 nsec	0.71 nsec	0.15 nsec

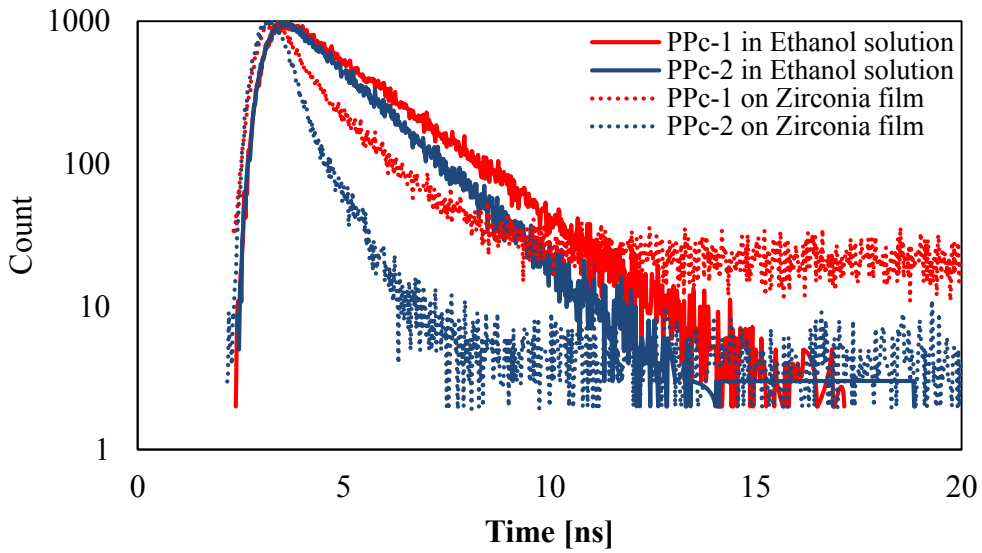

Figure 4.10 *Emission life time in ethanol solution and zirconia film.*

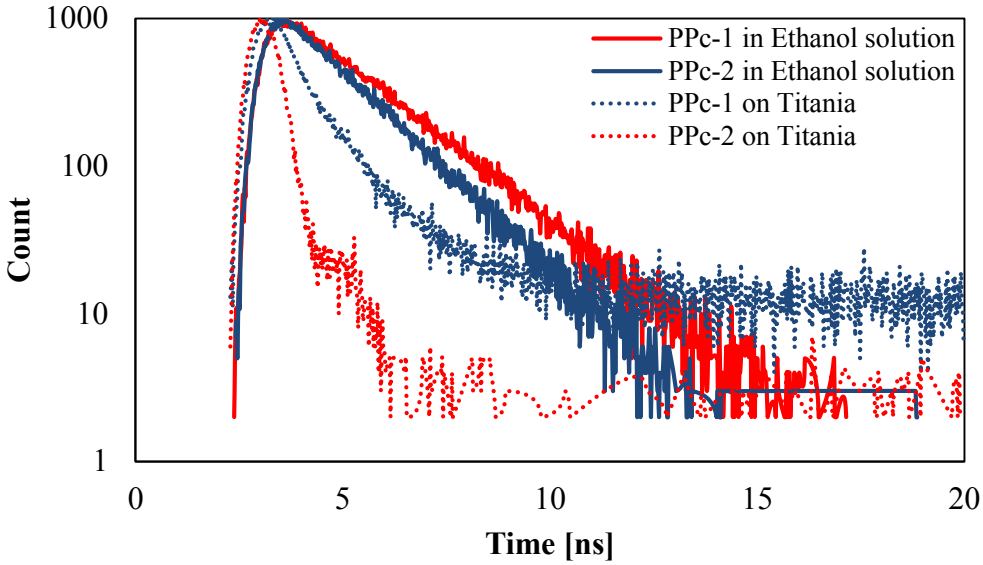

Figure 4.11 *Emission life time in ethanol solution and titania film.*

In addition, a lifetime component longer than 15 ns for PPc-1 on ZrO_2 remains. These results suggest that PPc-1 on ZrO_2 is less aggregated than PPc-2 on ZrO_2, in agreement with the FWHM results. The emission lifetimes of PPc-1/TiO_2 (0.71 ns) and PPc-2/TiO_2 (0.15 ns) are shorter than those of PPc-1/ZrO_2 (1.02 ns) and PPc-2/ZrO_2 (0.42ns). Therefore, in both cases, injection from the dye to TiO_2 occurs (Figure 4.11).

Figure 4.12 shows the energy band diagrams for PPc-1 and PPc-2. The HOMO of the previously reported phosphorous phthalocyanine is more negative than that of the I^-/I_3^- redox potential and does not match the requirement of the energy level diagram needed for DSSC. The introduction of electron withdrawing groups at the position of the phthalocyanine ring decreases the HOMO level, which matches the requirement of DSSCs. The LUMO levels of PPc-1 and PPc-2 are −3.67 and −3.44 eV, respectively. These LUMO energy levels are shallower than that of the TiO_2 conduction band (−4.0 eV), suggesting that the electron injection from these LUMOs to the TiO_2 conduction band is possible. The HOMO energy levels of PPc-1 and PPc-2 are −5.28 and −4.95 eV, respectively. Since the I^-/I_3^- redox potential is −4.9 eV, electron injection from the I^-/I_3^- redox level to the HOMO of PPc-1 is possible (dye regeneration). However, electron injection to the HOMO of PPc-2 may be difficult because of the small energy level difference (0.05 eV) between the I^-/I_3^- redox level and the HOMO of PPc-2.

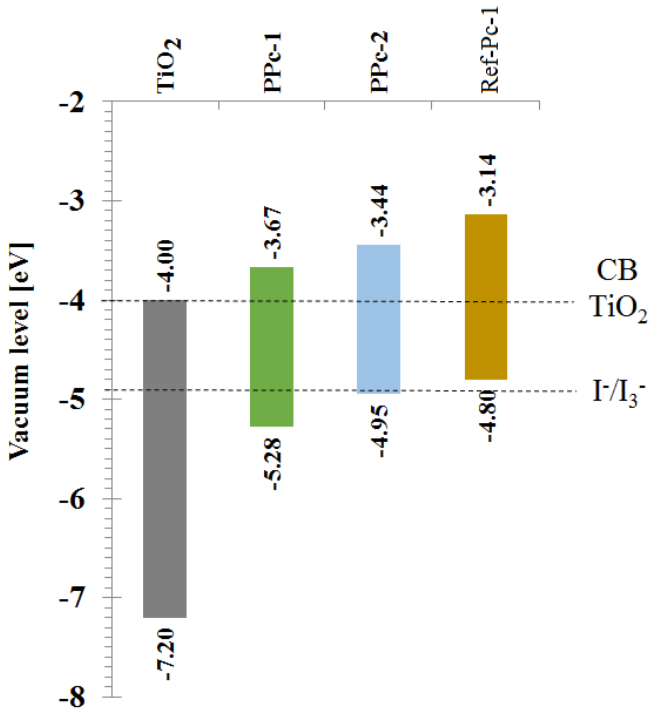

Figure 4.12 *Energy level diagrams for phosphorus phthalocyanines along with the energy levels of TiO_2 and I^-/I_3^- redox couple.*

Table 4.2 and Figure 4.13 shows the current–voltage (I–V) characteristics of DSSCs. The Voc, Jsc, FF, and power conversion efficiency (PCE) of DSSC-PPc-1 are 0.566 V, 6.879 mA/cm^2, 0.686, and 2.67%, respectively. PPc-2 has a lower efficiency with 0.573 V, 3.748 mA/cm^2, 0.731 and 1.57%, respectively. In both cases, Voc is almost the same, but the large difference in efficiency between them is brought about by that of Jsc. The lower Jsc of PPc-2 can be explained by the small energy gaps between the I^-/I_3^- redox potential and the HOMO level of PPc-2 (0.05 eV). In addition, this may be explained by the fact that the PPc-1 density on porous TiO_2 is higher than the PPc-2 density, because the absorbance of PPc-1 on porous TiO_2 is higher than that of PPc-2 with the same thickness, as shown in Fig. 4.8 and from dye loading measurement. In solution, the Soret band absorbances of both are between 1.2 and 1.6. However, on the porous titania layer, the Soret band absorbance of PPc-2 (0.25) is much smaller than that of PPc-1 (0.35). Since flexible fluoroalkyl groups (PPc-1) do not disturb the adsorption

of the phthalocyanine rings on porous titania through Ti–O–P (axial adsorption), the PPc-1 dye density on porous titania is larger than the PPc-2 dye density.

Table 4.2. I-V Characteristic of DSSCs with Dyes under investigation.

Dye	Jsc (mA/cm^2)	Voc (V)	FF	η (%)
PPc-1	6.879	0.566	0.686	2.67
PPc-2	3.748	0.573	0.731	1.57

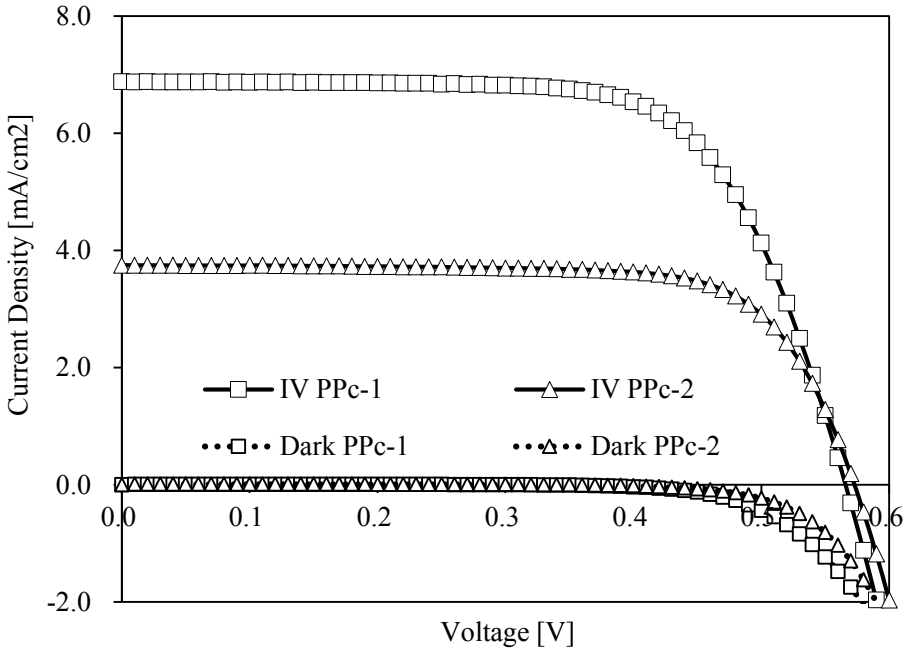

Figure 4.13 *I–V characteristics dark current for DSSCs stained with PPc-1 and PPc-2.*

Figure 4.14 shows IPCE curves of DSSCs. IPCE of DSSC-PPc-1 and DSSC-PPc-2 have two peaks (510 and 710 nm, and 430 and 710 nm, respectively), which are associated with the electronic absorption spectra of PPc-1 and PPc-2 adsorbed on the porous TiO_2 layer. The higher IPCE of PPc-1 is consistent with the higher Jsc of PPc-1. The IPCE curve edge reaches 800 nm.

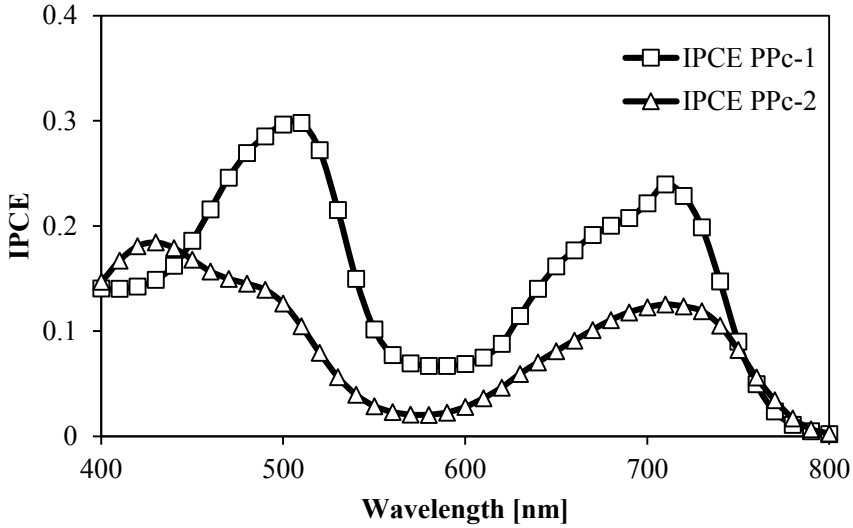

Figure 4.14 *IPCE spectra of DSSCs stained with PPc-1 and PPc-2*

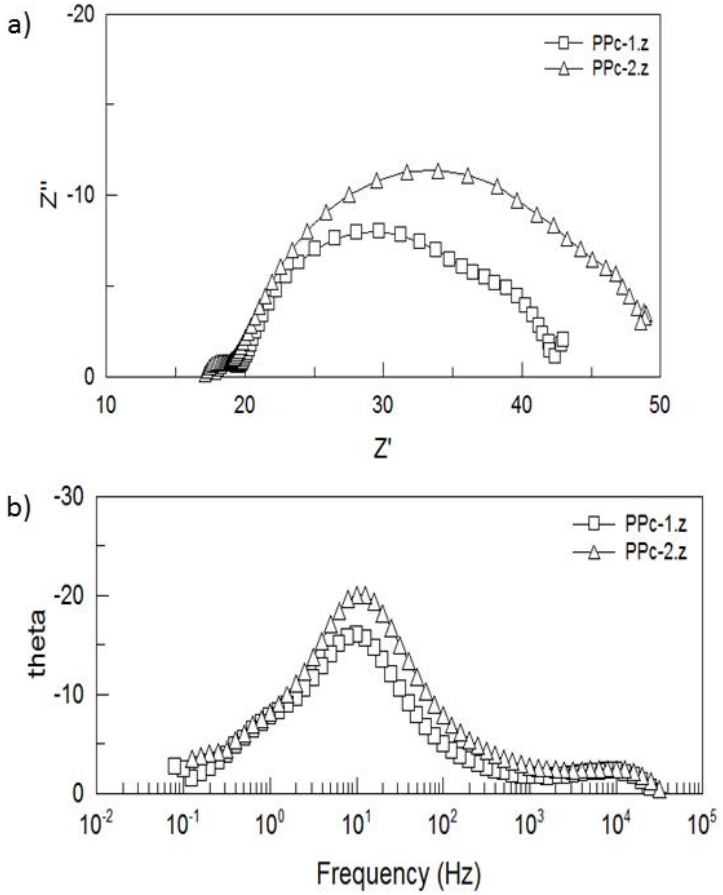

Figure 4.15 *Electrical impedance spectroscopic plot for PPc-1 and PPc-2. a) Cole-cole plot and b) Bode plot.*

Figure 4.15 shows electrical impedance spectra (EIS) of DSSC-PPc-1 and DSSC-PPc-2. The curves are divided into three parts. A semi-circle observed at higher frequency, middle frequency and lower frequency are associated with resistance of interface at Pt/electrolyte of the counter electrode, TiO_2/Dye/electrolyte and FTO/(Dye)/electrolyte interfaces, and diffusion of I^-/I_3^- redox in the electrolyte[18]. The second semi-circle in DSSC-PPc-1 was a little smaller than that of DSSC-PPc-2. This may be explained by the fact that PPc-1 density on porous TiO_2 is a little larger than PPc-2 as was described in the previous section. It has been reported that there are a lot of surface traps on the porous TiO_2 and the surface traps become centers for charge recombination[19]. In addition, the surface traps are passivated by adsorption of dye molecules[20]. The larger amount of PPc-2 adsorbed on the porous TiO_2 layer passivates the surface trap of porous TiO_2 layers and electron diffusions in porous TiO_2 layers would increase. Electron life time was measured by EIS, according to the following equation[21].

$$\tau = \frac{1}{2\pi f minimum} \quad (4.1)$$

The electron life time of DSSC-PPc-1was 15.9 ms which was longer than 13.2 ms of DSSC-PPc-2, also supporting the explanation that surface of porous titania of DSSC-PPc-1 is passivated more than that of DSSC-PPc-2.

4-*tert*-butylpyridine (TBP) is one of additive commonly used in electrolyte configurations. It have been reported that presence of TBP in DDSCs system will suppress the recombination of the injected electron and I_3^- ions[22,23]. TBP adsorbed on the TiO_2 surface not covered by the dye. Arakawa and his group reported that TBP was slightly adsorbed on bare titania surface and dramatically increased in the presence of LiI for titania coated with dye[24]. This phenomena indicated that TBP molecules interact with LiI cations especially on the TiO_2 surface area that not covered with dyes. TBP also reported shifting TiO_2 conduction band to higher level and observed slightly lower Jsc in presence of TBP as additive[25]. It also been reported that the shifting of TiO_2 conduction band in use of TBP as additive was also found on Cobalt-based electrolyte[26]. In order to get optimum injection, it is required sufficient energy difference between LUMO energy level and TiO_2 conduction band. At least 0.4-0.5 eV gap between them is required to ensure optimal electron injection. The gap between PPc-1 LUMO level (-

3.67 eV) and TiO_2 conduction band (-4.0 eV) were 0.33eV and in order to increase the energetic gap we try to remove TBP from the systems. However, the improvement of Jsc after removing the TBP hampered Voc more than 50% led to very low over all photovoltaic performance.

Figure 4.16 shows IPCE spectra and I-V characteristics from PPc-1 dye fabricated with TBP and without TBP. Jsc, Voc, FF and PCE for device without TBP are 9.77 mA/cm^2, 0.26 V, 0.38 and 0.95 %, respectively. Electron recombination was very high due to higher amount of surface traps on titania surface. The nature of axial ligation need more space occupy for dye-adsorption and leaves more un-passivated surface traps.

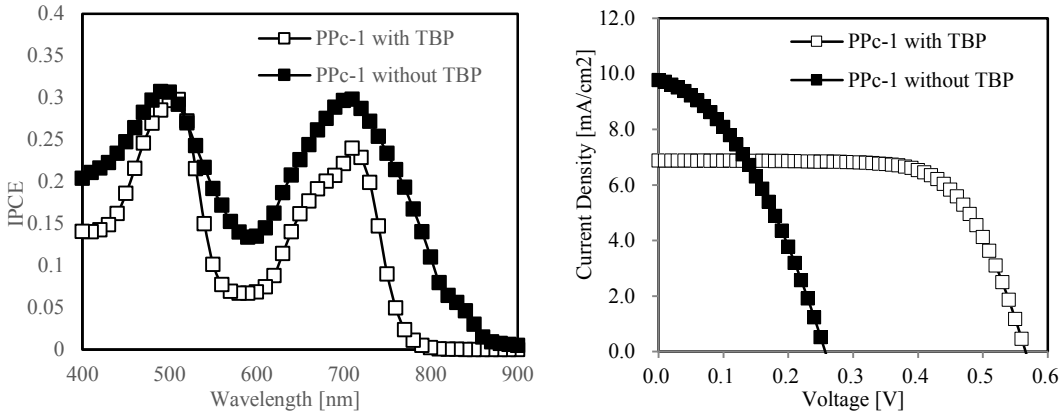

Figure 4.16 *IPCE spectra and I–V characteristics for DSSCs for PPc-1 with TBP and PPc-1 without TBP.*

4.4 Conclusion

In summary, it was found that phosphorous phthalocyanine without the conventional anchoring group (–COOH) can be well adsorbed on TiO_2 with Ti–O–P linkages. The higher efficiency of DSSC-PPc-1 can be explained by the longer excitation lifetime, higher dye concentration on a porous TiO_2 layer, sufficient energy level difference between the LUMO of PPc-1 and the TiO_2 conduction band, and that between the HOMO of PPc-1 and the I^-/I_3^- redox level. Higher Jsc could be achieved by removing TBP from electrolyte configurations. However, in absence of TBP, more surface trap

were left on titania surface and hampered Voc. We propose an approach to stain the TiO_2 surface with symmetrical phthalocyanine, which can be synthesized much easier than unsymmetrical phthalocyanine with carboxylic anchoring groups. This will provide a direction to photoconversion in IR regions where the synthesis of unsymmetrical phthalocyanine with carboxylic acids is much harder.

4.5 References for chapter 4

1) B. O'Reagan, and M. Grätzel, *Nature*, **353,** 737, (1991).

2) A. Yella, H.-W. Lee, H.N. Tsao, C. Yi, A.K. Chandiran, Md.K. Nazeeruddin, E.W.-G. Diau, C.-Y. Yeh, S.M. Zakeeruddin and M. Grätzel, *Science*, **334,** 629-633, (2011).

3) T. Kinoshita, J.T. Dy, S. Uchida, T. Kubo and H. Segawa, *Nature Photonics*, **7**, 535-539, (2013).

4) D. Joly, L. Pelleja, S. Narbey, F. Oswald, J. Chiron, J.N. Clifford, E. Palomares and R. Demadrille, *Scientific Reports,* **4**, 4033, (2014).

5) S. Mori, M. Nagata, Y. Nakahata, K. Yasuta, R. Goto, M. Kimura and M. Taya, *J.Am.Chem Soc.*, **132**, 4054-4055, (2010).

6) B. Lim, G.Y. Margulis, J.-H. Yum, E.L. Unger, B.E. Hardin, M. Grätzel, M.D. McGeHee and A. Sellinger, *Org. Lett*, **15** [4], 784-787, (2013).

7) M. Kimura, H. Nomoto, H. Suzuki, T. Ikeuchi, H. Matsuzaki, T.N. Murakami, A. Furube, N. Masaki, M.J. Griffith and S. Mori, *Chem. Eur. J.*, **19**, 7495-7502, (2013).

8) K. Sakamoto and E. O-Okumura, *Materials*, **2**, 1127-1179, (2009).

9) L. Macor, F. Fungo, T. Tempesti, E.N. Durantini, L. Otero, E.M. Brea, F.F. Santiago, and J. Bisquert, *Energy Environ. Sci.,* **2**, 529-534, (2009).

10) B.-W. Park, T. Inoue, Y. Ogomi, A. Miyamoto, S. Fujita, S.S. Pandey and S. Hayase, *Applied Physics Express*, **4**, 012301, (2011).

11) G.M. Shivashimpi, S.S. Pandey, A. Hayat, N. Fujikawa, Y. Ogomi, Y. Yamaguchi and S. Hayase, *J.JPhotochem,* **289**, 53-59, (2014).

12) J. Li, L. R. Subramanian, M. Hanack, *Eur. J. Org. Chem,* 2759-2767, (1998).

13) J. P. Fox and D. P. Goldberg, *Inorganic Chemistry,* **42**, 8181-8191, (2003).

14) N. Kobayashi, T. Furuyama and K. Satoh, *J. Am. Chem. Soc.*, **33** [49], 19642–19645, (2011).

15) Z. Li, X. Huang, S. Xu, Z. Chen, Z. Zhang, F. Zhang, and K. Kasatani, *Journal of Photochemistry and Photobiology A: Chemistry*, **188**, 311–316, (2007).

16) M. G. Walter, A. B. Rudine and C. C. Wamser, *J. Porphyrins Phthalocyanines*, **14**, 759-792, (2010).

17) K.J.A. Raj, R. Shanmugam, R. Mahalakshmi and B. Viswanathan, *Indian Journal of Chemistry,* **49A**, 9-17, (2010).

18) J. Bisquet, *J. Phys. Chem. B,* **106**, 325-333, (2002).

19) J. Nelson, S.A. Haque, D.R. Klug, and J.R. Durrant, *Phys. Rev. B63*, 205321, (2001).

20) Y. Noma, T. Kado, D. Ogata, Y. Hara and S. Hayase, *JJAP,* **47**, 505-508, (2008).

21) R. Kern, R. Sastrawan, J. Ferber, R. Stangl, J. Luther, *Electrochimica Acta*, **47**, 4213-4225, (2002).

22) A. Kay and M. Grätzel, *J. Phys. Chem.*, **97**, 6272-6277, (1993).

23) S.R. Raga, E.M. Barea, and F.F-Santiago, *J.Phys.Chem.Lett.,* **3**, 1629-1634, (2012).

24) K. Hara, Y. D-Oh, C. Kasada, Y. Ohga, A. Shinpo, S. Suga, K. Sayama and H. Arakawa, *Langmuir, **20,*** 10, 4205-4210, (2004).

25) P. Wang, S.M. Zakeeruddin, R. Humphry-Baker and M. Grätzel, *Chemistry of Materials,* **16,** 2694, (2004).

26) J. Gao, M.B. Achari and L. Kloo, *Chem. Commun.,* **50**, 6249-6251, (2014).

Chapter 5 TCO free Dye sensitized solar cell using flat Titanium sheet.

Structure modifications are commomnly done by engineers in order to improve the performance of the devices. For DSSCs, the structure modification to remove expensive parts on the standard structure are done in order to achieved lower manufacturing cost. TCO in DSSCs taking 24% of total production cost of DSSCs and the nature of rigid glass used as TCO parts make DSSCs application limited to flat architecture. In this chapter, we succesfully replaced TCO with flat titanium sheet as working and counter electrodes. The titanium sheets are also allow us to make cylindrical structure of DSSCs with high efficiency.

5.1 TCO-less back-contact DSSCs

Flat titanium sheet with micro holes (FTS-MH) was used to fabricate transparent-conductive oxide less dye-sensitized solar cells (TCO-less DSSCs) with back contact electrodes. FTS-MH allows us to fabricate solar cells with ease and simple, compared to TCO-less DSSCs reported before. Hydrogen peroxide (H_2O_2) treatments on FTS-MH were important factors to enhance the efficiency. H_2O_2 treatment changed the surface morphology of FTS-MH and created nanostructures on the surface that increase surface contact between FTS-MH and titanium dioxide (TiO_2) working as a photo anode. This surface change also hamper electron recombination resulting in increment of both short circuit current and open circuit voltage. Overall photo-conversion efficiency could reach up to 7.25 % under simulated solar irradiation.

5.1.1 Introduction

Dye sensitized solar cell (DSSCs) was reported for the first time in 1991 after Grätzel and his group demonstrated the potentials of this type of solar cells with relatively low cost to make[1)]. DSSCs have achieved relatively high efficiency over 13% with porphyrin dye and cobalt electrolyte configuration[2)]. Replacing glass substrate of

DSSCs with more flexible materials is desired for portability and easy-to-use. The rigid structure of DSSC is mainly due to utilization of transparent conductive oxide layered glasses (TCO glass). DSSCs utilize two TCO glasses, working as photo anodes and counter electrodes. Fluorine doped tin oxide coated glasses (FTO glass) have been most widely used to fabricate DSSCs. There are some reports to replace glass based TCO electrodes with polymer based TCO[3]. Unfortunately, semiconductor photo anode used for DSSCs, titanium dioxide (TiO_2), required calcination at around 450°C, which makes polymer based TCO unssuitable. Low temperature processes had been intensively proposed, such as low temperature sintering[4], hydrothermal treatment[5], chemical vapor deposition with UV irradiation[6], spray coating[7] *etc*. However, low necking (interconnection) between TiO_2 particles by low temperature process made it difficult to achieve the same results as high temperature calcination. Back-contact structure with metallic materials is strong candidate to replace the TCO in DSSCs[8,9].

Titanium is one of best candidates among metallic materials for TCO-less DSSCs application. Titanium is strong, light weight, non-reactive against electrolyte, which makes it easy to apply with various DSSC structures such as flexible and cylindrical solar cell. Fan *et al* have reported TCO-less DSSCs consisting of 150 µm thick titanium wire having overall efficiency of 1.49 %[10]. Recently, we have reported TCO-less DSSC by replacing the FTO on anode side with Ti sputtered Stainless Steel (Ti/SUS) metal mesh working as the supporter for the mesoporous TiO_2 and back contact conducting grid. It has been demonstrated that it needs the sputtering of thin titanium on the SUS in order to protect the surface and reduce electron recombination between electrons in metal electrode and redox species to enhance the photo-conversion efficiency[11].

Our group has also demonstrated that all metal type TCO-less DSSC with porous titanium directly sputtered onto TiO_2 surface leads to 7.4 % efficiency which was comparable with the corresponding TCO based DSSCs fabricated in a similar experimental condition[12]. Meanwhile, in order to reduce high energy and high cost processes, sputtering and thermal evaporation are some of the bottle-necks towards the commercialization of DSSCs[13]. Since the thickness of mesh (minimum diameter:

50µm) affected the diffusion length of electrolytes, we used 20µm thin Ti sheets with micro holes (FTS-MH) towards the fabrication of back contacted TCO-less DSSCs.

5.1.2 Experimental Detail

5.1.2.1 Materials

The sample of flat titanium sheet with micro holes (FTS-MH) was received from Ushio Inc., Japan. The FTS-MH (20µm) was much thinner than conventional titanium wire mesh (thickness: 150µm)[10]. In this experiment, FTS-MH treated with H_2O_2 was used as well as FTS-MH without the treatment. The hole diameter was 100µm and distance between these hole centers were about 150µm as shown in Figure 5.1. Titanium dioxide (TiO_2) PST-400C and PST-30NRD were purchased from Catalysts and Chemical Ltd in Japan. For sensitizer dye, Ruthenizer 535-bisTBA (OPV-N719; Di-tetrabutyl-ammoniumcis-bis(isothiocyanato)bis(2,2'-bipyridyl-4,4'-dicarboxylato)ruthenium(II)) from OPV Tech is utilized. Glass paper with 30µm thick used as spacer between photo anode and counter electrode was employed for this experiment.

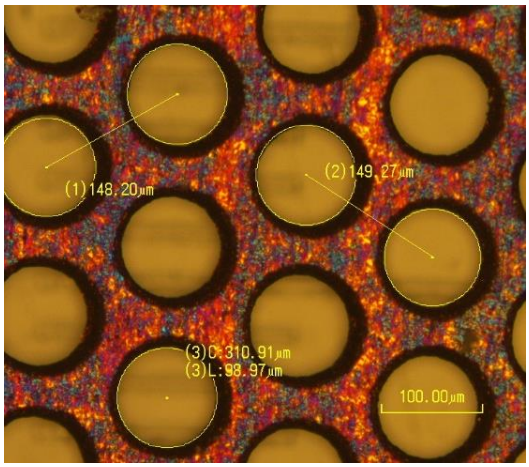

Figure 5.1 *Image of flat titanium sheet with micro holes (FTS-MH) used for back-contact electrode.*

5.1.2.2 Cell Fabrication and Measurement

A. Photo-anode

Photo-electrodes prepared for TCO-less DSSCs are different with conventional DSSCs. As a replacement of FTO glass, we used as FTS-MH as photo anode supporter. FTS-MH was cleaned with ultrasonic cleaner in acetone for 15 minutes. After drying with blower, untreated FTS-MH was directly coated with TiO_2. For treated FTS-MH, hydrogen peroxide (H_2O_2) treatment was applied on it.

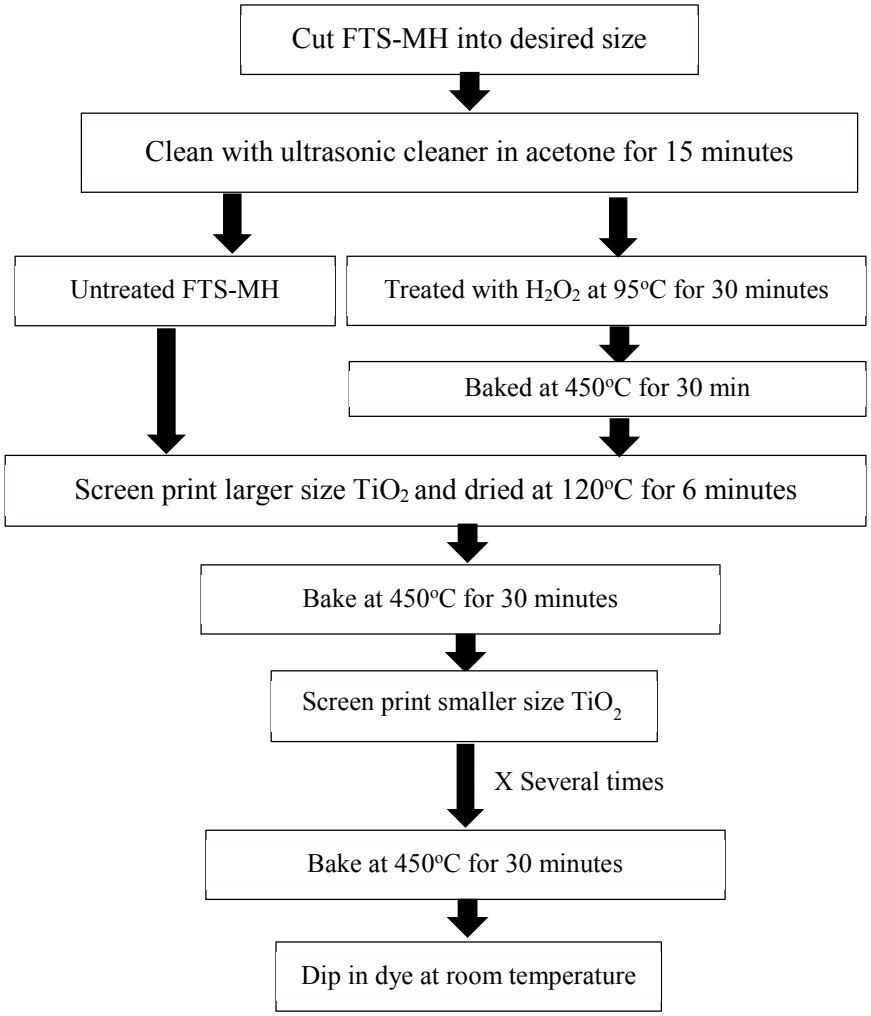

Figure 5.2 *Fabrication of Photo-anode for TCO-less DSSCs*

H_2O_2 30 % (w/w) in H_2O was directly used. The solution was put in a beaker along with FTS-MH and heated at 95°C for 30 minutes. After treatment, FTS-MH was rinsed with ethanol and dried with blower. To finish the treatment, calcination at 450°C for 30 min were needed.

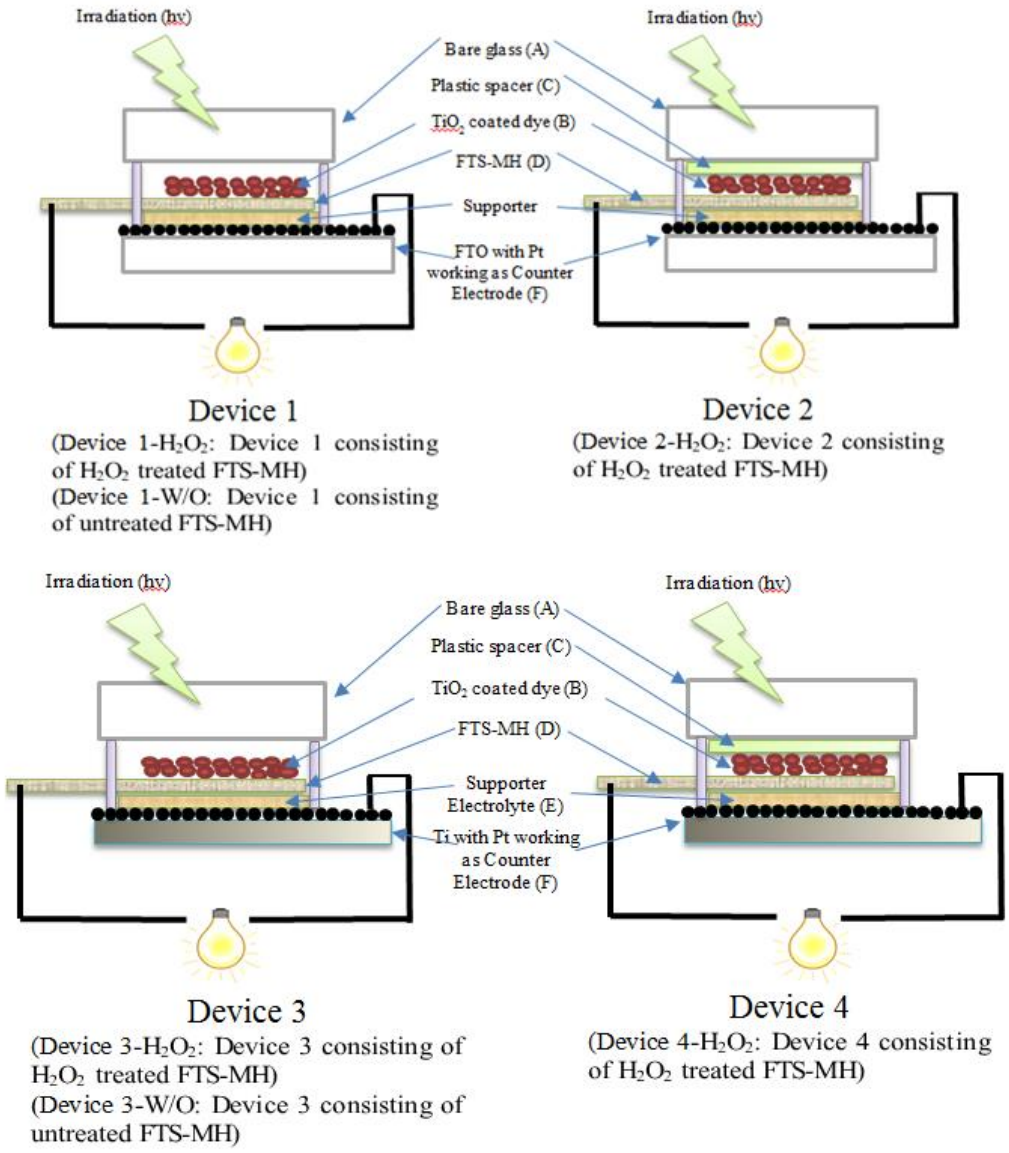

Figure 5.3 *DSSCs TCO-less structures and their abbreviations*

After cooling down to room temperature, TiO_2 paste with larger particle size (PST-400C paste) was screen printed onto both treated and untreated FTS-MH using metal mask (thickness: 40µm) while putting polytetrtafluoroethylene (PTFE) mesh above

the FTS-MH to hold the TiO_2. FTS-MH was dried at 125ºC for 6 minutes and PTFE was removed after cooled down to room temperature and baked again at 450ºC for 30 minutes. Above of larger size TiO_2, smaller size TiO_2 (PST-30NRD) was coated with same method mentioned above for several times to create 18µm thick of TiO_2. Finally, FTS-MH coated with TiO_2 immersed in 0.3 mM N719 dye. The flowchart for fabrication of photo anode is shown in Figure 5.2.

B. Counter electrode

Two type of substrates were used for preparing the counter electrode (CE). First is standard FTO glass and the other is titanium foil. The counter electrodes was prepared with same method mentioned in Chapter 4. Therefore, Titanium foil was cleaned only with acetone in ultrasonic cleaner without further cleaning with UV-Ozone cleaner.

C. Device Fabrications

Four types of solar cells were prepared as shown in Figure 5.3. One is TCO-less DSSCs with FTO glasses (FTO-CE) as the counter electrode (Device 1), consisting of Glass/porous TiO_2 layer stained with N719/FTS-MH/electrolyte layer/FTOglass with Pt working as the counter electrode. The second cell is TCO-less DSSC with Ti sheet as the counter electrode (Device 3), consisting of Glass/porous TiO_2 layer stained with N719/FTS-MH/electrolyte layer/Ti sheet with Pt (Ti-CE) working as the counter electrode. The third one has an adhesive plastic sheet layer between a glass and porous TiO_2 as shown in Device 2, consisting of glass/plastic layer/ porous TiO_2 layer stained with N719/FTS-MH/electrolyte layer/FTO with Pt working as the counter electrode. The fourth is Device 4, which is similar to Device 2 except Device 4 used Ti sheet sputtered Pt as counter electrode.

Device 4 consisting of H_2O_2-treated FTS-MH is abbreviated as Device 4-H_2O_2. The H_2O_2 treatment was done by dipping the FTS-MH in 30% aq. hydrogen peroxide solution (Wako) at 95ºC for 30 minutes. After rinsed in ethanol, the FTS-MH was baked at 450ºC for 30 min for cleaning the surface of Ti and fabricating

porous structures on the Ti surface. The working electrode has Ti-TiO_2 layer structures. The working electrode was fabricated by screen printing of 400 nm size of TiO_2 (PST-400C) on the FTS-MH (both untreated and H_2O_2 treated) and the sample was heated at 450°C for 30 min. Second layer of porous titania was fabricated by coating 30 nm size of TiO_2 (PST-30NRD) on the top of the first layer. The sample was baked at 450°C for 30 minutes to make porous titania layer with total thickness of 18μm. The sample was dipped in Ruthenizer 535-bis TBA solution in tert-buthanol/Acetonitrile (1:1 vol) for 24 hours at room temperature. Then, the FTS-MH was rinsed with solvent to remove the excess dye.

The photoactive area was 0.25 cm^2. Solaronix plastic sheet (Solaronix Meltonix 1170-25) (C in Fig. 5.3) was placed between the bare glass (A) and photo anode (B + C) and the sample was heated to 120°C while they were pressed to stick them together. The plastic sheet removes gap between the cover-glass and the photo anode. A glass (A in Fig. 5.3)/plastic films/a photo anode consisting of porous titania layer (B) and FTS-MH (D), a glass mesh paper (30μm thick) working as a supporter of electrolyte (E), and a counter electrode (F) were piled up consecutively for preparing the solar cell. Electrolyte (E1) was injected to the glass paper and the space of the glass paper was filled with E1. The electrolyte composition (E1) is as follows: 0.05 M Iodine (I_2), 0.1 M Lithium Iodine (LiI), 0.5 M 4-tert-Butylpyridine and 0.6 M 1,2-dimethyl-3 propylimidazolium iodine in acetonitrile. The glass mesh paper holds the electrolyte E1 and prevents the cell from short circuit. Finally, epoxy resin was used to seal the cell. Device 2- H_2O_2 was prepared in the method similar to the Device 4- H_2O_2 except that the counter Pt/Ti electrode was replaced with a Pt/FTO glass.

5.1.3 Result and discussion

A. Hydrogen Peroxide Treatment

It has been reported that by H_2O_2 treatment of titanium mesh nanosheets of TiO_2 on titanium mesh surface are grown[14]. Figure 5.4 shows the Scanning Electron

Microscopy (SEM) pictures of untreated (A) and H_2O_2 treated (B) FTS-MH sheet. The formation of nanosheets were clearly observed after the H_2O_2 treatment of the titanium surface (see Figure 5.4 for magnification up to nanoscale for untreated (C) and H_2O_2 treated (D)). We expected that these nanosheets increased surface contacts between the FTS-MH and TiO_2 porous layer and lead to better electron transport between Ti FTS-MH and the porous titania layer. In photo anode, the first layer of TiO_2 with 400nm particles size served as base layer and to cover 100µm holes in FTS-MH. Without the first layer, uniform coating was difficult to achieve and TiO_2 layers tended to crack after annealing process due to weak contact between them. This layer also works as light scattering layers to enhance light absorption inside the photo-anode. Second layer of TiO_2, 30nm particles size, serve as dye adsorption layer.

Table 5.1 and Figure 5.5 (A) shows the I-V characteristics of DSSCs with untreated FTS-MH and H_2O_2 treated FTS-MH with FTO counter electrode (Device 1) and DSSCs with untreated FTS-MH and H_2O_2 treated FTS-MH with Ti counter electrode (Device 3). Titanium sheet sputtered with platinum (Ti-CE) was used as the counter electrode along with FTO based counter electrode, since Ti Sheet has lower resistance compared with TCO glasses[15]. Untreated FTS-MH shows hampered PCE compared with treated one for both of Device 1 and Device 3. Efficiency, Jsc, Voc and fill factor were 4.94 %, 10.18 mA/cm^2, 0.67 V and 0.73, for untreated FTS-MH with Ti-CE (Device 3-W/O), respectively. TCO-less DSSC with untreated FTS-MH and FTO-CE (Device 1-W/O) had photovoltaic performances of PCE 4.68 %, Jsc 9.72 mA/cm^2, Voc 0.66 V and fill factor 0.73. Devices treated with hydrogen peroxide gave better results. Efficiency, Jsc, Voc and fill factor ware 6.33%, 11.92 mA/cm^2, 0.71 V and 0.75, for H_2O_2 treated FTS-MH with Ti-CE (Device 3- H_2O_2), respectively. TCO-less DSSC with H_2O_2 treated FTS-MH and FTO-CE (Device 1- H_2O_2) had slightly lower photovoltaic performances of PCE 6.05 %, Jsc 11.15 mA/cm^2, Voc 0.73 V and fill factor 0.75.

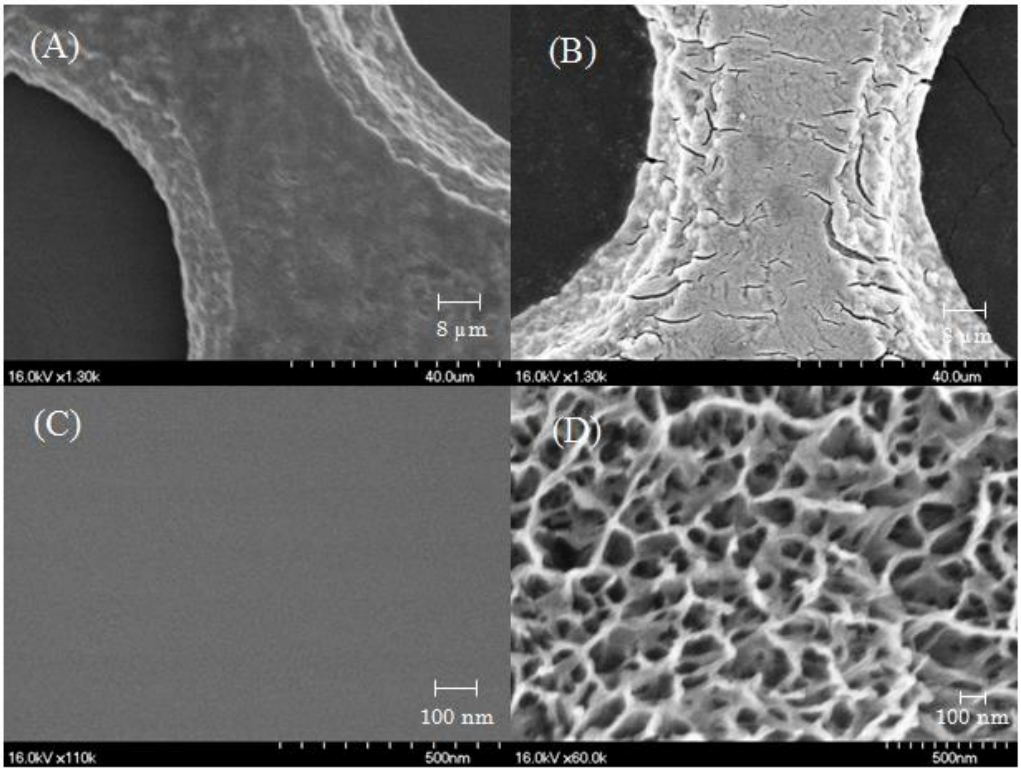

Figure 5.4 *SEM pictures of untreated FTS-MH (left) and H_2O_2 treated FTS-MH (right)*

Table 5.1 *I-V Characteristics for untreated and H_2O_2 treated cells*

	Ti-Pt Counter electrode		FTO-Pt Counter electrode	
	H_2O_2 Treated FTS-ME	untreated FTS-ME	H_2O_2 Treated FTS-ME	untreated FTS-ME
Jsc (mA/cm^2)	11.92	10.18	11.15	9.72
Voc (V)	0.71	0.67	0.73	0.66
FF	0.75	0.73	0.75	0.73
η (%)	6.33	4.94	6.05	4.68

The increase in the Jsc is explained by the lower interfacial resistance between H_2O_2 treated FTS-MH and porous titania. Another benefit from H_2O_2 treatment was the suppression of charge recombination between electrons in FTS-MH and I_3^- of electrolyte. It has been already known that titanium has oxidized overlayer on its

surface. The chemical reaction of FTS-MH surface by H_2O_2 further enhances the formation of TiOx layer, leading to suppress the charge recombination of electrons in FTS-MH and I_3^- of the electrolyte.

(A)

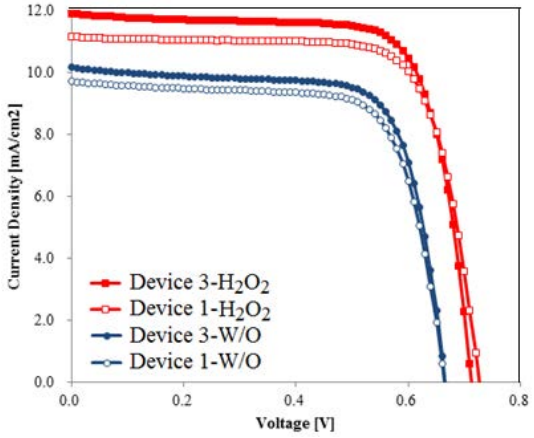

(B)

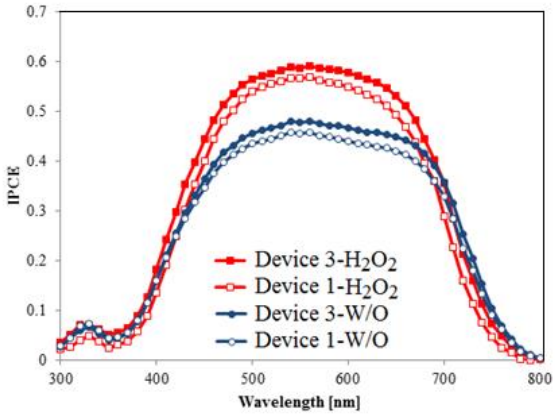

Figure 5.5 *I-V (A) and IPCE (B) characteristics for Device 1 and Device 3 before and after H_2O_2 treatment of FTS-MH. Device 3-H_2O_2: Device 3 consisting of H_2O_2 treated FTS-MH, Device 1-H_2O_2: Device 1 consisting of H_2O_2 treated FTS-MH, Device 3-W/O: Device 3 consisting of untreated FTS-MH, Device 1-W/O: Device 1 consisting of untreated FTS-MH.*

The enhancement of open circuit voltage (Voc)[16] is explained by the formation of charge recombination blocking layer. IPCE of TCO-less DSSC with FTS-MH treated with H_2O_2 was higher than that without H_2O_2 treatment for both of Device 1 and Device 3. However, the shape of the IPCE curve for the former was similar to that for the latter, suggesting that H_2O_2 treatment does not affect light scattering issue.

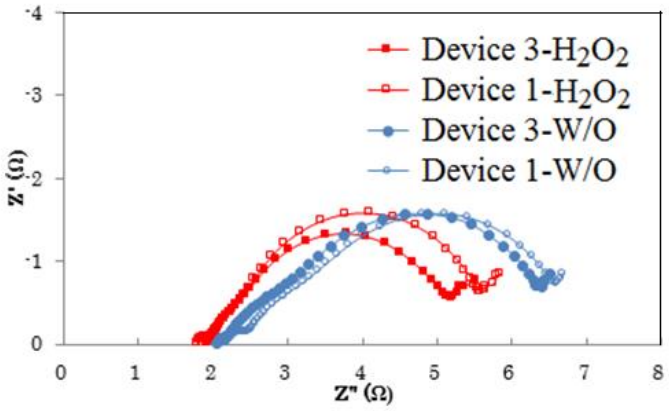

Figure 5.6 *Cole-cole plot for Device 1 and Device 3 before and after H_2O_2 treatment of FTS-MH.*

Electrochemical Impedance Spectroscopy (EIS) of TCO-less DSSCs with untreated FTS-MH and H_2O_2 treated FTS-MH for both of Device 1 and Device 3 are shown in Figure 5.6. A semi-circle observed at higher frequency, middle frequency and lower frequency are associated with resistance of interface at Pt/electrolyte of the counter electrode, TiO_2/Dye/electrolyte and FTO/(Dye)/electrolyte interfaces, and diffusion of I^-/I_3^- redox in the electrolyte. Treated FTS-MH showed lower series resistance and smaller semi-circle compared to the untreated FTS-MH for both of Device 1 and Device 3. The lower series resistance is attributed to the porous structure fabricated on the Ti sheet as shown in Figure 5.4, where the contact areas between FTS-MH and porous titania layer increase. In midde and high frequency, treated FTS-MH also gave lower semi-circle assosiated with lower resistance on TiO_2/Dye/electrolyte and FTO/(Dye)/electrolyte interfaces due to transformation of TiOx layer into TiO_2 nanosheets.

In order to obtain more informations about the reason behind higher the Jsc on treated FTS-MH, dye loading measurement was done by same method in previous chapter. Dye loading was measured and calculated by comparing the desorption of N719 dyes with calibration curve from known concentration of dye and divided by the total area of titania layer. Dye solutions with certain concentration was measured with UV-vis spectroscopy and plotted to determine the equation for calibration curve. In order to desorbed the dyes from titania surface, the mixture of NaOH (0.1mM), ethanol, t-butyl alcohol and acetonitrile (vol 1:1:1:1) was used. Desorption dye solution was

taken and calculated with calibration curve of knowing concentration. At last, the concentration of desorbed dyes from unterated and treated FTS-MH were divided by the active area.

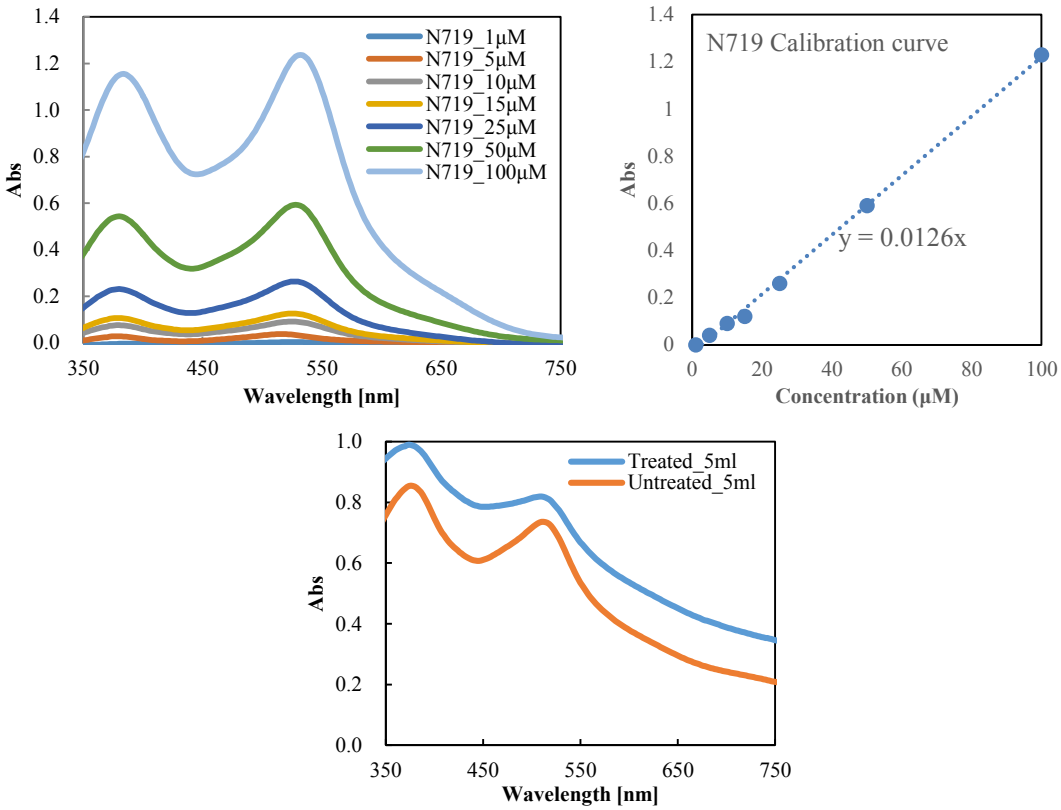

Figure 5.7 Calibration curves and UV-VIS spectra desorbed dye for treated and untreated FTS-MH.

Treated FTS-MH had absorption peak for desorbed dye of 0.81, which corresponds to concentration of 67.27 µM. Since the concentration taken in 5 ml, the concentration of dye desorbed was 336.35 nmole. The active area of titania is 1 cm^2, gave final dye loading for H_2O_2 treated is 336.35 nmole/cm^2. The same method was done for untreated FTS-MH. It had absorption peak for desorbed dye of 0.74, which corresponds to concentration of 61.71 µM. Since 5 ml of the solution was taken, the concentration of dye desorbed was 308.55 nmole. The active area of titania is 1 cm^2, gave final dye loading for untreated FTS-MH is 308.55 nmole/cm^2.

B. Reduction of electrolytic gap

In conventional DSSC with TCO layers, TiO_2 layer is prepared directly on the FTO-surface, therefore, there is almost no gap between them. However, in Device 1 and Device 3, a photo anode floats between a top cover glass and a counter electrode. Therefore, there is gap (C in Fig 5.3) between a top cover glass and the photo anode, where electrolyte with redox couple is filled. Redox electrolyte couple I^-/I_3^- used in the system has absorption peak at 360 nm, which decreases the photon density reaching the photo anode. To suppress this phenomenon, we put a plastic spacer (C in Fig. 5.3) to reduce the gap between the photo anode (B) and the top cover glass (A).

Table 5.2 *I-V Characteristics for H_2O_2 treated cells with plastic spacer.*

	H_2O_2 Treated FTS-ME With plastic spacer	
	Ti-Pt CE	FTO-Pt CE
Jsc (mA/cm^2)	13.46	12.34
Voc (V)	0.73	0.74
FF	0.73	0.71
η (%)	7.25	6.43

In Figure 5.8, IPCE at 300–400nm region for both of Device 4 and Device 2 structures increased to 30% which is higher than cells fabricated without plastic spacer (Device 1 and Device 3). Photovoltaic parameters and I-V characteristic shown in Table 5.2, shows Jsc enhancement from 11.15 mA/cm^2 (Device 1- H_2O_2) to 12.34 mA/cm^2 with PCE 6.43 % in FTO-CE (Device 2- H_2O_2) and from 11.92 mA/cm^2 (Device 3- H_2O_2) to 13.46 mA/cm^2 with overall PCE 7.25 % in case of Ti-CE (Device 4- H_2O_2) after the plastic sheet insertion.

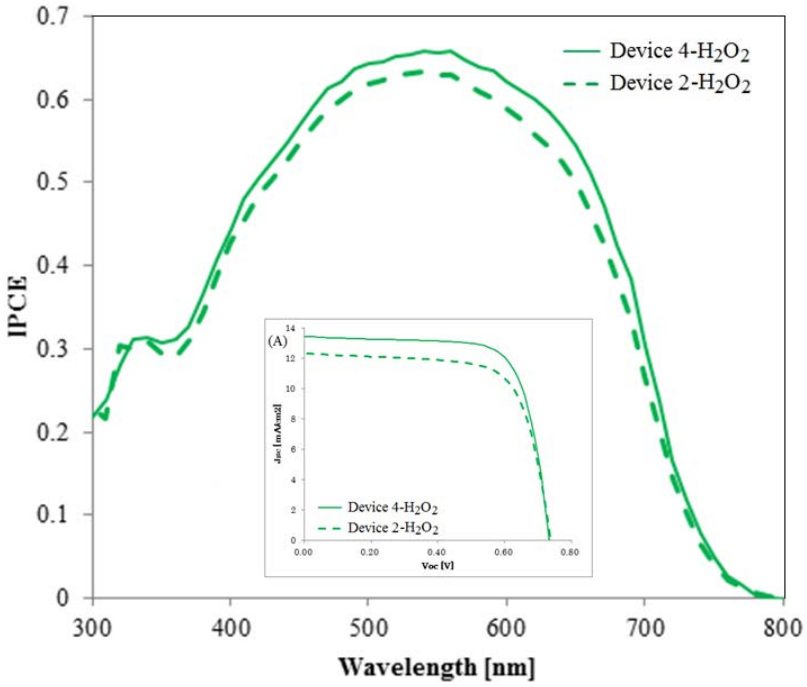

Figure 5.8 IPCE characteristic for devices with plastic spacer (Device 2 and Device 4). Device 2-H_2O_2: Device 2 consisting of H_2O_2 treated FTS-MH. Device 4-H_2O_2: Device 4 consisting of H_2O_2 treated FTS-MH. Inset; I-V graph.

5.1.4 Conclusion

In summary, TCO-less DSSCs consisting of FTS-MH treated with H_2O_2 gave better PCE compared to those with untreated one. Due to formation of the nano-titania on the sheets, the contact between FTS-MH and nanoporous TiO_2 layer were improved and enhancement of Jsc was observed. PCE of Device 3 was enhanced from 4.94% to 6.33% after the H_2O_2 treatment. Removing electrolytic gap in device (Fig. 5.3) increased IPCE in 300 – 400 nm wavelength region up to 30 % and overall efficiency of 7.25 % was observed for Device 4.

5.2 Cylinder TCO-less DSSCs

Flat titanium sheet with micro holes (FTS-MH) was successfully applied to fabricate cylinder transparent-conductive oxide less dye-sensitized solar cells (TCO-less DSSCs) with back contact electrodes. FTS-MH allows us to fabricate cylinder solar cells with ease and simplicily, compared to cylinder based TCO-less DSSCs reported before. FTS-MH allowed us to create flexible electrodes due to flexible nature of titanium sheet. FTS-MH utilized as working and counter electrodes with 20μm thick is bendable to 360 degrees without changing the structure. Overall photo-conversion efficiency could reach up to 8.5 % under simulated solar irradiation, making it among highest efficiency for cylinder TCO-less DSSCs structure.

5.2.1 Introduction

Nowadays, research on solar cells not only limited to materials research but also taking another step to strcutural design. Researchers have demanded to develop solar panels which is inexpensive and more efficient than conventional solar panels. The new technique consists of cylindrical solar cells which are made of thin-film semiconductor material that is deposited on a glass tube had already been carried on in past few years by Solyndra[17]. However, in september 2011 the company filled for bankruptcy due to decline of silicon price, which made them unable to compete with conventional crystalline silicon solar cells[18,19]. DSSCs itself is a low cost solar cells compared with silicon based solar cell[20]. With this predominance, cylindical DSSCs is expected to compete with silicon solar cell. Cylinderical structure has many advantages, compared to conventional flat structures. Cylindrical solar panels which absorb more light in a day, which means can produce more power. Besides generating more electricity, the cylindrical solar panels offer less wind resistance. These kinds of solar cells do not need to be secured or reinforced like conventional solar panels. The space between the tubes in cylindrical solar cell allow wind to past trough. At any point in a day, the sun will hit a part of the solar cells. Conventional flat solar panels need tracking systems that will change the photovoltaic cells facing the sun[21]. However, they are costly, difficult to maintain, cannot withstand heavy winds, and they consume a lot of space where solar panel can be intalled instead. Tachan and

his group reported the effectiveness of cylindrical architecture on sealing area which can be reduced up to one-third in similar area of flat solar cells[22]. Our group has been also working in cylindrical DSSCs in past 5 years. Learning from TCO-less structure, cylindrical TCO-less DSSCs with SUS mesh as photo anode supporter can produce 11.94 mA/cm^2 of Jsc with 5.58 % of PCE under AM1.5 simulated solar irradiation[23]. Nevertheless, SUS mesh required a blocking protection with sputtering Ti over it. Without the Ti protection, electron recombination will be much higher[24,25]. Our group also reported coil type of cylindrical DSSCs (CC-DSSCs) with titanium wire to subtitute SUS mesh in previous report[26]. Titanium is strong, light in weight and do not react with electrolyte, which makes it better choice than other metallic materials. However, coating methode on the top of wraped coil in CC-DSSCs is still not effective. In this report, we used flat titanium mesh with micro holes (FTS-MH) as photo anode supporter to replace SUS mesh and titanium wire in CC-DSSCs. FTS-MH (20μm thick) is flexible and strong material which is durable enough to bend 360 degree without damaging the photo anodes. FTS-MH has holes with 100μm diameter, allowing electrolyte to freely move between photo anode and counter electrodes.

5.2.2 Experimental detail

5.2.2.1 Materials

Flat titanium sheet with micro holes (FTS-MH) was received from Ushio Inc., Japan. In this experiment, untreated FTS-MH and one treated with H_2O_2 were used as photo-electrodes. Titanium dioxide (TiO_2) PST-400C and PST-30NRD were purchased from Catalysts and Chemical Co. Ltd Japan. Ruthenizer 535-bis TBA (OPV-N719; Di-tetrabutylammoniumcis-bis (isothiocyanato) bis (2,2'-bipyridyl-4,4'-dicarboxylato) ruthenium(II)) from OPV Tech was employed for this experiment. Glass paper with 50μm thickness as spacer between photo anode and counter electrode was used. Heat shrinkable tube (NF070, FEP) was purchased from JUNFLON Junkosha Inc. Japan.

5.2.2.2 Cell Fabrication

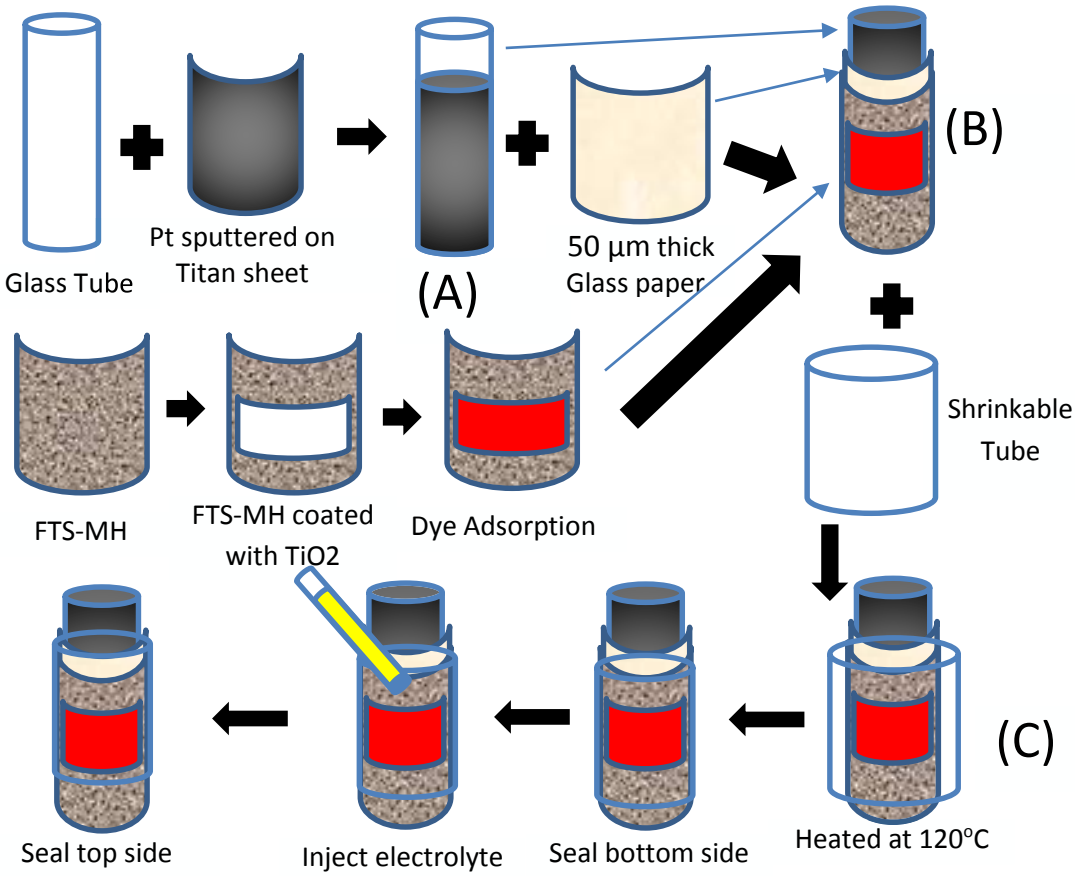

Figure 5.9 Device fabrication process for cylindical TCO-less DSSC with FTS-MH

Cylindrical glass was wrapped with Titanium foils sputtered with Pt. To stick them together, plastic spacer was used as a *glue*. Titanium foil/plastic spacer/cylinder glass was heated at 120°C on a hotplate to melt the spacer while applying a pressure on the sandwich structure (A in Fig. 5.8). Photo-electrodes for cylinder TCO-less DSSCs was prepared with the method same as that to flat TCO-less DSSCs mentioned above. Glass paper as a spacer and FTS-MH coated TiO_2 and dye was bent at 360 degree to wrap the counter electrode (B in Fig. 5.8). After all were wrapped together, its then inserted to heat shrinkable tube and heated at 120°C for 30 seconds (C in Fig. 5.8). This heat shrinkable tube will reduce the gap between photo anodes and counter

electrodes and held the structure tightly. One side of the cylinder was sealed with UV-resin and solidified with UV-light. Electrolyte (E1) was inserted into the glass paper gap. Finally, the other sides of device was sealed with UV resin. Silver paste was applied on both poles. Preparation and assembly process are shown in Figure 5.9.

5.2.3 Result and discussion

Figure 5.10 shows the I-V characteristics of cylinder TCO-less DSSCs with untreated FTS-MH and H_2O_2 treated FTS-MH with Ti counter electrode. Titanium sheet sputtered with platinum (Ti-CE) was used as the counter electrode not only because Ti Sheet has lower resistance compared with TCO glasses but also that Ti sheet has flexibility, allowing us to bend it up to 360 degree.

Device fabricated with untreated FTS-MH showed lower PCE compared with treated one. Efficiency, Jsc, Voc and fill factor were 5.76 %, 10.79 mA/cm^2, 0.74 V and 0.72, for untreated FTS-MH, respectively. Devices treated with hydrogen peroxide gave better results. Efficiency, Jsc, Voc and fill factor were 8.59%, 16.19 mA/cm^2, 0.76 V and 0.70, for H_2O_2 treated FTS-MH, respectively.

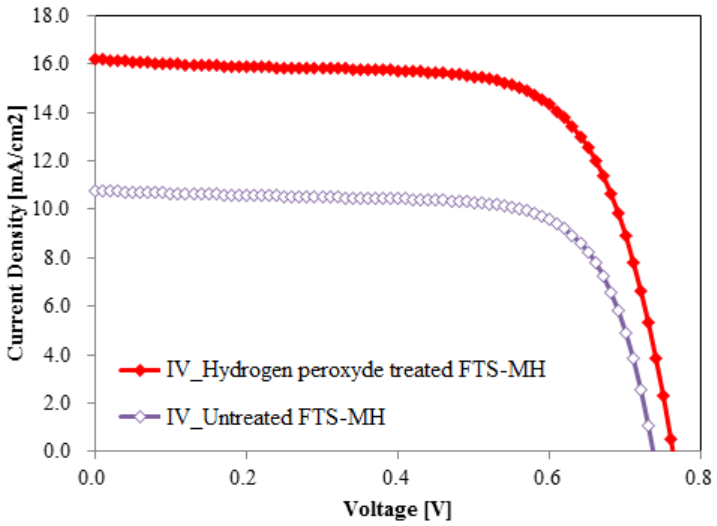

Figure 5.10 I-V characteristics for device before and after H_2O_2 treatment of FTS-MH.

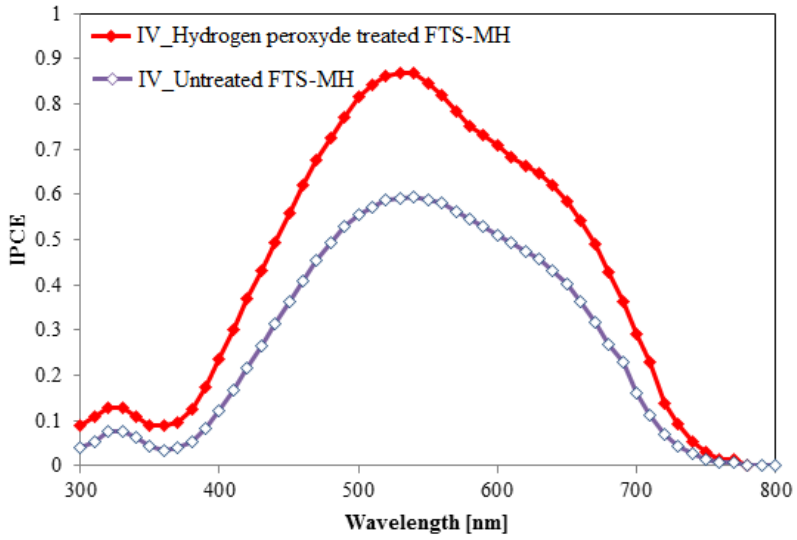

Figure 5.10 *IPCE characteristics for devices with and without H_2O_2 treatment on FTS-MH of Cylinder TCO-less DSSCs.*

The H_2O_2 treatment plays important role to enhance the PCE. The nanosheets were created by chemical etching process between titanium surface and hydrogen peroxide as shown in Figure 5.4. The enhancement of open circuit voltage (Voc) is explained by the formation of charge recombination blocking layer. Nanosheets on treated FTS-MH suppress the charge recombination of electrons in FTS-MH and I_3^- in the electrolyte. IPCE of TCO-less DSSC with FTS-MH treated with H_2O_2 was higher than that without H_2O_2 treatment because of enhancement of electron injections clarified by the lower interfacial resistance between H_2O_2 treated FTS-MH and porous titania.

5.2.4 Conclusion

In conclusion, cylindrical TCO-less DSSCs have been successfully fabricated with high efficiency. Formation of the nano-titania on the titanium sheets made the contact between FTS-MH and nanoporous TiO_2 layer better, which led to enhancement of

Jsc. Suppression of electron recombination leading to improvement Voc. PCE was enhanced from 5.76% to 8.59% after the H_2O_2 treatment. According to our knowledge, this result is highest PCE for TCO-less DSSCs with cylindrical structure.

5.3 References for Chapter 5

1) B. O'Reagan, M. Grätzel, *Nature*, **353**, 737, (1991).

2) S. Mathew, A. Yella, P. Gao, R.H.-Baker, B.F.E. Curchod, N.A.-Astani, I. Tavernelli, U. Rothlisberger, Md.K. Nazeeruddin and M. Grätzel, *Nature Chemistry***, 6**, 242–247, (2014).

3) A.F. Nogueira, C. Longo and M.-A. De Paoli, *Coordination Chemistry Reviews*, **248** 13–14, 1455–1468, (2004).

4) C. Longo, A. F. Nogueira, M. A. De Paoli and H. Cachet, *J. Phys.Chem. B*, **106**, 5925, (2002).

5) J. Nemoto, M. Sakata, T. Hoshi, H. Ueno and M. Kaneko, *J. of Electroanalytical Chemistry*, **599**, 23–30, (2007).

6) T. N. Murakami, Y. Kijitori, N. Kawashima and T. Miyasaka, *Chem.Lett.*, 1076, (2003).

7) S. Uchida, M. Tomiha, H. Takizawa and M. Kawaraya, *J. Photochem.Photobiol., A*, **164**, 93, (2004).

8) N. Fuke, A. Fukui, A. Islam, R. Komiya, R. Yamanaka, L. Huan and H. Harima, *Journal of Applied Physics,* **104**, 064307, (2008).

9) X. Huang, P. Shen, B. Zhao, X. Feng, S. Jiang, H. Chen, H. Li and S. Tan, *Solar Energy Materials & Solar Cells,* **94**, 1005-1010, (2010).

10) X. Fan, F. Wang, Z. Chu, L. Chen, C. Zhang, and D. Zou. *Applied Physics Letters*, **90**, 073501, (2007).

11) Md.Z. Molla, N. Mizukoshi, H. Furukawa, Y. Ogomi, S.S. Pandey, T. Ma and S. Hayase, *Prog. Photovolt: Res. Appl.,* (2014).

12) Y. Kashiwa, Y. Yoshida and S. Hayase, *Applied Physics Letters*, **92**, 033308-1–033308-3, (2008).

13) J.M. Kroon, N.J. Bakker, H.J.P. Smit, P. Liska, K.R. Thampi, P. Wang, S.M. Zakeeruddin, M. Grätzel, A. Hinsch, S. Hore, U. Wűrfel, R. Sastrawan, J.R. Durrant, E. Palomares, H. Pettersson, T. Gruszecki, J. Walter, K. Skupien and G. E. Tulloch, *Prog. Photovolt: Res. Appl*., **15**, 1–18, (2007).

14) T.-Y. Tsai, C.-M. Chen, S.-J. Cherng and S.-Y. Suen, *Prog. Photovolt: Res. Appl.*, **21**, 226–231, (2013).

15) J. Jaus, H. Pantsar, O.F. Adurodija, B. Li, B. Regaard, H. Herfurth and D. Doble, *35th IEEE Photovoltaic Specialists Conference (PVSC)*, 002429 – 002432, (2010).

16) G. Kapil, S.S. Pandey, Y. Ogomi, T. Ma and S. Hayase, *Organic Electronics*, **15**, 3399–3405, (2014).

17) C.L. Melissa "Solyndra — Illuminating Energy Funding Flaws?", *Scientific American*, (2011).

18) M. Bathon, "Solyndra Lenders Ahead of Government Won't Recover Fully". *Bloomberg Business*. (2011). Retrieved 2 May 2015.

19) R.D. White, "Solar panel firm Solyndra to cease operations". Los Angeles Times (2011). Retrieved 2 May 2015.

20) J. Kalowekamo and E. Baker, *Solar Energy*, **83***,* 8, 1224-1231, (2009).

21) S. Rahman, R.A. Ferdaus, M.A. Mannan and M.A. Mohammed, *American Academic & Scholarly Research Journal*, **5***,* 1, 47-54, (2013).

22) Z. Tachan, S. Rühle and A. Zaban, *Solar Energy Materials and Solar Cells*, *94*(2), 317-322, (2010).

23) J. Usagawa, S.S. Pandey, Y. Ogomi, S. Noguchi, Y. Yamaguchi and S. Hayase, *Progress in Photovoltaics: Research and Applications*, **21***,* 4, 517-524, (2013).

24) A.K. Baranwal, T. Shiki, Y. Ogomi, S.S. Pandey, T. Ma and S. Hayase, *RSC Advances*, **4***,* 88, 47735-47742, (2014).

25) J. Usagawa, T. Kogo, K. Sadamasu, S.S. Pandey, Y. Ogomi and S. Hayase, *Journal of Photonics for Energy*, *2*(1), 021011-1, (2012).

26) G. Kapil, J. Ohara, Y. Ogomi, S.S. Pandey, T. Ma and S. Hayase, *RSC Advances*, **4***,* 44, 22959-22963, (2014).

Chapter 6 Conclusion and Future Prospects

6. 1 Conclusions

In this work, we studied the axially anchored Phosphorus-Phthalocyanine dye on TiO_2 surface without special anchoring groups and utilization of flat titanium sheet with micro holes for TCO-less application on flat and cylindrical structures.

We found that phosphorous-phthalocyanine without the conventional anchoring group (–COOH) can be well adsorbed on TiO_2 with Ti–O–P linkages. XPS measurement showed shifted binding energy on TiO_2 surface after the introduction of PPc dyes. The higher efficiency of DSSC-PPc-1 can be explained by the longer excitation lifetime and higher dye concentration on a porous TiO_2 layer. The introduction of electron withdrawing groups at the α-position of the phthalocyanine ring on PPc-1 decreased the HOMO level, which matched the requirement of DSSCs. The LUMO levels of PPc-1 and PPc-2 are −3.67 and −3.44 eV, respectively. These LUMO energy levels were shallower than that of the TiO_2 conduction band (−4.0 eV), suggesting that the electron injection from these LUMOs to the TiO_2 conduction band is possible. The HOMO levels of PPc-1 and PPc-2 are −5.28 and −4.95 eV, respectively. Since the I^-/I_3^- redox potential is −4.9 eV, electron injection from the I^-/I_3^- redox level to the HOMO of PPc-1 is possible (dye regeneration). However, electron injection to the HOMO of PPc-2 may be difficult because of the small energy level difference (0.05 eV) between the I^-/I_3^- redox level and the HOMO of PPc-2. These sufficient energy level differences between the LUMO of PPc-1 and the TiO_2 conduction band, and that between the HOMO of PPc-1 and the I^-/I_3^- redox level help to enhance PPc-1 performances than PPc-2. We have proposed an approach to stain the TiO_2 surface with symmetrical phthalocyanine, which can be synthesized much more easily than unsymmetrical phthalocyanine with carboxylic anchoring groups. This will provide a direction to photo conversion in IR regions where the synthesis of unsymmetrical phthalocyanine with carboxylic acids is much harder.

We found that TCO-less DSSCs consisting of FTS-MH treated with H_2O_2 gave better PCE compared to those with untreated one. The increase in the Jsc was

explained by the lower interfacial resistance between H_2O_2 treated FTS-MH and porous titania. Another benefit from H_2O_2 treatment was the suppression of charge recombination between electrons in FTS-MH and I_3^- in electrolyte. It has been already known that titanium has oxidized overlayer on its surface. The chemical reaction of FTS-MH surface by H_2O_2 further enhanced the formation of TiOx layer, leading to suppress the charge recombination of electrons in FTS-MH and I_3^- in the electrolyte. Due to formation of the nano-titania on the sheets, the contact between TiO_2 and metal grid collectors was improved, leading to iprovement of Jsc.

In the devices with flat structures, PCE was enhanced from 4.94% to 6.33% after the H_2O_2 treatment. Another enhancement was acquired from removing gap in the device by inserting plastic spacer, which increased IPCE in 300 – 400 nm regions up to 30 %. Overall efficiency of 7.25 % was observed.

In the devices with cylindrical structures, the same effect of H_2O_2 treatment resulting in formation of the nano-titania on the titanium sheets made the contact between FTS-MH and nanoporous TiO_2 layer better and led to enhancement of Jsc. Suppression of electron recombination that improved Voc was also observed. PCE was enhanced from 5.76% to 8.59% after the H_2O_2 treatment. According to our knowledge, this result is highest PCE for cylindrical structure TCO-less DSSCs.

6.2 Future Prospects

We propose an approach of narrow gap electron injection from axial ligation of phthalocyanine dyes to TiO_2 surfaces, which opens possibilities of other dyes with symmetrical structure to be used as sensitizer in DSSCs. Synthesizing symmetrical dyes are much easier than unsymmetrical structure with carboxylic anchoring groups. This report will provide a direction to photo conversion in IR regions where the synthesis of unsymmetrical phthalocyanine with carboxylic acids is much harder.

CONCLUSION AND FUTURE PROSPECTS

FTS-MH has been shown to have advantage in flat and cylindrical structure. This will open possibilities to use TCO-less with FTS-MH in tandem structure or hybrid dyes in cylindrical structure to achieve high efficiency DSSCs.

PPc-1 synthetizes process

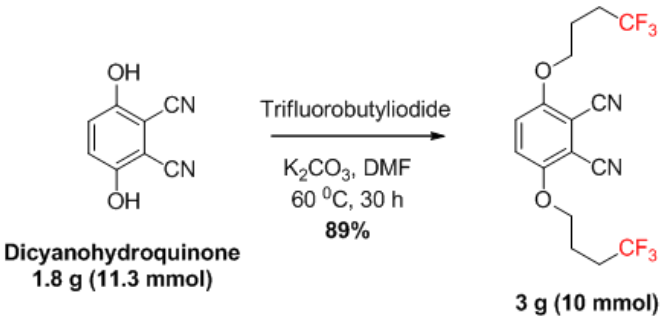

Dicyanohydroquinone
1.8 g (11.3 mmol)

3 g (10 mmol)

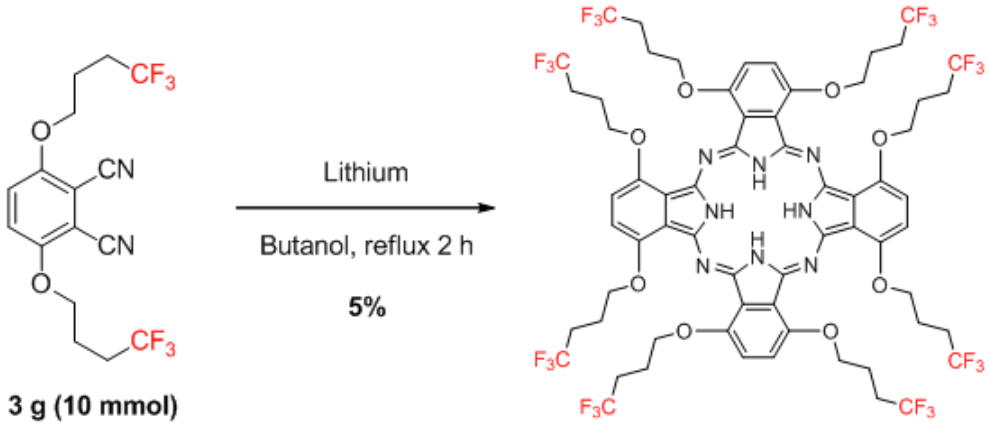

3 g (10 mmol)

600 mg (0.4 mmol)

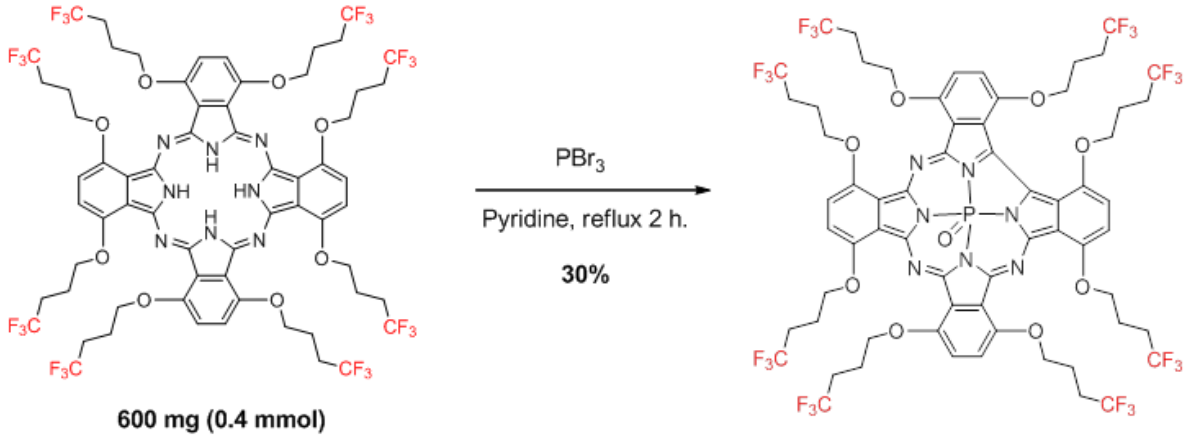

600 mg (0.4 mmol)

PPc-2 synthetizes process

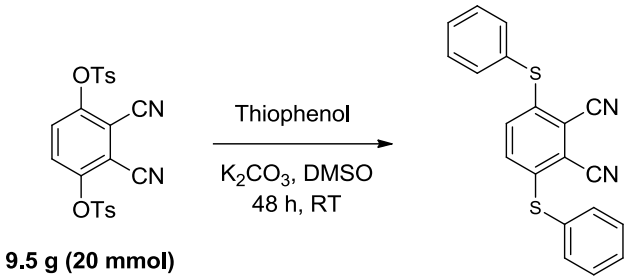

9.5 g (20 mmol)

1st purification batch = 1.3 g (3.8 mmol)

2nd purification batch = 2.5 g (7.3 mmol)

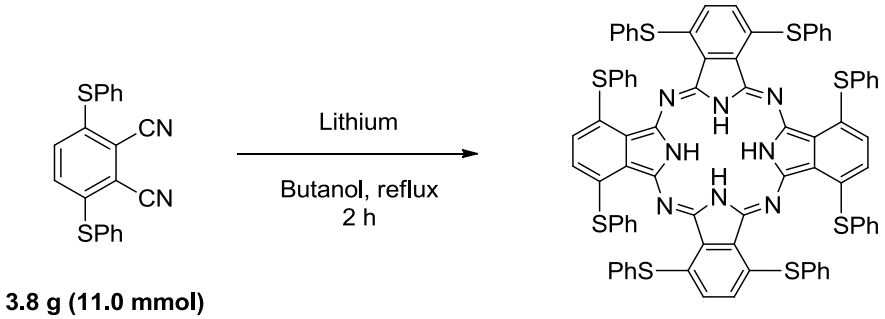

3.8 g (11.0 mmol)

2 g
after column purification

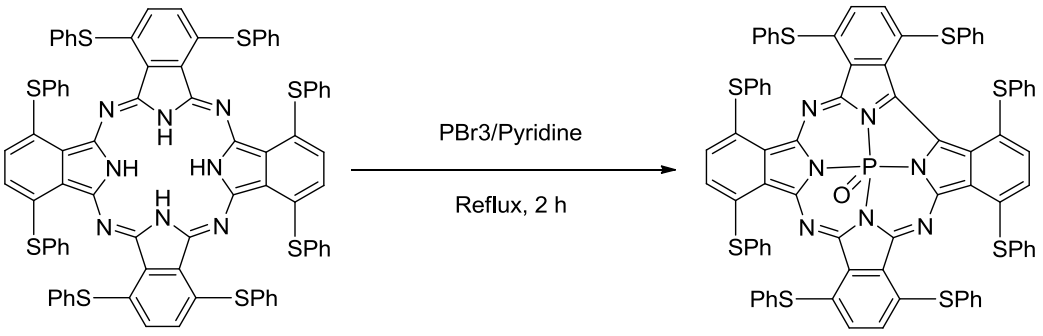

2.0 g (1.5 mmol)

1.46 g
(Crude before column)

APPENDIX

H_2O_2 treated FTS-MH and Untreated FTS-MH

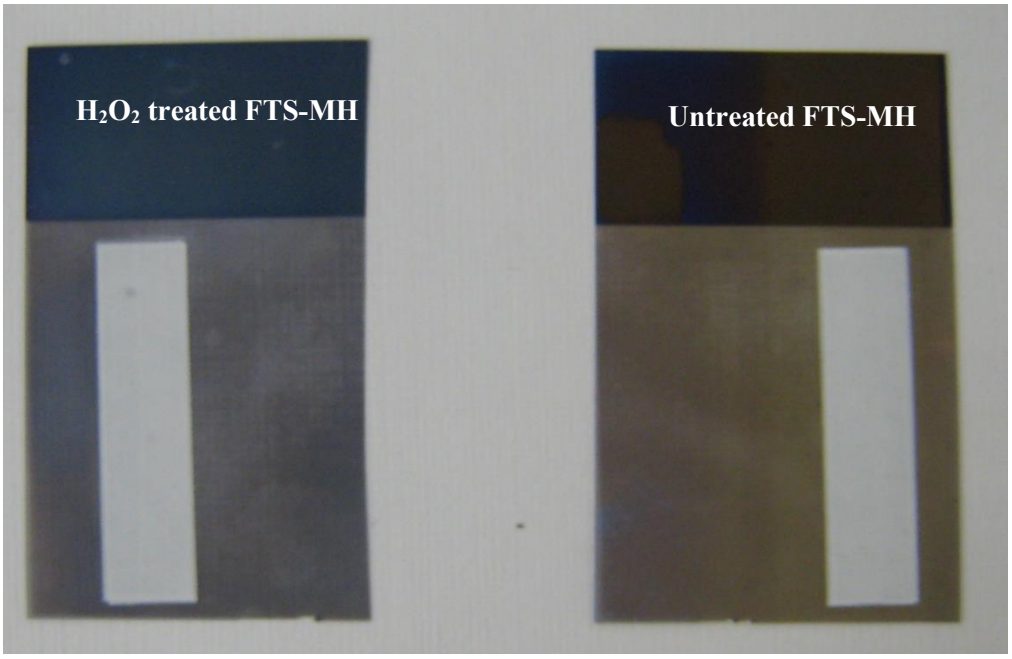

Glass paper as spacer and electrolyte holder

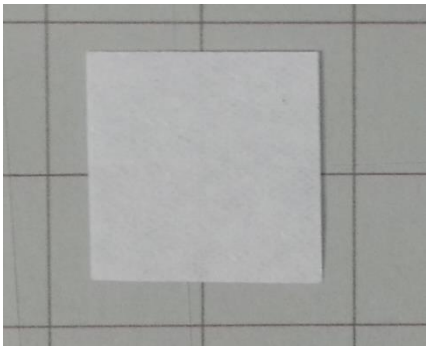

FTS-MH coated with TiO_2 and Dye

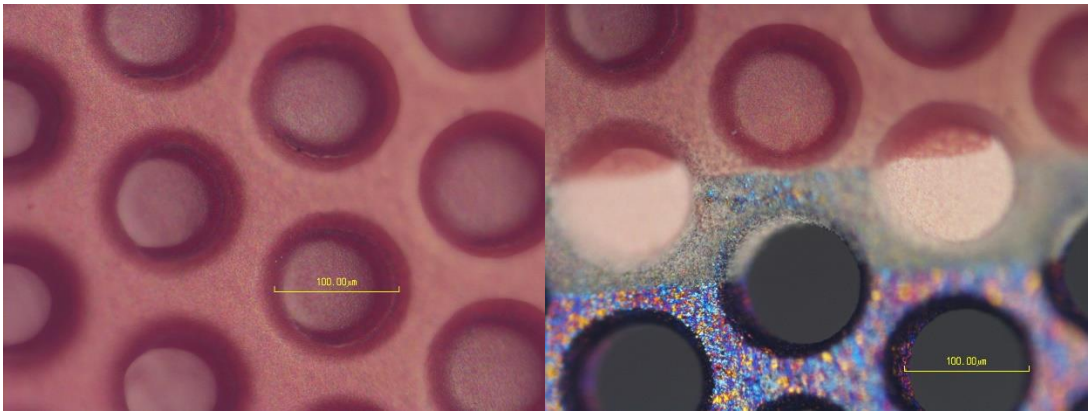

FTS-MH from Top side

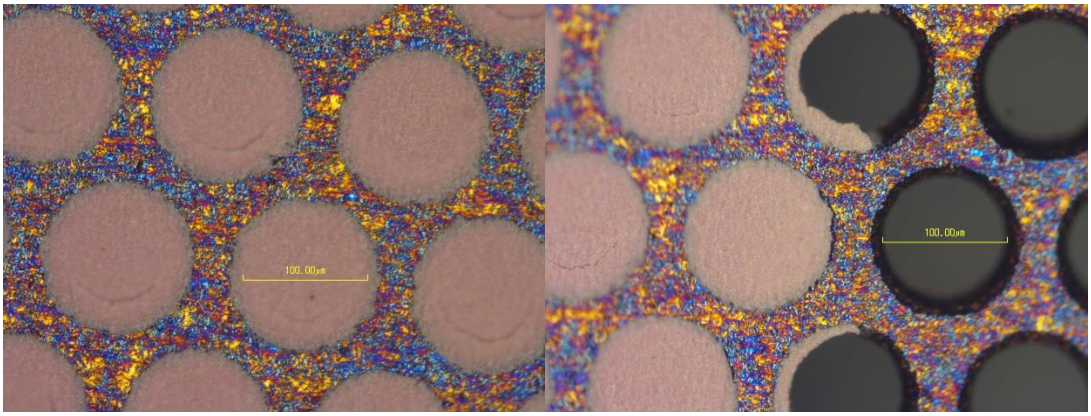

FTS-MH from back side

Cylindrical TCO-less DSSCs with FTS-MH

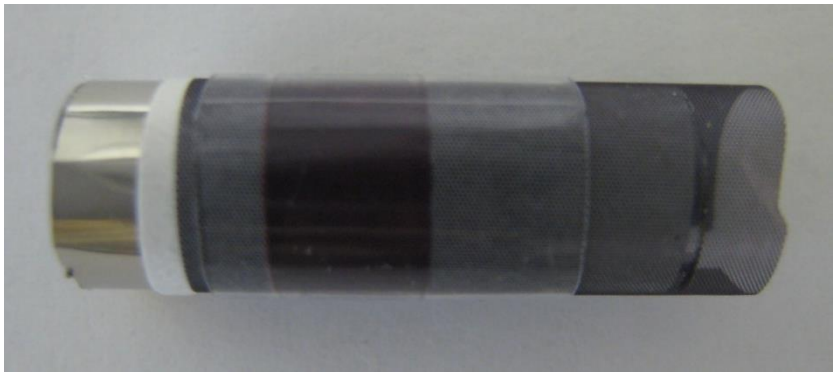

Cylindrical TCO-less with FTS-MH before inserting the electrolyte

Final cell after injecting the electrolyte and sealing with UV-resin.

APPENDIX

FEP Heat-Shrinkable tube Specification

Features	• Excellent heat and cold resistance. • Temperature range for continuous no-load use FEP<-65 ~ +200ºC. • Inactive in regard to almost chemicals and solvents. • Excellent resistance to weather and does not change with age. • Almost nothing sticks to it, and even if it does, it is easily to remove. • Flame-resistant. • Excellent electrical characteristics.
Uses	• Protective covering for electrical leads of thermistors, liquid transport equipment and applications which require chemical resistance and non-adhesiveness. • Protection of tiny elements such as sensors. • To give rolls and similar items non-adhesiveness. • Protective covering that give chemical resistance at high temperatures.

Achievement

Publications

1. **Azwar Hayat**, Gururaj M. Shivashimpi, Terumi Nishimura, Naotaka Fujikawa, Yuhei Ogomi, Yoshihiro Yamaguchi, Shyam S. Pandey, Tingli Ma and Shuzi Hayase, **Dye sensitized solar cells based on axially ligated Phosphorus-Phthalocyanine dyes**, *Applied Physics Express*, **8**, 047001 (2015).

2. Gururaj M. Shivashimpi, Shyam S. Pandey, **Azwar Hayat**, Naotaka Fujikawa, Yuhei Ogomi, Yoshihiro Yamaguchi and Shuzi Hayase, **Far-red sensitizing octatrifluorobutoxy phosphorous triazatetrabenzocorrole: Synthesis, spectral characterization and aggregation studies**, *Journal of Photochemistry and Photobiology A: Chemistry,* **289**, 53-59 (2014).

Publications unrelated to thesis

1. **Azwar Hayat**, Shyam S. Pandey, Yuhei Ogomi and Shuzi Hayase, **Relationship between I_3^- diffusion in titania nanopores modified with dyes and open circuit voltage of Dye-sensitized solar cell**, *Journal of the Electrochemical Society*, **158**, 7, B770-B771 (2011).

2. Shyam S. Pandey, Kyung-Young Lee, **Azwar Hayat**, Yuhei Ogomi and Shuzi Hayase, **Investigating the role of dye dipole on open circuit voltage in solid-state Dye-sensitized solar cells**, *Japanese Journal of Applied Physics*, **50**, 06GF08 (2011).

Conferences

1. **Oral**; Dye sensitized solar cells based on axially ligated Phosphorus (III) Phthalocyanine dyes, **Azwar Hayat**, Terumi Nishimura, Shivashimpi Gururaj, Yuhei Ogomi, Shyam S. Pandey and Shuzi Hayase, **2013 JSAP-MRS Joint Symposia as part of 74th Japan Society of Applied Physics Autumn Meeting**, September 16-20, 2013, Doshisha University, Kyoto, Japan.

2. **Oral**; Photovoltaic performance of Dye Sensitized Solar Cells consisting of P-Substituted Phthalocyanine, **Azwar Hayat**, Shivashimpi Gururaj, Terumi Nishimura, Naotaka Fujikawa, Yuhei Ogomi, Shyam S. Pandey, Yoshiro Yamaguchi, Tingli Ma and Shuzi Hayase, **81st The Electrochemical Society Of Japan Spring Meeting**, March 29-31, 2014, Kansai University, Osaka, Japan

3. **Oral**; Axially anchored Phosphorus-Phthalocyanine dyes as NIR Sensitizer for Dye Sensitized Solar Cells, **Azwar Hayat**, Shivashimpi Gururaj, Terumi Nishimura, Naotaka Fujikawa, Yuhei Ogomi, Shyam S. Pandey, Yoshiro Yamaguchi, Tingli Ma and Shuzi Hayase, **IUMRS-ICA 2014**, August 24-30, 2014, Fukuoka University, Fukuoka, Japan.

4. **Poster**; Phosphorus (III)-Phthalocyanine as Potential NIR Sensitizer for Dye Sensitized Solar Cells, **Azwar Hayat**, Shivashimpi Gururaj, Terumi Nishimura, Naotaka Fujikawa, Yuhei Ogomi, Shyam S. Pandey, Yoshiro Yamaguchi, Tingli Ma and Shuzi Hayase, **50th Kyushu Branch Chemical Society Meeting**, July 2013, Kitakyushu, Japan.

5. **Oral**; Transparent Conductive Oxide free Dye sensitized solar cell using flat Titanium sheet, **Azwar Hayat**, Shyam S. Pandey, Tingli Ma and Shuzi Hayase, **11th International Conference on Nano-Molecular Electronics**, December 17-19, 2014, Kobe International Conference Center, Kobe, Japan.

6. **Oral**; Flat Titanium Based Photo Anode and Counter Electrode for Transparent Conductive Oxide-Less Dye Sensitized Solar Cell, **Azwar Hayat**, Shyam S. Pandey, Yuhei Ogomi, Tingli Ma and Shuzi Hayase, **ICMAT 2015&IUMRS-ICA 2015**, June 28- July 3, 2015, Suntec Singapore, Singapore.

Acknowledgement

Alhamdulillahirabbilalamin, Thanks to Allah SWT and Prophet Muhammad SAW. From my deepest gratitude, I would like to thank **Prof. Shuzi Hayase** for accepting me in his laboratory and giving me chance to work under his guidance from 2009-2011 in Master degree and 2012-2015 for Doctoral degree. His enormous knowledge and understanding have given me an excellent background in this field. I also would like to thanks **Prof. Shyam S. Pandey** for his valuable support and encouragement. My truthful thanks to **Prof. Tingli Ma**, for her valuable input and suggestions for this work. My honest thanks to **Prof. Wataru Takashima** and **Prof. Hirokazu Yamane** for valuable comments and suggestions in this thesis.

I would also like to thank **Dr. Gururaj Shivashimpi**, for synthetized the Phthalocyanine dyes in Hayase laboratory. I would also like to thanks **Mr. Md. Zaman Molla, Mr. Gaurav Kapil, Mr. Ajay K. Baranwal, Mr. Tarun** and all **Hayase lab members** for making my study unforgettable in Japan.

I am also grateful to Kyushu Institute of Technology for all kind supports, especially I would like to thanks **Miss Yasuko Nagamatsu** for her constant help during my stay in Japan.

Moreover, I thank my parents (**Mr. Abdul Hayat** and **Mrs. Asmaidar**), my beloved wife (**Andi Dian Sry Rezki**) and my adored Son (**Al Bukhari Ryoichi Azwar**) for their love, cooperation and encouragement which was a constant source of inspiration for me. At last, my gratitude to Indonesia government with Indonesian Higher Education for Doctoral Program Scholarship 2012-2015.